UNIVERSIDAD MICHOACANA DE SAN NICOLÁS DE HIDALGO

"A TWO-TIME SCALE-BASED APPROACH FOR THE ANALYSIS OF SHORT-TERM AND LONG-TERM DYNAMICS IN ELECTRIC POWER SYSTEMS"

by

REYMUNDO RAMÍREZ BETANCOUR

THESIS

REQUIREMENT FOR THE DEGREE OF

DOCTOR IN SCIENCES IN ELECTRICAL ENGINEERING

División de Estudios de Posgrado
Facultad de Ingeniería Eléctrica

ADVISOR:
CLAUDIO RUBÉN FUERTE ESQUIVEL, Ph.D.

CO-ADVISOR:
THIERRY VAN CUTSEM, Ph.D.

MORELIA, MICHOACÁN APRIL 2012

A TWO-TIME SCALE-BASED APPROACH FOR THE ANALYSIS OF SHORT-TERM AND LONG-TERM DYNAMICS IN ELECTRIC POWER SYSTEMS

by

REYMUNDO RAMÍREZ BETANCOUR

THESIS

Requirement for the degree of
DOCTOR IN SCIENCES IN ELECTRICAL ENGINEERING

Universidad Michoacana de San Nicolás de Hidalgo
División de Estudios de Posgrado
Facultad de Ingeniería Eléctrica

Advisor:
CLAUDIO RUBÉN FUERTE ESQUIVEL, Ph.D.

Co-Advisor:
THIERRY VAN CUTSEM, Ph.D.

April 2012

A TWO-TIME SCALE-BASED APPROACH FOR THE ANALYSIS OF SHORT-TERM AND LONG-TERM DYNAMICS IN ELECTRIC POWER SYSTEMS

Los Miembros del Jurado de Examen de Grado aprueban
la **Tesis de Doctorado en Ciencias en Ingeniería Eléctrica** de ***Reymundo Ramírez Betancour***

Dra. Elisa Espinosa Juárez
Presidente

Dr. Claudio R. Fuerte Esquivel
Director de Tesis

Dr. Thierry Van Cutsem
Co-Director de Tesis

Dr. J. Aurelio Medina Rios
Vocal

Dr. Daniel Ruiz Vega
Revisor Externo
Instituto Politécnico Nacional

Dr. J. Aurelio Medina Ríos
Jefe de la División de Estudios de Posgrado
En Ingeniería Eléctrica.

UNIVERSIDAD MICHOACANA DE SAN NICOLÁS DE HIDALGO
Marzo 2012

Abstract

In this thesis an approach for the simulation of power system short-term and long-term dynamics is developed. It combines the good characteristics of both Full-Time Scale (accuracy) and Quasi Steady-State (efficiency) simulation in a unified simulation tool. According to this approach, the short-term dynamics are computed with the Full-Time Scale simulation while the long-term dynamics are calculated by the Quasi Steady-State approximation. The singular perturbation and the two-time scale techniques are applied to obtain a suitable criterion for switching from Full-Time Scale to Quasi Steady-State simulation. The switching occurs automatically once the fast part of the dynamic variables remains below a specified tolerance during a specified period of time.

The benefits and main characteristics of the proposed method are shown by numerical simulations in both small and large power systems: 2-machine, 4-bus system; 3-machine, 9-bus Western System Coordinating Council (WSCC) system; 10-machine, 39-bus New England system and 46-machine, 190-bus equivalent model of the Mexican system.

Acknowledgements

First and foremost, I would like to express my sincere appreciation to my thesis supervisor, Prof. Claudio Rubén Fuerte Esquivel, for his invaluable assistance, time, patience and guidance throughout the entire duration of my Ph.D. research work. I would express many thanks for his sincere friendship.

I thank my co-advisor Prof. Thierry Van Cutsem by accepting me as a visiting student in department of Electrical Engineering and Computer Science in the University of Liège. His help and suggestions improved my research work.

I would also thank my examiners Professors, for fruitful discussions and persistently revising the thesis report. Their valuable comments improved the level of this thesis report.

I acknowledge the financial assistance that I have received from the Consejo Nacional de Ciencia y Tecnología (CONACyT) of México. I must also acknowledge the División de Estudios de Posgrado de la Facultad de Ingeniería Eléctrica de la Universidad Michoacana de San Nicolás de Hidalgo, for the hospitality and the opportunity of carrying out my Doctoral studies.

None of this would have been possible without the love, patience, encouragement, and support of my wife during these many years. I wish to thank a lot my wife, Isela.

Especial acknowledge to my mother, father, aunt, sisters and brother for their constant support and good wishes at any moment of my life.

To family Vega-Loya for its hospitality and support, but especially for its help to my wife during my absence due to my doctoral studies in Belgium.

Finally, I would like to thank everybody who was important to the realization of this research work.

Table of Contents

List of Tables

List of Figures

List of Publication

The publications derived of this research work are

Journal

- Ramírez-Betancour R., Fuerte-Esquivel C. R. and Van Cutsem T., "*A two-time scale simulation for dynamic analysis of power systems,*" Electric Power System Research, ISSN: 0378-7796, Vol. 83, No. 1, Feb. 2012, pp. 185-195.

Conference

- Ramírez-Betancour R., Gutierrez-Martinez V. J. and Fuerte-Esquivel C. R., "*Static simulation of voltage instability considering effects of governor characteristics and voltage and frequency dependence of loads,*" North American Power Symposium 2010, NAPS 2010, ISBN: 978-1-4244-8046-3, Sept. 26-28, Arlington, TX, 7 pages.

- Ramírez-Betancour R. and Fuerte-Esquivel C. R., "*Flujos de potencia no-iterativo usando series de potencia y expansión de fracciones continuas,*" in Proc. 5^{o} Congreso Internacional de Ingeniería Electromecánica y de Sistemas, Noviembre 10-14, 2008, México City, México, pp. 163-169.

- Ramírez-Betancour R. and Fuerte-Esquivel C. R., "*Control de Intercambio de Áreas en Flujos de Potencia con Regulación Primaria y Cargas no Lineales,*" IEEE-ROPEC- 2006, Octava Reunión de Otoño de Potencia, Electrónica y Computación, Noviembre 8-10, 2006, Morelia, Mich., México, 6 pages.

- Ramírez-Betancour R. and Fuerte-Esquivel C. R., "*Flujos de Potencia con Regulación Primaria y Cargas no Lineales*," IEEE Sección México RVP-AI/2006, Décimo Novena Reunión de Verano de Potencia, Aplicaciones Industriales y Exposición Industrial, Julio 9-15, 2006, Acapulco Gro., México, 6 pages.

Nomenclature

t_0:	Initial time of the study period
t_{sw}:	Switching time
t_{end}:	Final time of the study period
Tol_{sw}:	Switching tolerance
t_{TOL}:	Pre-specified fixed number of time steps
E_{fd}:	Voltage proportional to the field voltage
δ:	Rotor angle position relative to a certain rotating reference
E'_q:	Voltage magnitudes behind synchronous *q*-axis reactances
E'_d:	Voltage magnitudes behind synchronous *d*-axis reactances
ψ_{1d}:	Flux linkage per second of *d*-axis damping winding
ψ_{2q}:	Flux linkage per second of *q*-axis damping winding
T'_{qo}, T'_{do}:	*q*-, *d*-axis transient open-circuit time constant
T''_{qo}, T''_{do}:	*q*-, *d*-axis subtransient open-circuit time constant
V:	Magnitude of the voltage measured at bus terminal
θ:	Phase angle of the voltage measured at bus terminal
n:	Number of buses in the system
P_g:	Active power generated by the synchronous machine
Q_g:	Reactive power generated by the synchronous machine
P_L:	Active power demanded by the load
Q_L:	Reactive power demanded by the load
$P_{inj\,i}$:	Active power flows injected at *i-th* bus
$Q_{inj\,i}$:	Reactive power flows injected at *i-th* bus
$\boldsymbol{J}$:	Jacobian Matrix

S_{sys}: System nominal power

S_{gen}: Generator nominal power

S_{mot}: Motor nominal power

AGC: Automatic Generation Control

AVR: Automatic Voltage Regulator

BLC: Boundary Layer Correction

BE: Backward Euler

COI: Center-of-Inertia

DAE: Differential-Algebraic Equation

DF: Derivative Feedback

FTS: Full-Time Scale

LFC: Load-Frequency Control

LTC: Load Tap Changers

ODE: Ordinary Differential Equation

OXL: OvereXcitation Limiter

PSS: Power System Stabilizer

QSS: Quasi Steady-State

SPT: Singular Perturbation Technique

TR: Trapezoidal Rule

Chapter 1

INTRODUCTION

1.1 Motivation and justification

Generally speaking, modern power systems are large-scale systems composed of the interconnection of electric components whose dynamics are interacting at widely-varying speeds [Chow, 1982]. Therefore, the power system stability problem is commonly studied in different categories according to the time scale instead of a single problem. In the context of power system analysis, the stability is defined as “the ability of a power system to recover a state of operating equilibrium after being subjected to a disturbance from a given initial operating condition, with most system variables bounded so that practically the entire system remains intact” [Kundur et al. 2004], and it can be classified as shown in Figure 1.1.

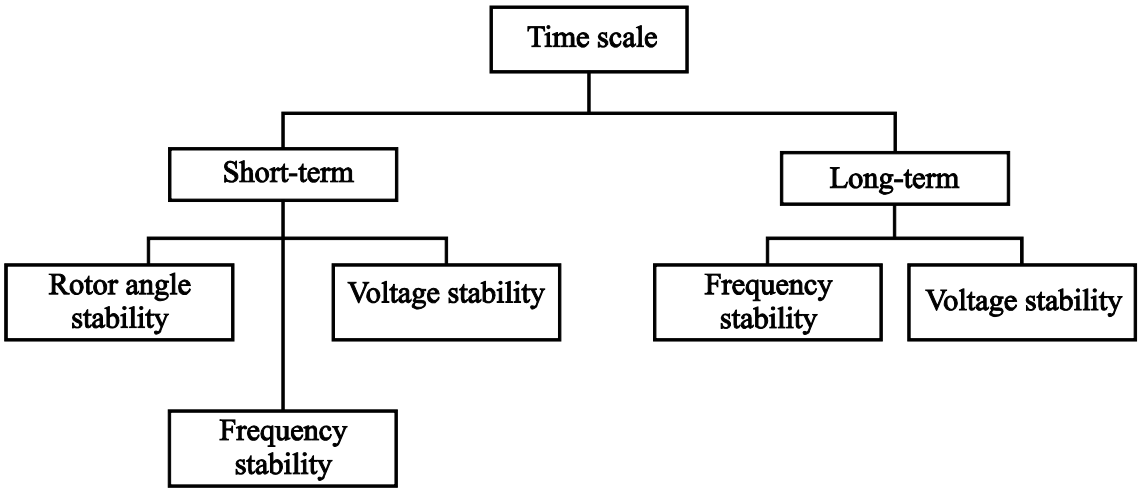

Figure 1.1: Power system stability classification.

Immediately after a power system has been subject to a disturbance, short-term dynamics are excited first. The short-term time scale is mainly concerned with the rotor angle, frequency and voltage transient stability involving the fast components, lasting typically for a few seconds. Some dynamic components acting within this period of time are considered fast: generators, Automatic Voltage Regulators (AVRs), turbines, governors, induction motors, Static Var Compensators (SVCs), High Voltage Direct Current (HVDC), etc. [Van Cutsem and Vournas, 1998].

Following the disturbance which does not cause short-term instability, the multi-time scale dynamics can persist over periods of time spanning from several minutes to several hours. This is called long-term dynamics. The focus of this slower time frame is to evaluate the effects of wide excursions of voltage and frequency for prolonged periods of time. Several dynamic components are acting in this time frame, such as boiler, load self-restoration, secondary frequency and voltage control, switching of shunt compensation, changes in generator set points, Load Tap Changers (LTCs), OvereXcitation Limiters (OXLs), etc, [Van Cutsem and Vournas, 1998]. Consequently, long-term dynamic simulations considering both fast and slow dynamics of the system must be performed to accurately analyze the effects of large excursions of voltage, frequency and power flows that may invoke the action of slow processes, controls and protections. This analysis requires the step-by-step numerical integration of a large-scale nonlinear stiff set of differential-algebraic equations (DAEs), where the time step is largely determined by fast states associated with the very small time constants of generators and their controls, such that long-term simulations may demand a huge computational effort if appropriate techniques are not used.

There are two main numerical approaches based on time scales to reduce the computational burden of long-term dynamic simulations: i) Full-Time Scale (FTS) simulation techniques using a variable time step size of integration in conjunction with explicit or implicit integration methods [Stubbe et al., 1989], [de Mello et al., 1992], [Astic et al., 1994], [Sanchez-Gasca et al., 1995], [Yang and Ajjarapu, 2006]; and ii) model reduction-simplification techniques in conjunction with implicit integration methods

[Chow, 1982], [Xu et al., 1998], [Peponides et al., 1982], being the Quasi Steady-State (QSS) method widely used for its high efficiency [Van Cutsem et al., 2006], [Grenier et al., 2005], [Loud et al., 2001].

This thesis proposes a two-time scale simulation approach for a unified solution of both fast and slow dynamics combining FTS simulation and QSS simulation. The proposed method is inspired of Singular Perturbation (SP) theory to model the interaction between short- and long-term dynamics [Xu et al., 1998], [Peponides et al., 1982]. Based on this interaction, a suitable criterion is proposed to accurately determine when the QSS model of a power system can be considered as a uniform approximation of the FTS model, which also determines the appropriate switching time between these models. The main contributions of the proposed approach are the following: i) simulation efficiency is achieved by both time step size adjustment and model reduction, which are implemented in a single simulation tool instead of using only the former [Stubbe et al., 1989], [de Mello et al., 1992], [Astic et al., 1994], [Sanchez-Gasca et al., 1995] or only the latter [Grenier et al., 2005]; ii) the proposed criterion to automatically switch from the FTS to QSS models preserves a uniform approximation of state and algebraic variables, so that a process to initialize variables for the QSS simulation is not necessary; and iii) finally, the proposed switching criterion is easily computed from the FTS simulation by monitoring the rate of change of the fast time-varying state variables.

1.2 State of the art

An interconnected power system is an extremely complex sizable dynamic system because of its multi-time scale nature, as well as its large-scale and nonlinear characteristics, which make numerical simulation over long time intervals very demanding. Approaches that automatically adjust the time step of integration in accordance with the system's dominant transients used to study both short-term and long-term dynamic phenomena in integrated simulation tools have been reported [Stubbe et al., 1989], [de Mello et al., 1992], [Astic et al., 1994], [Sanchez-Gasca et al., 1995], [Yang and Ajjarapu, 2006]. The main idea behind

these approaches is to automatically reduce the time step to capture fast transients. As fast modes decay during the solutions process, the time step is gradually increased to reduce the computation time required to capture slow transients. A predictor-corrector approach based on the Gear-type Backward Differentiation Formula (BDF) is used in [Stubbe et al., 1989] to solve the set of DAEs. The time step size (and possibly the order) of the integration method are adjusted according to a local truncation error defined as the difference between predicted and corrected solutions. A similar idea is applied in [de Mello et al., 1992], but the full power system model is solved by a simplified time-domain simulation based on the Backward Euler (BE) method and large time steps of integration to filter out the fast dynamics. Simulation is performed by integrating the set of DAEs with a specified maximum step size, which is automatically reduced when the Newton method used to solve the set of nonlinear equations exhibits convergence difficulties. As the convergence of the Newton method improves over successive time steps, the time step is increased until reaching the maximum step time value. A drawback of these approaches is that an unstable mode of oscillation can lie in the stability domain of the integration methods so that a real unstable phenomenon will be simulated as a stable one. This problem can be avoided by using the mixed Adams-BDF variable step size and variable order algorithm proposed in [Astic et al., 1994]. The Adams method is applied to solve the set of ordinary differential equations (ODEs) and to check the errors in dynamic variables, whilst the BDF method is applied with the same purpose but to the algebraic equations and variables. The selection of both step size length and order of the integration method is based on a global truncation error, which depends on the weighted root mean square norm of all corrected values of dynamic and algebraic variables. In the proposed implementation, the step size adjustment can be done once it has been kept constant in at least the number of time steps that equals the order of the mixed integration method [Astic et al., 1994]. A variable time step integration based on the Theta (θ) method is used in [Sanchez-Gasca et al., 1995] to solve the set of DAEs representing the power system. This method is A-stable for values of $\theta \leq 0.5$, and a value for θ in the range of 0.47-0.49 avoids the following: i) the problem of sustained numerical oscillations, which is often encountered following the occurrence of

switching events in simulations using the trapezoidal rule of integration [Yang and Ajjarapu, 2006], and ii) the problem of hyper-stability presented in the numerical methods used in [Stubbe et al., 1989], [Astic et al., 1994]. The time step adjustment is done based on a local truncation error defined as a function of predicted and corrected values of both state and algebraic variables. The time step is increased if the maximum norm of the local error vector is below a specified tolerance for a number of time steps. On the other hand, if this norm exceeds the tolerance, the time step is reduced to a fixed value for a number of time steps before attempting to increase it. When a severe disturbance occurs, the simulation algorithm temporary changes to an explicit integration method with the time step fixed to a pre-specified minimum value. During this stage, the magnitude of the local error of integration is monitored to return to the solution based on the θ method. The integration steps have to be further adjusted in order to fall on the time instants where discrete state events (such as variables hitting their limits) take place. In case where the long-term dynamics are driven by many discrete controls – such as the widely used Load Tap Changers (LTCs) – this may prevent the step size from being increased to the extent allowed by the slow continuous-time dynamics

Alternatively, the multiple time scales inherent to the dynamics of a power system can be exploited to obtain reduced order models relevant to a particular time scale [Chow, 1982], [Cate et al., 1984], [Van Cutsem and Vournas, 1998] with the objective of simulating those reduced models much more efficiently [Van Cutsem and Vournas, 1998], [Xu et al., 1998]. A first step toward model simplification was proposed in [Frowd et al. 1982] with a unified approach to short- and long-term dynamic simulation using the fixed-step trapezoidal integration method. The simulation mode is determined by the integration step size, and the switching from one mode to the other is defined by the degree of damping of synchronizing oscillations. An artificial damping term is included in the rotor swing equations of each generator to allow synchronizing oscillations to be artificially suppressed and to allow a larger integration time step when simulating the long-term mode. Based on the idea of combining the advantages of implicit and explicit integration methods to solve the set of DAEs representing the system under study [Astic et al., 1994], a

decoupled time-domain based on invariant subspace partition and fixed-step integration simulation is proposed in [Yang and Ajjarapu, 2006]. The original set of nonlinear ordinary ODEs are grouped in two decoupled sets of stiff and nonstiff equations, respectively, based on eigenvalue analysis of the linearized set of ODEs. The set of stiff ODEs is integrated by those equations whose eigenvalues are located outside the stability domain of a selected explicit method. These equations, together with the set of algebraic equations, are solved using the trapezoidal integration method, and the forward Euler method is used to solve the rest of the nonstiff ODEs.

An alternative to deal with the complexity of considering fast and slow phenomena in long-term dynamic simulations consists on using the model simplification concept. In recent years, the well-known Quasi Steady-State (QSS) approximation has been used for long-term dynamic studies [Van Cutsem and Vournas, 1998], [Xu et al., 1998]. This approximation relies on time-scale decomposition, which consists of decomposing the dynamic state variables into a set of fast time-varying state variables and a set of slow time-varying state variables. By assuming that the former set changes instantaneously with variations of the slow state variables, the set of differential equations associated with the fast (short-term) dynamics are represented by their equilibrium condition [Van Cutsem and Vournas, 1998], significantly reducing the computational effort for long-term dynamic simulation. However, when the power system is subjected to a severe contingency, the QSS simulation has some limitations [Loud et al., 2001]: 1) The assumption that the short-term dynamics can be replaced by their equilibrium equations is also based on the fact that these dynamics are transiently stable. However, the system may lose stability in the short-term and not even enter the long-term period. When this happens, the QSS simulation could exhibit singularity problems [Van Cutsem and Vournas, 1998]; 2) A large disturbance may trigger controls associated with discrete events with great impact on the system's long-term evolution. The sequence of controls depends on the system dynamics, and hence may not be correctly identified from the simplified model.

An alternative to tackling these QSS limitations consists of combining the FTS simulation for the short-term period and QSS approximation for the long-term time frame

as proposed in [Loud et al., 2001] and [Van Cutsem et al., 2006]. The time to switch from FTS to QSS simulation is chosen once the dynamics of rotor angles or frequency have died out [Loud et al., 2001]. In this case, the QSS model is initialized by setting the continuous long-term variables and the algebraic variables to the values computed by FTS simulation at the switching time t_{sw}. The short-term variables are initialized at the values associated with the equilibrium point of the set of differential equations at t_{sw}. Lastly, the operation and waiting state of discrete events have to be considered to determine their initial conditions at t_{sw} and to establish the sequence of discrete controls during the QSS simulation with reasonable accuracy. The initialization process is avoided in [Van Cutsem et al., 2006] by performing an off-line coupling of both approaches based on the discrete events taking place during the detailed simulation. The FTS simulation is executed until the switching time t_{sw} is detected as proposed in [Loud et al., 2001], and the sequence of discrete events that have occurred over this interval are identified. The QSS simulation is then implemented from the initial time with those discrete events imposed as external disturbances, without allowing the discrete devices to act by themselves until the simulation arrives at t_{sw}. From there on, the study proceeds with the usual QSS approximation.

1.3 Objectives

The general goal of this work is to develop an accurate single unified program for long-term dynamics analysis, which combines the accurate of FTS simulation and the efficiency of QSS simulation without the necessity of initializing the QSS models at switching time. The single program obtains the reliability of the FTS simulation when dealing with the short-term dynamics and the efficiency of the QSS simulation when the long-term dynamics is studied.

The general goal can be achieved if an appropriate switching criterion is developed. Therefore, another goal is to develop a suitable criterion for switching from the FTS to the QSS model. The correct switching time has to correspond to the time when the QSS model

is a uniform approximation of FTS model, such that a process to initialize variables for the QSS simulation is not necessary. Also, the switching criterion has to be easily computed in order to reduce the computational burden. For this purpose the singular perturbation technique and the concept of boundary layer correction are used [Kokotovic et al. 1986].

1.4 Methodology

In order to reach the proposed objectives, this research work was developed according to the following methodology:

- Review of the state of the art of dynamic power system simulation (short-term and long-term).
- Review of the singular perturbation and the two-time scales theories.
- Development of the switching criterion.
- Development of the FTS model of a power system based on the power balance formulation.
- Computational implementation of the FTS model in a digital program.
- Development of the QSS model of a power system based on the power balance formulation.
- Computational implementation of the QSS model in a digital program.
- Computational implementation of the switching criterion in the digital program in order to combine FTS and QSS models.
- Development of experiments in order to validate the proposed approach.

1.5 Thesis outline

The rest of this thesis is organized as follows:

Chapter 2 presents the FTS models of the power system components to be considered in this work. The solution process of the differential equations of the models is developed, and the equations representing the dynamic behavior of large-scale power systems are described based on the two frames of references.

Chapter 3 provides the QSS models of the power system components explored in this work. The dynamic state variables are split up into fast and slow variables, and the differential equations associated with the fast variables are replaced by their equilibrium equations. The solution process of this new set of differential and algebraic equations is then presented.

Chapter 4 presents the development of a suitable switching criterion between FTS and QSS simulation by applying the singular perturbation and two-time scale techniques. The proposed approach is then illustrated by studying a single power system.

Chapter 5 addresses the application of the proposed approach to illustrate its suitability for the analysis of short-term and long-term dynamics in electric power systems. It combines the FTS and the QSS models by using the switching criterion developed in Chapter 4. The proposed approach is then tested on several systems: a simple system, the Western System Coordinating Council (WSCC) system, the New England system, and a reduced representation of the Mexican power system.

Chapter 6 gives the general conclusions of this research and presents suggestions for future research work.

Chapter 2

FULL-TIME SCALE MODELLING OF POWER SYSTEM

2.1 Introduction

The dynamic stability analysis of power system is an integral part in the design, planning and operation of large interconnected power systems. The aim of dynamic simulations is the monitoring of the power system and the planning of preventive or corrective control action strategies suitable for mitigating the impact of several disturbances presented in the system. Thus, the development of accurate digital programs and numerical methods for dynamic analysis is very important for secure power grid expansion, and it significantly impacts the future design and operation of large interconnected power systems [Khaitan et al., 2008].

Power system dynamics and stability analyses require performing numerical simulations of a large set of equations of devices, involving dynamic characteristics in a wide range of time scales and nonlinear effects [Van Cutsem et al. 2006]. Therefore, Full-Time Scale (FTS) models must be included in order to obtain more realistic results.

In the present Chapter, the FTS models of the fundamental elements (e.g. network, generator, controls, loads, etc.) that form the power system are developed. Consequently, the resulting differential and algebraic equations are transformed into pure algebraic equations (AEs) using ether the Trapezoidal Rule or the Backward Euler integration method. Thus, the Newton-Raphson algorithm can be used to solve the AEs under a single frame of reference based on power flow formulation.

2.2 Full-time scale formulation

In stability studies, the derivation of a general dynamic model of the power system is given by the sets of differential-algebraic-discrete equations (2.1)-(2.3). Likewise, the numerical integration of the whole set of equations is referred to as Full-Time Scale simulation [Van Cutsem and Vournas, 1998]

$$\dot{x} = f(x, y, z) \qquad f : \Re^{n+m+p} \to \Re^{n} \qquad x \in X \subset \Re^{n} \tag{2.1}$$

$$0 = g(x, y, z) \qquad g : \Re^{n+m+p} \to \Re^{m} \qquad y \in Y \subset \Re^{m} \tag{2.2}$$

$$z(t_k^+) = h(x, y, z(t_k^-)) \qquad h : \Re^{n+m+p} \to \Re^{p} \qquad z \in Z \subset \Re^{p} \quad t \in \left[t_0, t_{end}\right] \tag{2.3}$$

where t_0 and t_{end} are the initial and final times, respectively, of the study time period.

The differential equations (2.1) involve two time scales of dynamic phenomena: short-term dynamics of generators, turbines, governors, AVRs, induction motors, etc. and long-term dynamics of boiler, load self-restoration, secondary frequency and voltage control, etc.

The algebraic equations (2.2) consider the dynamic phenomena practically instantaneous, such as electromagnetic and network transients, etc.

The discrete-time equations (2.3) represent the discrete controls and protections that act on the system: switching of shunt compensation, changes in generator set points, LTCs, OXLs, etc.

In the following Section, the mathematical full-time scale models of the principal devices (generators, voltages regulators, governors, turbines, for example) that compose the power system are developed. The appropriate procedure to solve the equations (2.1)-(2.3) is also presented.

2.3 Generator modelling

The performance of synchronous machines (generators) plays an important role in power system stability because they have to be rotating in synchronism. The generator model commonly used in stability analysis is based on a two-axis formulation of the machine equations as shown in Figure 2.1 [Sauer and Pai, 1998], [Van Cutsem and Vournas, 1998]. The stator (or armature) circuit is composed of three identical sinusoidally distributed armature winding, displaced 120°, with voltages v_a, v_b, v_c and currents i_a, i_b, i_c respectively. The rotor circuit consists of four windings with the field winding (denoted by fd) on the direct axis. Two windings (denoted by *1d* and *1q*) represent amortisseur (or damper) bar effects. The *1d* winding has the same magnetic axis as the field winding, while the magnetic axis of the *1q* winding (called the quadrature axis) is displaced 90° ahead of the direct axis. Furthermore, eddy currents are represented by the second winding (denoted by *2q*) on the quadrature axis [Van Cutsem and Vournas, 1998], [Krause et al., 2002].

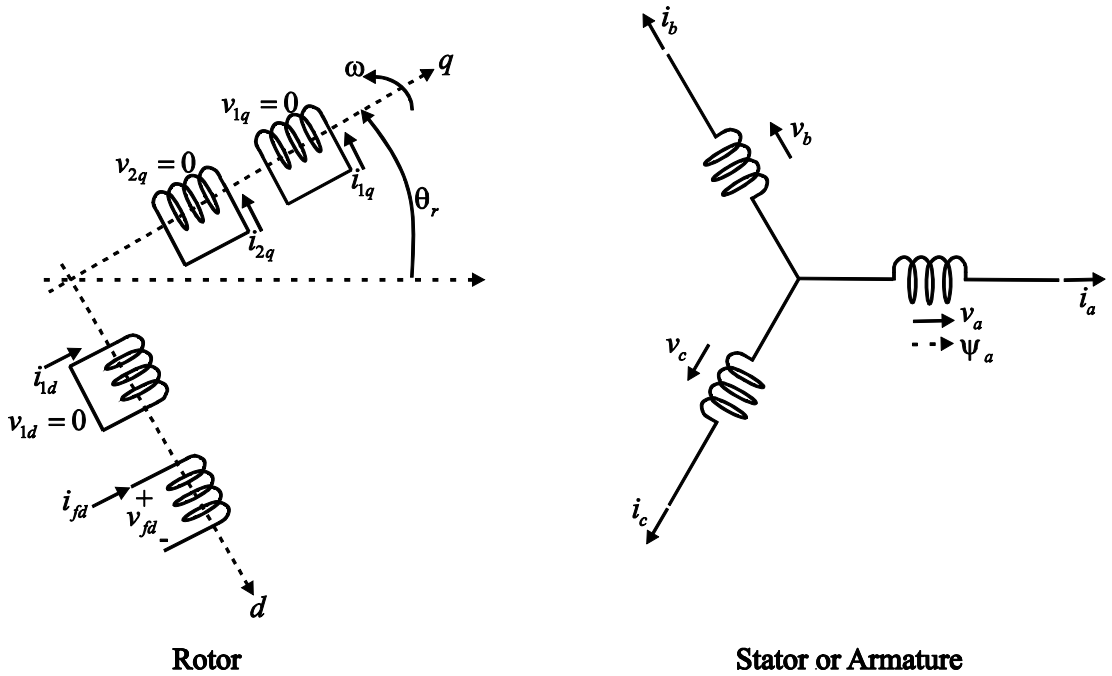

Figure 2.1: Schematic diagram of the synchronous machine.

The stator and rotor equations are obtained by applying the fundamental Kirchhoff's and Faraday's laws as well as the Park transformation [Sauer and Pai, 1998], [Krause et al., 2002]:

$$\begin{bmatrix} V_d \\ -V_{fd} \\ 0 \end{bmatrix} = -\begin{bmatrix} R_a & 0 & 0 \\ 0 & R_{fd} & 0 \\ 0 & 0 & R_{d1} \end{bmatrix}\begin{bmatrix} I_d \\ I_{fd} \\ I_{d1} \end{bmatrix} - \begin{bmatrix} \frac{\omega}{\omega_0}\psi_q \\ 0 \\ 0 \end{bmatrix} - \frac{1}{\omega_0}\frac{d}{dt}\begin{bmatrix} -\psi_d \\ \psi_{fd} \\ \psi_{d1} \end{bmatrix} \tag{2.4}$$

$$\begin{bmatrix} V_q \\ 0 \\ 0 \end{bmatrix} = -\begin{bmatrix} R_a & 0 & 0 \\ 0 & R_{q1} & 0 \\ 0 & 0 & R_{q2} \end{bmatrix}\begin{bmatrix} I_q \\ I_{q1} \\ I_{q2} \end{bmatrix} + \begin{bmatrix} \frac{\omega}{\omega_0}\psi_d \\ 0 \\ 0 \end{bmatrix} - \frac{1}{\omega_0}\frac{d}{dt}\begin{bmatrix} -\psi_q \\ \psi_{q1} \\ \psi_{q2} \end{bmatrix} \tag{2.5}$$

with the flux linkages per second expressed as

$$\begin{bmatrix} \psi_d \\ \psi_{fd} \\ \psi_{1d} \end{bmatrix} = \begin{bmatrix} -X_d & X_{md} & X_{md} \\ -X_{md} & X_{fd} & X_{md} \\ -X_{md} & X_{md} & X_{1d1d} \end{bmatrix}\begin{bmatrix} I_d \\ I_{fd} \\ I_{1d} \end{bmatrix} \tag{2.6}$$

$$\begin{bmatrix} \psi_q \\ \psi_{1q} \\ \psi_{2q} \end{bmatrix} = \begin{bmatrix} -X_q & X_{mq} & X_{mq} \\ -X_{mq} & X_{1q1q} & X_{mq} \\ -X_{mq} & X_{mq} & X_{2q2q} \end{bmatrix}\begin{bmatrix} I_q \\ I_{1q} \\ I_{2q} \end{bmatrix} \tag{2.7}$$

where ω_0 is the synchronous speed, and ω is the actual rotor speed. X_{md} and X_{mq} are the *d* and *q* magnetizing reactance, respectively, R_s is the stator resistance, V_d is the *d* winding voltage, I_d is the *d* winding currents and X_d is the *d* leakage reactance. Appropiate variables are also associated with the *q* axis and the rotor circuit.

According to the dynamic of interest in the present work, the generator model considered in this work relied on the following assumptions [Van Cutsem and Vournas, 1998]:

- The transformer voltages are neglected $(\dot{\psi}_d = \dot{\psi}_q = 0)$.
- The usual speed deviations are small compared to the synchronous speed, $(\omega \approx \omega_0)$.
- The armature resistance (which is very small) is neglected.
- Magnetic saturation is neglected.

Therefore, under these assumptions and through algebraic manipulation (see Appendix A), the FTS synchronous machine model of order VI can be expressed only in terms of meaningful bus variables:

$$\frac{d}{dt}\begin{bmatrix} E'_q \\ \psi_{1d} \\ E'_d \\ \psi_{2q} \end{bmatrix} = \begin{bmatrix} \frac{K_1}{T'_{do}} & \frac{K_2}{T'_{do}} & 0 & 0 \\ \frac{K_4}{T''_{do}} & \frac{K_5}{T''_{do}} & 0 & 0 \\ 0 & 0 & \frac{K_7}{T'_{qo}} & \frac{K_8}{T'_{qo}} \\ 0 & 0 & \frac{K_{10}}{T''_{qo}} & \frac{K_{11}}{T''_{qo}} \end{bmatrix} \begin{bmatrix} E'_q \\ \psi_{1d} \\ E'_d \\ \psi_{2q} \end{bmatrix} + \begin{bmatrix} \frac{1}{T'_{do}} & \frac{K_3}{T'_{do}} & 0 \\ 0 & \frac{K_6}{T''_{do}} & 0 \\ 0 & 0 & \frac{K_9}{T'_{qo}} \\ 0 & 0 & \frac{K_{12}}{T''_{qo}} \end{bmatrix} \begin{bmatrix} E_{fd} \\ V\cos(\delta-\theta) \\ V\sin(\delta-\theta) \end{bmatrix} \tag{2.8}$$

$$\frac{d\delta}{dt} = \omega - \omega_0 \tag{2.9}$$

$$\frac{d\omega}{dt} = \frac{\omega_0}{2H}\left(P_m - P_g - D(\omega - \omega_0)\right) \tag{2.10}$$

with

$$\begin{aligned} P_g = {} & K_{13}E'_dV\cos(\delta-\theta) + K_{14}\psi_{2q}V\cos(\delta-\theta) + K_{15}E'_qV\sin(\delta-\theta) \\ & + K_{16}\psi_{1d}V\sin(\delta-\theta) + K_{17}V^2\sin(2(\delta-\theta)) \end{aligned} \tag{2.11}$$

$$\begin{aligned} Q_g = {} & -K_{13}E'_dV\sin(\delta-\theta) - K_{14}\psi_{2q}V\sin(\delta-\theta) + K_{15}E'_qV\cos(\delta-\theta) \\ & + K_{16}\psi_{1d}V\cos(\delta-\theta) - V^2\left(K_{18}\cos(\delta-\theta)^2 + K_{19}\sin(\delta-\theta)^2\right) \end{aligned} \tag{2.12}$$

where K_j are constants associated to the generator's reactances, E_{fd} is the voltage proportional to the field voltage determined by exciters or it can be considered as constant and δ is the generator's rotor angle relative to a certain rotating reference with respect to the quadrature axis. The voltage magnitudes behind transient *q*- and *d*-axis reactances are E'_q and E'_d. Flux linkages per second related to damping windings are given by ψ_{1d} and ψ_{2q}. T'_{do}, T'_{qo} and T''_{do}, T''_{qo} are the *q*-, *d*-axis transient and subtransient open-circuit time constant, respectively. *H* is the moment of inertia, *D* is the damping constant, P_m is the turbine mechanical power injection and P_g is the generator's electrical power output. Lastly, *V* and θ are the magnitude and phase angle of the voltage measured at bus terminal.

2.3.1 Initial condition for the synchronous generator

In power system dynamic analysis, computing the initial value of all the dynamic states (E'_q, E'_d, ψ_{1d}, ψ_{2q}, δ, ω) is necessary, as well as the fixed inputs (E_{fd}, P_m). These values are normally obtained from a base study power flow solution. After the power flow study has been solved, the initial condition is computed by solving the steady-state synchronous generator model represented by the steady-state equivalent circuit of Figure 2.2 [Sauer and Pai, 1998].

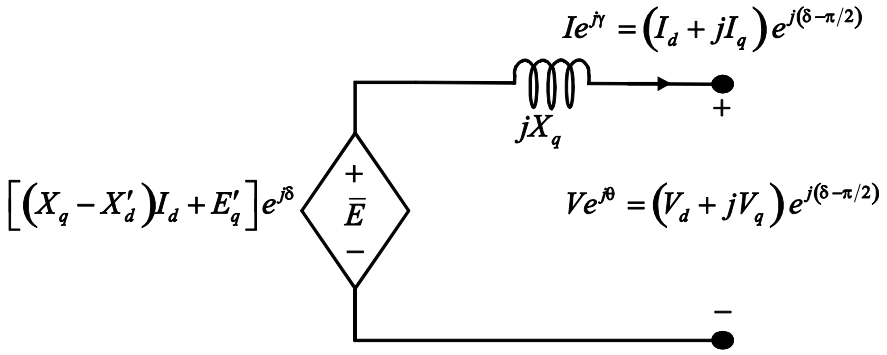

Figure 2.2: Equivalent circuit for steady-state operation of synchronous generator.

Application of Kirchhoff's voltage law to Figure 2.2 yields the stator equation in steady-state

$$\bar{E} = Ve^{j\theta} + jX_q Ie^{j\gamma} \tag{2.13}$$

where $Ve^{j\theta}$ and $Ie^{j\gamma}$ are the terminal voltage and current, respectively; $\bar{E}$ represents a voltage behind reactance X_q.

Thus, the initial condition for the generator model is normally carried out by the following steps:

- The terminal current is found as

$$Ie^{j\gamma} = \frac{P_g + jQ_g}{Ve^{j\theta}}. \tag{2.14}$$

- $\bar{E}$ is computed by (2.13), and the internal angle of generator is obtained from

$$\delta = \text{angle of } \bar{E}. \tag{2.15}$$

- From Figure 2.2 and the result of the previous step, E'_q is computed as

$$E'_q = \left|\bar{E}\right| - \left(X_q - X'_d\right) I_d \tag{2.16}$$

where $I_d = I\cos(\gamma - \delta + \pi/2)$.

- Since the derivatives are zero, the rest of the state variables are given by

$$\begin{bmatrix} \psi_{1d} \\ E'_d \\ \psi_{2q} \end{bmatrix} = -\begin{bmatrix} K_5 & 0 & 0 \\ 0 & K_7 & K_8 \\ 0 & K_{10} & K_{11} \end{bmatrix}^{-1} \begin{bmatrix} K_4 & K_6 & 0 \\ 0 & 0 & K_9 \\ 0 & 0 & K_{12} \end{bmatrix} \begin{bmatrix} E'_q \\ V\cos\left(\delta - \theta\right) \\ V\sin\left(\delta - \theta\right) \end{bmatrix} \tag{2.17}$$

$$\omega = \omega_0. \tag{2.18}$$

- While the fixed inputs are computed as

$$E_{fd} = -\left(K_1 E'_q + K_2 \psi_{1d} + K_3 V \cos\left(\delta - \theta\right)\right) \tag{2.19}$$

$$P_m = P_g . \tag{2.20}$$

2.4 Automatic voltage regulators

The generators are normally operated at constant terminal voltage through an automatic voltage regulator (AVR) that controls the amount of current supplied to the generator field winding by the exciter. The general functional block diagram of the automatic voltage regulator system is shown in Figure 2.3 [Machowski et al., 2008].

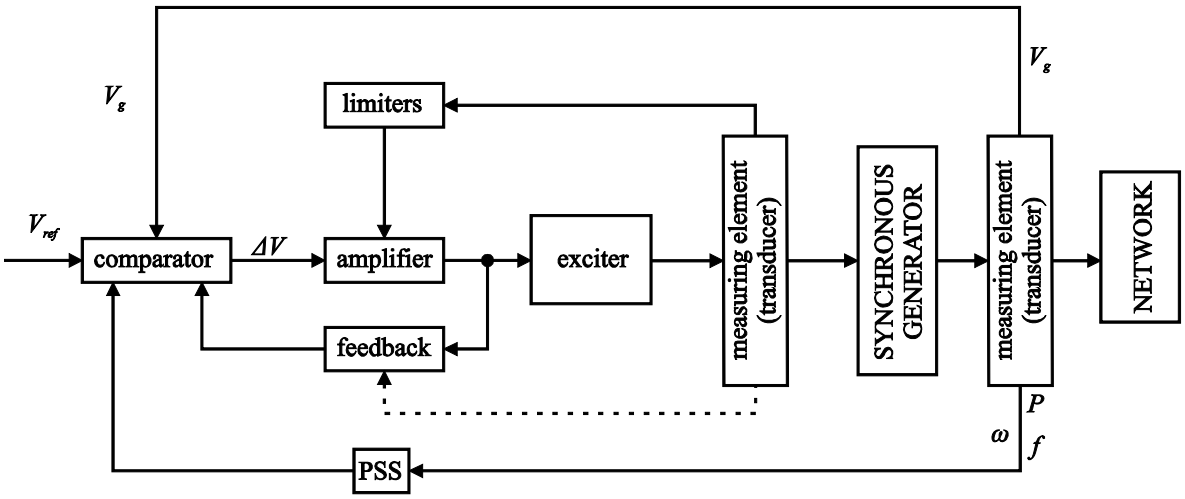

Figure 2.3: Block diagram of the AVR system.

The AVR system includes several subsystems which work together for the correct operation of the voltage control loop. These subsystems are presented in the following Sections.

2.4.1 Excitation modelling

The principal function of the electric field exciter is to control the terminal voltage magnitude at a reference value by changing the machine excitation, E_{fd}. Figure 2.4 shows a detailed dynamic model of the electric field exciter used in this work, which corresponds to the IEEE Type 1 without saturation representation [Anderson and Fouad, 1994], [Rafian et al. 1988].

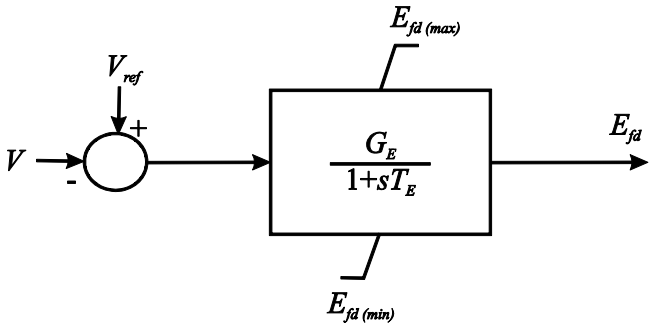

Figure 2.4: Electric field exciter.

From the block diagram of the model, the differential equation of the exciter can be expressed as

$$T_E \frac{dE_{fd}}{dt} = G_E \left(V_{ref} - V\right) - E_{fd} \qquad E_{fd(\min)} \le E_{fd} \le E_{fd(\max)} \tag{2.21}$$

where T_E is the exciter time constant, and G_E is the open-loop steady-state gain of excitation. The voltage reference (V_{ref}) is calculated as [Rafian et al., 1988],

$$V_{ref} = \frac{E_{fd}^0}{G_E} + V^0 \tag{2.22}$$

where E_{fd}^0 and V^0 are the initial excitation and terminal voltages of the generator whose values are obtained with the generator initialization procedure.

2.4.2 Feedback compensation

The excitation control system stabilization (comprised of a feedback compensation) is used to improve the dynamic performance of the control system. The most commonly used form of compensation is a derivative feedback (DF), as shown in Figure 2.5. The effect of the compensation is to minimize the phase shift introduced by the time delays over a selected frequency range [Kundur, 1994].

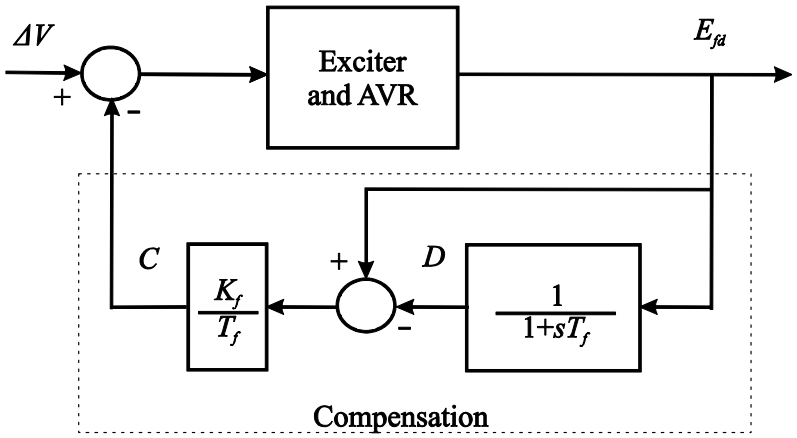

Figure 2.5: Derivative feedback compensation.

The mathematical model of DF compensation is obtained using Figure 2.5 as

$$T_f \frac{dD}{dt} = E_{fd} - D \tag{2.23}$$

$$C = \frac{K_f}{T_f}\left(E_{fd} - D\right) \tag{2.24}$$

where T_f is the time constant, and K_f is the gain of the DF compensation system. The initial condition of D must be equal to E_{fd}^0, since the initial compensation has to be zero, i.e. $C^0 = 0$.

2.4.3 Power system stabilizer

The power system stabilizer (PSS) adds damping to the generator rotor oscillations by controlling its excitation using an auxiliary stabilizing signal. This device is employed to improve the damping of rotor oscillations over a range of frequencies, rather than a single frequency. Normally, the frequency range of interest is 0.1 to 2.0 Hz [Kundur, 1994].

The functional block diagram of the PSS system is shown in Figure 2.6 [Kundur, 1994]. It consists of three blocks: a phase compensation block (lead-lag), a signal washout block and a gain block. The compensation block provides the appropriate phase-lead characteristic to compensate for the phase lag between the exciter input and the generator electrical (air-gap) torque. The PSS responds only to changes in rotor speed due to the signal washout block operation. This block operates as a high-pass filter with the time constant T_w high enough to allow signals associated with oscillations in ω to pass unchanged. The stabilizer gain K_S determines the amount of damping introduced by the PSS [Kundur, 1994], [Xu et al., 1998].

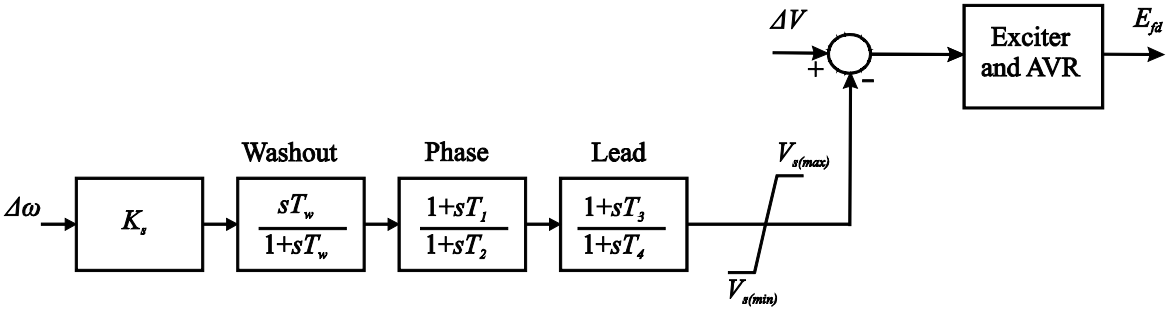

Figure 2.6: Power system stabilizer.

From Figure 2.6, the mathematical model of the PSS represented by first order differential equations cannot be directly obtained. However, this is reached by subdividing each block in an appropriate form, as shown Figure 2.7 (see Appendix B).

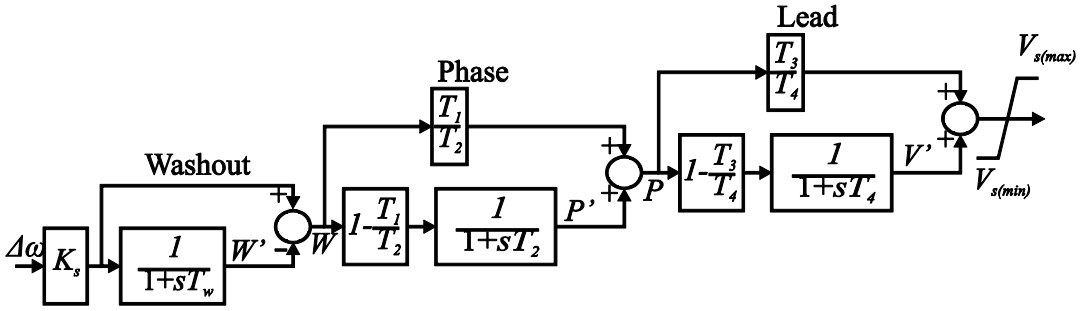

Figure 2.7: Block diagram of the PSS.

Using the block diagram of Figure 2.7, the mathematical model of the PSS takes the following form:

$$T_w \frac{dW'}{dt} = K_S \Delta\omega - W' \tag{2.25}$$

$$T_2 \frac{dP'}{dt} = c_1 \left(K_S \Delta\omega - W' \right) - P' \tag{2.26}$$

$$T_4 \frac{dV'}{dt} = c_2 \left(K_S \Delta\omega - W' \right) - c_3 P' - V' \tag{2.27}$$

where W', P' and V' are the state variables associated with the washout block, phase and lead, respectively. T_w and T_i are the time constants related to each block, while the gain c_1, c_2 and c_3 are given by

$$c_1 = 1 - \frac{T_1}{T_2}, \quad c_2 = 1 - \frac{T_3}{T_4}, \quad c_3 = \frac{T_1}{T_2} - \frac{T_1 T_3}{T_2 T_4}. \tag{2.28}$$

The compensation V_s of the PSS, which is incorporated in the exciter, can be expressed as

$$V_s = c_4 \left(K_s \Delta\omega - W' \right) + c_5 P' + V' \tag{2.29}$$

where the gain c_4 and c_5 are given by

$$c_4 = \frac{T_1 T_3}{T_2 T_4}, \quad c_5 = \frac{T_3}{T_4}. \tag{2.30}$$

The initial condition of the state variables W', P' and V' are equal to zero in order to start simulation without PSS compensation.

2.4.4 OvereXcitation limiters

The OvereXcitation Limiter (OXL) of synchronous generators plays an important role in the voltage stability of power systems. It modifies the reference voltage of automatic voltage regulators to protect the field winding of the synchronous generator from overheating [Van Cutsem and Vournas, 1998]. For the generator model presented in Section 2.3, the field current is given by the following expression:

$$I_{fd} = -K_1 E'_q - K_2 \psi_{1d} - K_3 V \cos(\delta - \theta) \tag{2.31}$$

where K_1, K_2 and K_3 are constants associated to the generator reactances; these are given in Appendix A.

This device is generally inactive, unless the field current is greater than its thermal limit, $I_{fd}^{\lim}$, as shown in Figure 2.8 [Van Cutsem and Vournas, 1998].

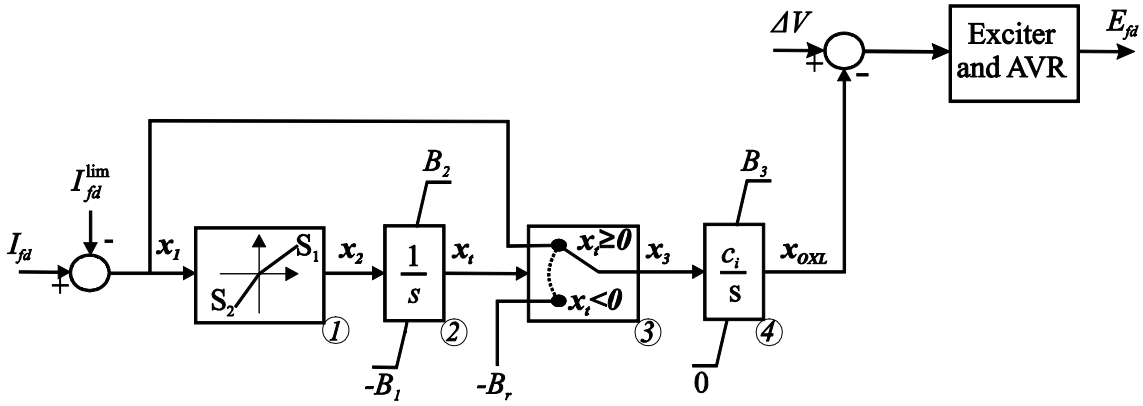

Figure 2.8: Block diagram of the OXL model.

Block 1 corresponds to a two-slope gain whose output depends on the value of x_1:

$$\begin{aligned} x_2 &= S_1 x_1 \qquad \text{if } x_1 \geq 0 \\ x_2 &= S_2 x_1 \qquad \text{if } x_1 < 0 \end{aligned} \tag{2.32}$$

where $x_1 = i_{fd} - i_{fd}^{\lim}$ and S_1, S_2 are constants bigger than zero. The output of the first limited integrator (block 2) is initially at its lower bound, $x_t = -B_1$, and hereafter it is expressed as

$$\begin{aligned} &\dot{x}_t = 0 \quad \text{if} \quad \left(x_t = B_2 \text{ and } \dot{x}_t \geq 0\right) \text{ or } \left(x_t = -B_1 \text{ and } \dot{x}_t < 0\right) \\ &\dot{x}_t = x_2 \quad \text{otherwise} \end{aligned} . \tag{2.33}$$

When i_{fd} becomes larger than $i_{fd}^{\lim}$, the output of block 2 starts increasing. As soon as x_t becomes positive, block 3 switches its input as indicated in Figure 2.8.

The output of the second limited integrator (block 4) must be initialized at zero, $x_{OXL} = 0$. Right after block 3 has switched, the output x_{OXL} increases according to the following expression [Van Cutsem and Vournas, 1998]:

$$\begin{aligned} &\dot{x}_{OXL} = 0 \quad \text{if} \quad \left(x_{OXL} = B_3 \text{ and } \dot{x}_{OXL} \geq 0\right) \text{ or } \left(x_{OXL} = 0 \text{ and } \dot{x}_{OXL} < 0\right) \\ &\dot{x}_{OXL} = c_i x_3 \quad \text{otherwise} \end{aligned} . \tag{2.34}$$

Therefore, the field current decreases as a result of subtracting the output signal x_{OXL} from the AVR inputs as shown in Figure 2.8.

2.5 Automatic generation control

The role of an Automatic Generation Control (AGC) is to maintain the power plant frequency close to its nominal values by controlling the generation of active power. This control is applied at two levels, designed for primary and secondary frequency control [Elgerd and van der Puije, 1998]. The AGC control loops are shown in Figure 2.9.

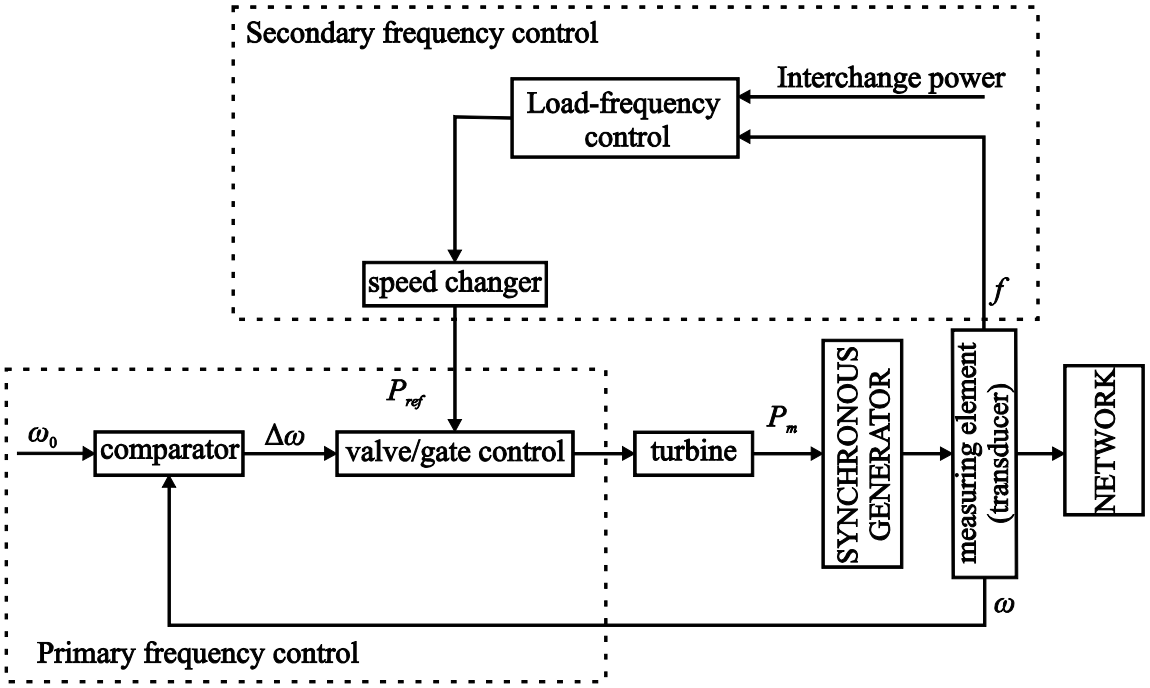

Figure 2.9: Automatic generation control.

The primary frequency control performs the initial adjustment of the frequency. This control responds relatively quickly to a measured sign of frequency. For "quickly" we mean the changes that happen in some seconds. Through the speed governor this control loop regulates active power output to match the fluctuations in the load [Elgerd and van der Puije, 1998].

The secondary control loop performs the fine tuning of the frequency. To achieve this, the load-frequency control adjusts the speed changer according to some convenient control strategy. The secondary control loop is a support of the governor, which allows lessening the frequency deviation to an acceptable value and keeps the interchanged power between neighboring electric areas at the scheduled value.

For the purposes of the present investigation, only the primary frequency control of the steam plants is considered. This loop control acts according to the speed governor and the steam turbine, as detailed in the next Sections.

2.5.1 Speed governor

The governor adjusts the steam input to the turbine through the valve position, P_{GV}. This is shown in the block diagram of Figure 2.10 [IEEE Committee Report, 1973].

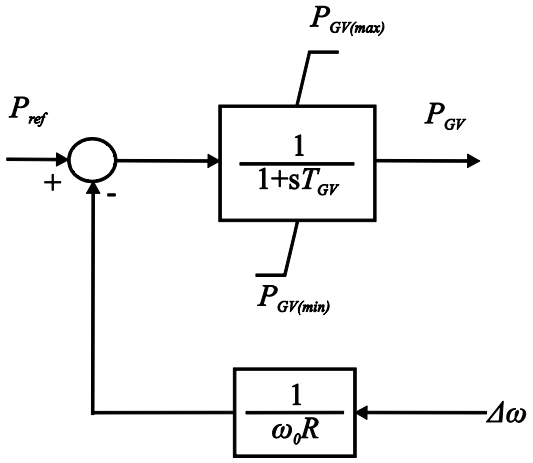

Figure 2.10: General models for speed governor systems.

The valve position is proportional to the changes of both the power reference, P_{ref}, and the deviation of angular speed, $\Delta\omega = \omega - \omega_0$. The power reference is fixed by the Load-Frequency Control (LFC) on the AGC secondary control. Therefore, the mathematical expression that represents the changes of the valve position takes on the following form:

$$T_{GV}\frac{dP_{GV}}{dt} = P_{ref} - \frac{1}{R}\frac{(\omega - \omega_0)}{\omega_0} - P_{GV} \tag{2.35}$$

where R is the speed droop characteristic and represents the regulation ability of the generator against the changes in the power system. This regulation is given in terms of the generated frequency and active power,

$$R = -\frac{\Delta f}{\Delta P_g}. \tag{2.36}$$

The value of P_{GV} and its derivative should be constrained by the limit on the valve position and rate limits, respectively [IEEE Committee Report, 1973], [Sauer and Pai, 1998]:

$$0 \le P_{GV} \le P_{GV(\max)} \tag{2.37}$$

$$\frac{dP_{GV}}{dt}^{\min} \le \frac{dP_{GV}}{dt} \le \frac{dP_{GV}}{dt}^{\max} . \tag{2.38}$$

The output of the governor is initially at the power reference value. This is determined by the LFC at the steady-state as follows:

$$P_{ref} = \frac{P_g^0}{P_g^{nom}} \tag{2.39}$$

where P_g^0 and P_g^{nom} are the initial and the rated active power generation, respectively.

2.5.2 Steam turbine

The steam turbine adjusts the mechanical power according to the steam flow, which is regulated by the valve position. The valve position is then the input signal to the turbine. The mathematical model that represents this relation varies according to the type of turbine employed in the generation plant: nonreheat, single reheat, double reheat.

For power system dynamic stability studies, a turbine of single reheat with multiple sections of pressure is commonly used [Kundur, 1994]. Hence, this type of turbine is adopted in the present work, and it is called tandem-compound steam turbine [IEEE Committee Report 1973].

The tandem-compound turbine is integrated by three sections: the high (HP), intermediate (IP) and low (LP) pressure turbines, respectively. All sections are mounted on the same shaft as shown in Figure 2.11a [IEEE Committee Report 1973]. Moreover, the

block diagram that corresponds to a linear approximation of this turbine is shown in Figure 2.11b [IEEE Committee Report, 1973], [Kundur, 1994].

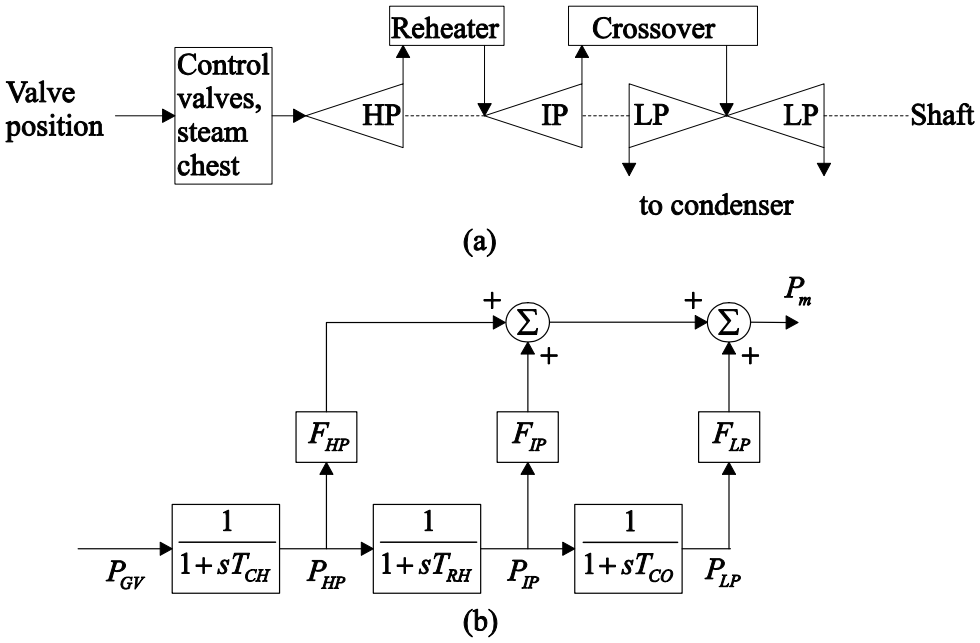

Figure 2.11: Steam turbine: (a) Tandem compound, single reheat; (b) Block diagram.

The mathematical equations that represent the steam turbine are [Rafian et al. 1988]

$$\frac{dP_{HP}}{dt} = \frac{P_{GV} - P_{HP}}{T_{CH}} \tag{2.40}$$

$$\frac{dP_{IP}}{dt} = \frac{P_{HP} - P_{IP}}{T_{RH}} \tag{2.41}$$

$$\frac{dP_{LP}}{dt} = \frac{P_{IP} - P_{LP}}{T_{CO}} \tag{2.42}$$

with a mechanical power injected to the generator given by

$$P_m = P_{HP}F_{HP} + P_{IP}F_{IP} + P_{LP}F_{LP} \tag{2.43}$$

where T_{CH}, T_{RH} and T_{CO} are the time constants which represent delays at the steam chest and inlet piping, reheaters and crossover piping, respectively. F_{HP}, F_{IP} and F_{LP} represent a portion of the total turbine power developed in the different stages [Sauer and Pai, 1998]. Furthermore, these fractions have to satisfy $F_{HP} + F_{IP} + F_{LP} = 1$.

The initial condition of each stage, P_{HP}, P_{IP} and P_{LP} is equal to the value of the output of governor P_{GV}.

2.6 Loads

In power system stability analysis, the impact of the loads in the system must be suitably characterized. However, the load demanded depends on a large number of devices that are continuously changing, which makes the accurate modelling the load composition in a power system very difficult and impractical. Therefore, a simplified load modelling is commonly used in power system studies.

In general, load modelling in a power system is split up into two categories. One is the steady-state load (also called static load) model, and the other is the dynamic load model.

In this Section, the widely used exponential and polynomial static loads are described. Additionally, the dynamic loads are presented from the viewpoint of load power restoration, which allows the introduction of the load tap changers. The characteristics and modelling of the induction motors are also discussed.

2.6.1 Static load models

A static load model represents the load at any instant of time *t* as an algebraic function of the bus voltage magnitude and frequency [Kundur, 1994]. Nonetheless, the frequency dependence of loads is not addressed in this work, which is a common practice in stability analysis [Van Cutsem and Vournas, 1998].

The voltage dependency of a load commonly used is the well-known exponential model, which has the general form

$$P_L = z_P P^0 \left(\frac{V}{V^0} \right)^{\alpha_t} \tag{2.44}$$

$$Q_L = z_Q Q^0 \left(\frac{V}{V^0} \right)^{\beta_t} \tag{2.45}$$

where z_P and z_Q are dimensionless demand variables, and P and Q are active and reactive components of the load when the bus voltage magnitude is V. The superscript *0* represents the values of the respective variable at the initial operation condition. The exponents α_t and β_t depend on the type of load (motor, heating, lighting, etc.).

When the exponents take integer values such as 2, 1, or 0, the model represents constant impedance load (often noted Z), constant current load (often noted I) or constant power load (often noted P), respectively. Thus, an alternative model which has been widely used to represent the voltage dependency of loads is the polynomial model [IEEE Task Force, 1993]. This model is commonly referred to as the ZIP model, as it is made up of three components: constant impedance, constant current and constant power. The active and reactive characteristic of this model is given by the following quadratic equations:

$$P_L = z_P P^0 \left[a_P \left(\frac{V}{V^0} \right)^2 + b_P \frac{V}{V^0} + c_P \right] \tag{2.46}$$

$$Q = z_Q Q^0 \left[a_Q \left(\frac{V}{V^0} \right)^2 + b_Q \frac{V}{V^0} + c_Q \right] \tag{2.47}$$

where the coefficients a_P, b_P, c_P, a_Q, b_Q and c_Q define the proportion of each component. These coefficients should satisfy $a_P + b_P + c_P = a_Q + b_Q + c_Q = 1$.

2.6.2 Load restoration dynamics

After a disturbance occurs in a power system, a deviation of load power is presented, which causes that various load components and control mechanisms act to restore the load power at its initial value. This process is known as load restoration and can be captured by the so-called generic models of self-restoring load [Van Cutsem and Vournas, 1998]. In this work, the multiplicative model of the generic load models are adopted. It is presented using an exponential static load model, but it can be applicable to a polynomial or any other type of static load models.

At any time the power consumed by the multiplicative generic load model is given by (2.44) and (2.45), which is called the transient load characteristic. While the steady-state load characteristic is represented by the following algebraic equations:

$$P_s = P^0 \left(\frac{V}{V^0} \right)^{\alpha_s} \tag{2.48}$$

$$Q_s = Q^0 \left(\frac{V}{V^0} \right)^{\beta_s} \tag{2.49}$$

where α_s and β_s are the steady-state load exponents. Generally, the transient load characteristic is more sensitive to voltage than the steady-state load characteristic, so that the transient load exponents α_t, β_t have larger values than the steady-state ones α_s, β_s [Van Cutsem and Vournas, 1998].

The multiplicative model leads the transient load characteristics towards the steady-state load characteristics by adjusting the value of z_P and z_Q. Thus, z_P and z_Q are considered new state variables and their value is opposite to the deviation of load; e.g., when the transient load characteristic suffers a drop, the variables z_P and z_Q will start to increase, and according to (2.44)-(2.45), both active and reactive power loads are forced towards to go to their steady-state characteristics. The behavior of the state variables z_P, z_Q is given by the following differential equations:

$$T_P \frac{dz_P}{dt} = \left(\frac{V}{V^0} \right)^{\alpha_s} - z_P \left(\frac{V}{V^0} \right)^{\alpha_t} \tag{2.50}$$

$$T_Q \frac{dz_Q}{dt} = \left(\frac{V}{V^0} \right)^{\beta_s} - z_Q \left(\frac{V}{V^0} \right)^{\beta_t} \tag{2.51}$$

where T_P and T_Q are time constants associated with the active and reactive power load, respectively.

Before any disturbance, the load power is equal to its steady-state characteristic and, therefore, the initial condition of the state variables z_P and z_Q are equal to one.

2.6.3 Load tap changer modelling

The basic function of a Load Tap Changer (LTC) is to control the voltage magnitude at a specified value, despite of variations in the input voltage by changing the transformer ratio *r*. For this reason, the LTC indirectly manipulates the process of load restoration when it restores the voltage magnitude to its reference value; the load power is also restored because in general depends on the bus voltage magnitude. Normally, the variable tap is on the high voltage side because on this side the current is lower and there are more turns, which makes commutation easier and more precise [Van Cutsem and Vournas, 1998].

To illustrate the LTC discrete model, the single-phase transformer is considered in Figure 2.12 with a constant leakage reactance and a negligible magnetizing branch.

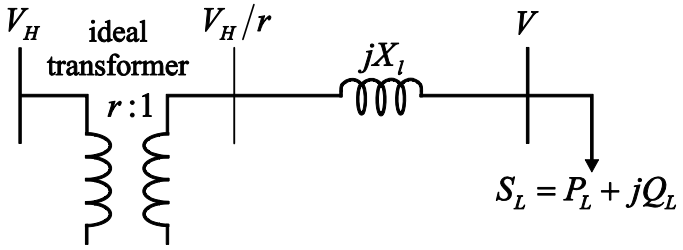

Figure 2.12: Equivalent circuit of a two-winding transformer.

The LTC raises or decreases the transformer ratio by one tap step, Δr, at discrete time instants. This process is shown in Figure 2.13.

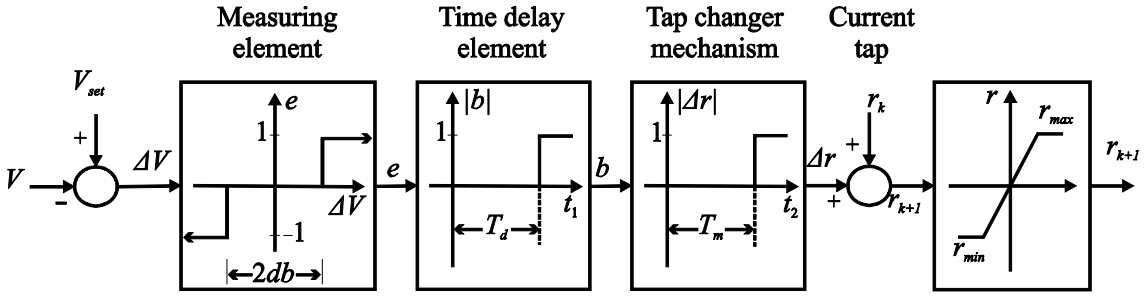

Figure 2.13: Block diagram of process operation for LTC.

The deviation of voltage magnitude ΔV is monitored by a measuring element. It produces an error signal based on the following rules:

$$e = \begin{cases} 0 & \text{if} \quad -db \le \Delta V \le +db \\ +1 & \text{if} \quad \Delta V > db \\ -1 & \text{if} \quad \Delta V < -db \end{cases} \tag{2.52}$$

where *db* represents the deadband. The LTC does not act with typical values for North American (NA), and for European practice are 0.625% and 1-2% voltage tap steps, respectively [IEEE Task Force, 1995], [Van Cutsem and Vournas, 1998].

The voltage error is the input signal of time delay element which produces an output according to (2.53)

$$\begin{aligned} & t_1 = 0 && \text{if} \quad e = 0 \\ & t_1 = t_1 + \Delta t && \text{otherwise} \\ & T_d = T_{d0} && \text{for first tap} \\ & T_d = T_{d1} && \text{for subsequent taps} \\ & b = \begin{cases} -1 & \text{if} \quad t_1 > T_d, \; e = -1 \\ +1 & \text{if} \quad t_1 > T_d, \; e = +1 \\ 0 & \text{otherwise} \end{cases} \end{aligned} \tag{2.53}$$

where T_d is the maximum initial time delay; typical values for NA and European practice are 30-120 and 25-140 seconds, respectively.

Finally, the tap is changed by the tap changer mechanism according to the following rules:

$$\begin{aligned} &t_2 = 0 \qquad \text{if} \quad b = 0 \\ &t_2 = t_2 + h \quad \text{otherwise} \\ &r_{k+1} = \begin{cases} r_k + \Delta r & \text{if} \quad t_2 > T_m,\ b = 1 \text{ and } r_k < r^{\max} \\ r_k - \Delta r & \text{if} \quad t_2 > T_m,\ b = -1 \text{ and } r_k < r^{\min} \\ r_k & \text{otherwise} \end{cases} \end{aligned} \tag{2.54}$$

where r^{max}, r^{min} are the upper and lower tap limits, and T_m is the mechanical time necessary to perform the tap change. Typical values of the mechanical time for NA and European practice are 5-10 and 5 seconds, respectively. Besides, typical values of the lower limit are 0.85-0.90 p.u. and the upper limit at 1.10-1.15 p.u. [IEEE Task Force, 1995], [Van Cutsem and Vournas, 1998].

Once the process discussed above has finished, the admittance matrix of the transformer associated with the LTC must be updated. The admittance matrix of the transformer models adopted in this work is developed in Section 2.7.2.

2.6.4 Induction motor modelling

The induction motors are approximately 60% to 70% of the total system load [Kundur, 1994]. Therefore, one needs a model that represents the dynamic characteristics of the power consumed by the motors in the power system.

A three-phase induction motor carries alternating current in both the stator and rotor windings. The rotor windings are either internally short-circuited (called squirrel-cage rotor) or connected through a slip ring to a passive external circuit (called wound rotor). Figure 2.14 shows the winding arrangement for a 2-pole, 3-phase (v_a, v_b, v_c), symmetrical induction motor. The stator and rotor windings are identical sinusoidally distributed

winding, displaced 120°, respectively. This representation can be employed for both the squirrel-cage rotor and the wound rotor.

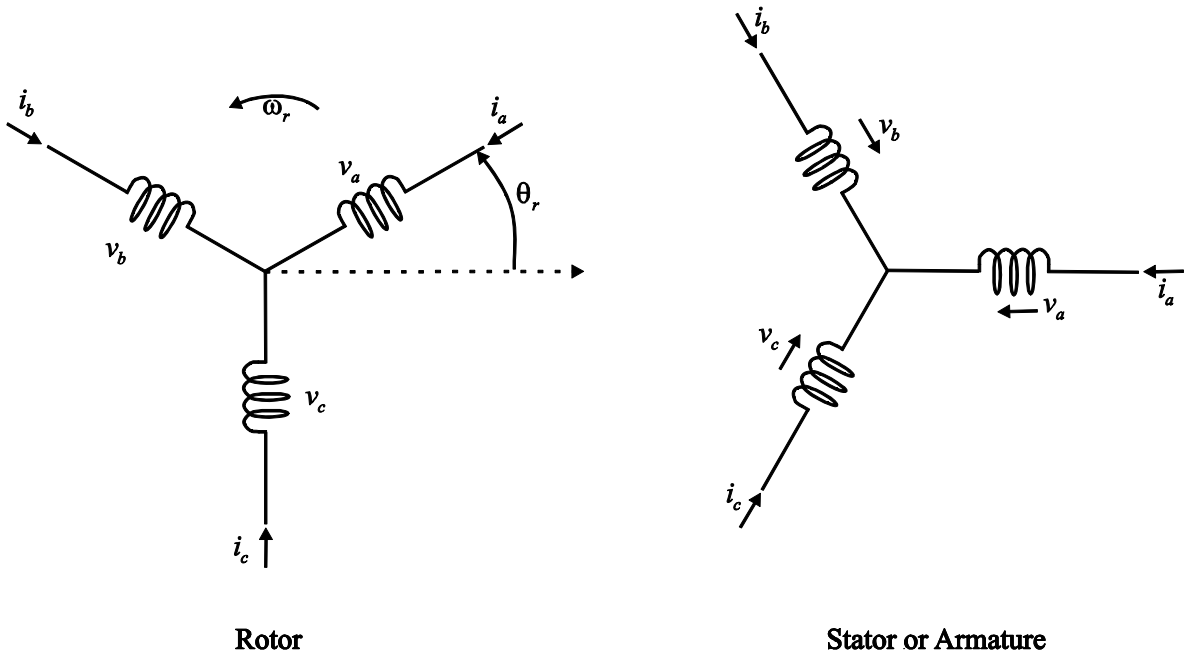

Figure 2.14: Schematic diagram of the induction machine.

The stator and rotor equations in terms of *d*, *q* variables are obtained applying the fundamental Kirchhoff's and Faraday's laws as well as the Park transformation [Krause et al., 2002], [Kundur, 1994]:

$$\begin{bmatrix} V_{ds} \\ V_{dr} \end{bmatrix} = \begin{bmatrix} R_s & 0 \\ 0 & R_r \end{bmatrix} \begin{bmatrix} I_{ds} \\ I_{dr} \end{bmatrix} - \begin{bmatrix} \frac{\omega_e}{\omega_0} & 0 \\ 0 & (1-\omega_r) \end{bmatrix} \begin{bmatrix} \psi_{qs} \\ \psi_{qr} \end{bmatrix} + \frac{1}{\omega_0} \frac{d}{dt} \begin{bmatrix} \psi_{ds} \\ \psi_{dr} \end{bmatrix} \tag{2.55}$$

$$\begin{bmatrix} V_{qs} \\ V_{qr} \end{bmatrix} = \begin{bmatrix} R_s & 0 \\ 0 & R_r \end{bmatrix} \begin{bmatrix} I_{qs} \\ I_{qr} \end{bmatrix} + \begin{bmatrix} \frac{\omega_e}{\omega_0} & 0 \\ 0 & (1-\omega_r) \end{bmatrix} \begin{bmatrix} \psi_{ds} \\ \psi_{dr} \end{bmatrix} + \frac{1}{\omega_0} \frac{d}{dt} \begin{bmatrix} \psi_{qs} \\ \psi_{qr} \end{bmatrix} \tag{2.56}$$

with the flux-current relations [Lesieutre et al., 1995],

$$\begin{bmatrix}\psi_{ds}\\ \psi_{dr}\end{bmatrix}=\begin{bmatrix}X_s+X_m & X_m\\ X_m & X_r+X_m\end{bmatrix}\begin{bmatrix}I_{ds}\\ I_{dr}\end{bmatrix} \tag{2.57}$$

$$\begin{bmatrix}\psi_{qs}\\ \psi_{qr}\end{bmatrix}=\begin{bmatrix}X_s+X_m & X_m\\ X_m & X_r+X_m\end{bmatrix}\begin{bmatrix}I_{qs}\\ I_{qr}\end{bmatrix} \tag{2.58}$$

where ω_r is the actual rotor speed, and ω_e represents the speed of a rotating reference frame. X_s and X_r are the stator and rotor leakage reactances, whereas X_m is the magnetizing reactance. R_s is the stator resistance, V_{ds} and V_{qs} are the *d* and *q* stator voltage, I_{ds} and I_{qs} are the *d* and *q* stator currents, ψ_{ds} and ψ_{qs} are the *d* and *q* stator flux linkage and similarly for the rotor circuit.

Based on the dynamics of interest in the present work, the motor model relies on the following assumptions:

- The transformer voltages are neglected $(\dot{\psi}_{ds}=\dot{\psi}_{qs}=0)$.
- The reference frame is rotating at synchronous speed, $(\omega_e=\omega_0)$.
- The rotor is assumed to be a squirrel-cage, $(V_{dr}=V_{qr}=0)$.
- Magnetic saturation is neglected.

Hence, an induction motor model of order III is obtained through some algebraic manipulations of (2.55)-(2.58), taking into account the assumptions of Appendix C

$$\frac{d}{dt}\begin{bmatrix}e'_q\\ e'_d\end{bmatrix}=\begin{bmatrix}\dfrac{M_3}{T'_0} & \dfrac{M_2+M_1(1-\omega_r)}{T'_0}\\ \dfrac{-M_2+M_1(1-\omega_r)}{T'_0} & \dfrac{M_3}{T'_0}\end{bmatrix}\begin{bmatrix}e'_q\\ e'_d\end{bmatrix}+\begin{bmatrix}\dfrac{-M_2}{T'_0} & \dfrac{M_4}{T'_0}\\ \dfrac{M_4}{T'_0} & \dfrac{M_2}{T'_0}\end{bmatrix}\begin{bmatrix}V\cos(\theta)\\ V\sin(\theta)\end{bmatrix} \tag{2.59}$$

$$\frac{d\omega_r}{dt}=\frac{1}{2H_m}(T_e-T_m) \tag{2.60}$$

with

$$T_e = -M_5 e'_d V \cos\theta + M_6 e'_d V \sin\theta - M_6 e'_q V \cos(\theta) - M_5 e'_q V \sin\theta + M_5 \left[(e'_d)^2 + (e'_q)^2 \right] \tag{2.61}$$

$$T_m = T_0 + T_1 \omega_r + T_2 \omega_r^2 \tag{2.62}$$

$$P_{Lm} = M_5 e'_d V \cos\theta + M_6 e'_d V \sin\theta - M_6 e'_q V \cos\theta + M_5 e'_q V \sin\theta - M_5 V^2 \tag{2.63}$$

$$Q_{Lm} = -M_6 e'_d V \cos\theta + M_6 e'_d V \sin\theta - M_5 e'_q V \cos\theta - M_6 e'_q V \sin\theta + M_6 V^2 \tag{2.64}$$

where M_j are constants associated to the motor reactances, and T'_0 is the transient open-circuit time constants; V and θ are the magnitude and phase terminal voltage; e'_q and e'_d are the e.m.f. behind transient reactance; H_m is the moment of inertia, T_e and T_m are the electromagnetic and the mechanical load torque, respectively; T_0, T_1 and T_2 are constants whose values are calculated as discussed in the next Section; P_{Lm} and Q_{Lm} represent the active and reactive power consumed by the induction motor. Lastly, the rotor angular speed, ω_r, is in p.u. of the base value of ω_0.

2.6.4.1 Initial condition for the induction motor

The initial condition of the state variables for the induction motor model is similar to that of a synchronous machine described in Section 2.3.1. Once the power flow study is carried out, the initial condition is then computed by solving the steady-state induction motor model, as detailed hereafter.

The induction motor can be represented by the well-known steady-state equivalent circuit of Figure 2.15 [Van Cutsem and Vournas, 1998], [Ruiz-Vega et al., 2002], [Ruiz et al., 1999].

The motor slip is defined as

$$s = 1 - \omega_r \tag{2.65}$$

where ω_r is given in per unit.

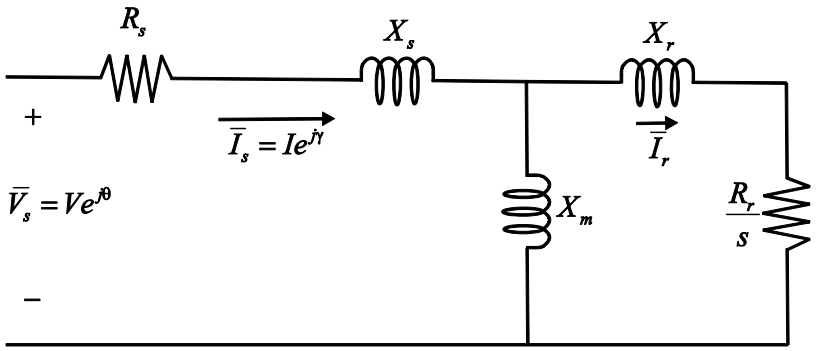

Figure 2.15: Equivalent circuit for steady-state operation of induction motor.

The equivalent impedance $Z_e = R_e + jX_e$ added to the stator impedance depends on *s* and is given by

$$Z_e = R_e + jX_e = \frac{jX_m\left(\frac{R_r}{s} + jX_r\right)}{\frac{R_r}{s} + j\left(X_m + X_r\right)}, \tag{2.66}$$

and the stator current can be obtained as

$$\bar{I}_0 = \frac{\bar{V}_0}{\left(R_s + R_e\right) + j\left(X_s + X_e\right)}. \tag{2.67}$$

Using (2.67) and Figure 2.15, the active and reactive power absorbed by the induction motor at the steady-state are given by

$$P_{Lm} = \frac{\left(R_s + R_e\right)\left(V^0\right)^2}{\left(R_s + R_e\right)^2 + \left(X_s + X_e\right)^2} \tag{2.68}$$

$$Q_{Lm} = \frac{\left(X_s + X_e\right)\left(V^0\right)^2}{\left(R_s + R_e\right)^2 + \left(X_s + X_e\right)^2}. \tag{2.69}$$

As the active power at steady-state is considered independent of voltage variations, (2.68) can be rewritten by the following quadratic expressions [Ruiz-Vega et al., 2002]:

$$A\left(\frac{R_r}{s}\right)^2 + B\left(\frac{R_r}{s}\right) + C = 0 \tag{2.70}$$

with

$$A = P_{Lm}\left(R_s^2 + X_{ss}^2\right) - \left(V^0\right)^2 R_s \tag{2.71}$$

$$B = 2P_{Lm}\left(R_s K_X + R_s X_{ss} X_{rr}\right) - \left(V^0\right)^2 \left(K_X + X_{ss} X_{rr}\right) \tag{2.72}$$

$$C = P_{Lm}\left(K_X^2 + R_s^2 X_{rr}^2\right) - \left(V^0\right)^2 R_s X_{rr}^2 \tag{2.73}$$

$$K_X = X_m^2 - X_{ss} X_{rr} \tag{2.74}$$

$$K_{ss} = X_s + X_m \tag{2.75}$$

$$K_{rr} = X_r + X_m \tag{2.76}$$

$$P_{Lm} = f_p \times P_L^0 \tag{2.77}$$

where f_p is a constant that defines the portion of the total active load power (P_L^0) consumed by the induction motor.

The initialization process is then normally carried out as follows:

- Equation (2.70) is solved, and two values of R_r/s are obtained. The larger value (represented by X_{root}) is selected because it is in the stable region of the active power-slip curve of the motor [Ruiz-Vega et al., 2002].

- The initial value of the motor slip is given by

$$s = \frac{R_r}{X_{root}}. \tag{2.78}$$

- The rotor speed is computed from (2.65)

$$\omega_r = 1 - s. \tag{2.79}$$

- The actual induction motor reactive power Q_{Lm} is given by (2.69). However, a difference between Q_{Lm} and the initial reactive power (a portion of the total reactive load Q_L at bus) is presented. Hence, a compensation Q_c must be placed at the bus where the motor is connected, which is given by

$$Q_c = Q_{Lm} - f_Q \times Q_L \tag{2.80}$$

where f_Q is a constant that represents the portion of the total reactive load power Q_L^0 consumed by the induction motor.

- Since the derivatives are zero, the state variables are given by

$$\begin{bmatrix} e'_q \\ e'_d \end{bmatrix} = -\begin{bmatrix} \frac{M_3}{T'_0} & \frac{M_2 + M_1(1-\omega_r)}{T'_0} \\ \frac{-M_2 + M_1(1-\omega_r)}{T'_0} & \frac{M_3}{T'_0} \end{bmatrix}^{-1} \begin{bmatrix} \frac{-M_2}{T'_0} & \frac{M_4}{T'_0} \\ \frac{M_4}{T'_0} & \frac{M_2}{T'_0} \end{bmatrix} \begin{bmatrix} V\cos(\theta) \\ V\sin(\theta) \end{bmatrix}. \tag{2.81}$$

- The electromagnetic torque is computed by (2.61).
- The initial mechanical load torque is equal to T_e in steady-state, while the constant associated with (2.62) is computed by

$$T_0 = \frac{T_e}{1 + C_{T1}\omega_r + C_{T2}\omega_r^2} \tag{2.82}$$

where C_{T1} and C_{T2} are the linear and quadratic mechanical torque coefficients, respectively. The value of these coefficients are given by the characteristic of the induction motor

$$C_{T1} = \frac{T_1}{T_0} \quad \text{and} \quad C_{T2} = \frac{T_2}{T_0}. \tag{2.83}$$

Therefore the constants T_1 and T_2 are obtained from (2.83)

$$T_1 = T_0 C_{T1} \quad \text{and} \quad T_2 = T_0 C_{T2}. \tag{2.84}$$

2.7 Network modelling

The network response is commonly considered instantaneous in power system stability analysis [Van Cutsem y Vournas 1998]. Thus, the network model can be represented by a set of algebraic equations that describes the power flow balance at all buses of the system at any time. Hence, the network model is given by the following constrains [Acha et al., 2004]:

$$\Delta P_i = P_{g\,i}^{sys} - P_{inj\,i} - P_{L\,i} = 0 \qquad i = 1, \cdots, n \tag{2.85}$$

$$\Delta Q_i = Q_{g\,i}^{sys} - Q_{inj\,i} - Q_{L\,i} = 0 \qquad i = 1, \cdots, n \tag{2.86}$$

with

$$P_{g\,i}^{sys} = \frac{S_{gen}}{S_{sys}} P_{g\,i} \tag{2.87}$$

$$Q_{g\,i}^{sys} = \frac{S_{gen}}{S_{sys}} Q_{g\,i} \tag{2.88}$$

where n is the number of buses in the system. $P_{g\,i}$ and $Q_{g\,i}$ are the active and reactive electric output power of the generator (see Section 2.3), respectively. S_{sys} and S_{gen} are the system and generator nominal power, respectively. $P_{L\,i}$ and $Q_{L\,i}$ are the active and reactive

power demanded by the load (see Section 2.6), respectively. $P_{inj\,i}$ and $Q_{inj\,i}$ are the active and reactive power flows injected at the *i-th* bus through the transmission elements and are computed from [Acha et al., 2004]:

$$P_{inj} = V_i^2 G_{ii} + V_i \sum_{j=1}^{n} V_j \left(G_{ij} \cos\left(\theta_i - \theta_j\right) + B_{ij} \sin\left(\theta_i - \theta_j\right)\right) \tag{2.89}$$

$$Q_{inj} = -V_i^2 B_{ii} + V_i \sum_{j=1}^{n} V_j \left(G_{ij} \sin\left(\theta_i - \theta_j\right) - B_{ij} \cos\left(\theta_i - \theta_j\right)\right) \tag{2.90}$$

where G_{ij} and B_{ij} are the equivalent conductance and susceptance of the transmission element (lines, transformer, etc.) connected between nodes *i* and *j*, respectively. Their values for several transmission elements are given in the following Sections.

2.7.1 Transmission line

The transmission line is represented by a pi-equivalent circuit with a series $\overline{y}_{ij}$ and a shunt $\overline{y}_{ij}^{sh}$ admittance, as shown in Figure 2.16. This transmission line representation is symmetric: $\overline{y}_{ij} = \overline{y}_{ji}$ and $\overline{y}_{ij}^{sh} = \overline{y}_{ji}^{sh}$.

By applying Kirchhoff's current law at buses *i* and *j*, the injected complex currents at buses may be expressed as follows:

$$\overline{I}_i = \overline{y}_{ij} \left(\overline{V}_i - \overline{V}_j \right) + \overline{y}_i^{sh} \overline{V}_i \tag{2.91}$$

$$\overline{I}_j = \overline{y}_{ji} \left(\overline{V}_j - \overline{V}_i \right) + \overline{y}_j^{sh} \overline{V}_j \,. \tag{2.92}$$

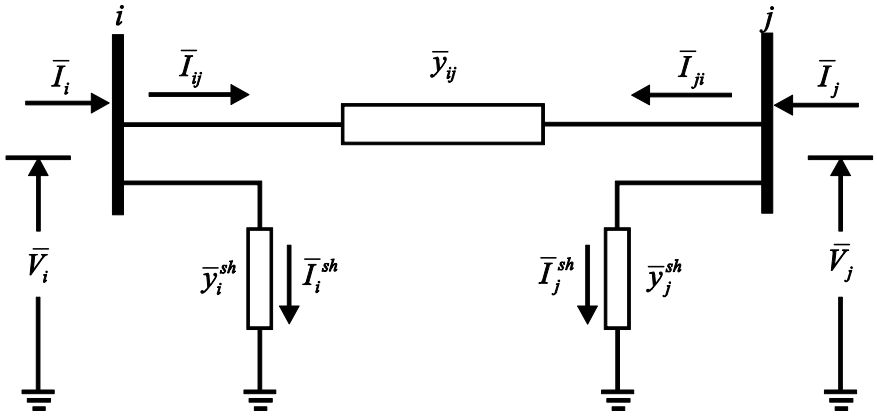

Figure 2.16: Pi-equivalent of transmission line.

The above equations can be written in a matrix form as

$$\begin{bmatrix} \bar{I}_i \\ \bar{I}_j \end{bmatrix} = \begin{bmatrix} \bar{y}_{ij} + \bar{y}_i^{sh} & -\bar{y}_{ij} \\ -\bar{y}_{ji} & \bar{y}_{ji} + \bar{y}_j^{sh} \end{bmatrix} \begin{bmatrix} \bar{V}_i \\ \bar{V}_j \end{bmatrix} \tag{2.93}$$

or simply

$$\begin{bmatrix} \bar{I}_i \\ \bar{I}_j \end{bmatrix} = \begin{bmatrix} \bar{Y}_{ii} & \bar{Y}_{ij} \\ \bar{Y}_{ji} & \bar{Y}_{jj} \end{bmatrix} \begin{bmatrix} \bar{V}_i \\ \bar{V}_j \end{bmatrix} \tag{2.94}$$

where

$$\bar{Y}_{ii} = \bar{y}_{ij} + \bar{y}_i^{sh} = G_{ii} + jB_{ii} \tag{2.95}$$

$$\bar{Y}_{ij} = -\bar{y}_{ij} = G_{ij} + jB_{ij} \tag{2.96}$$

$$\bar{Y}_{ji} = -\bar{y}_{ji} = G_{ji} + jB_{ji} \tag{2.97}$$

$$\bar{Y}_{ji} = \bar{y}_{ji} + \bar{y}_j^{sh} = G_{jj} + jB_{jj}\,. \tag{2.98}$$

2.7.2 Transformer

The conventional transformer (implemented in this work) was modelled with complex taps on both primary and secondary windings. Its magnetizing branch is also considered in the

model to account for the core losses. The schematic equivalent circuit of the transformer model is shown in Figure 2.17 [Fuerte-Esquivel, 1997].

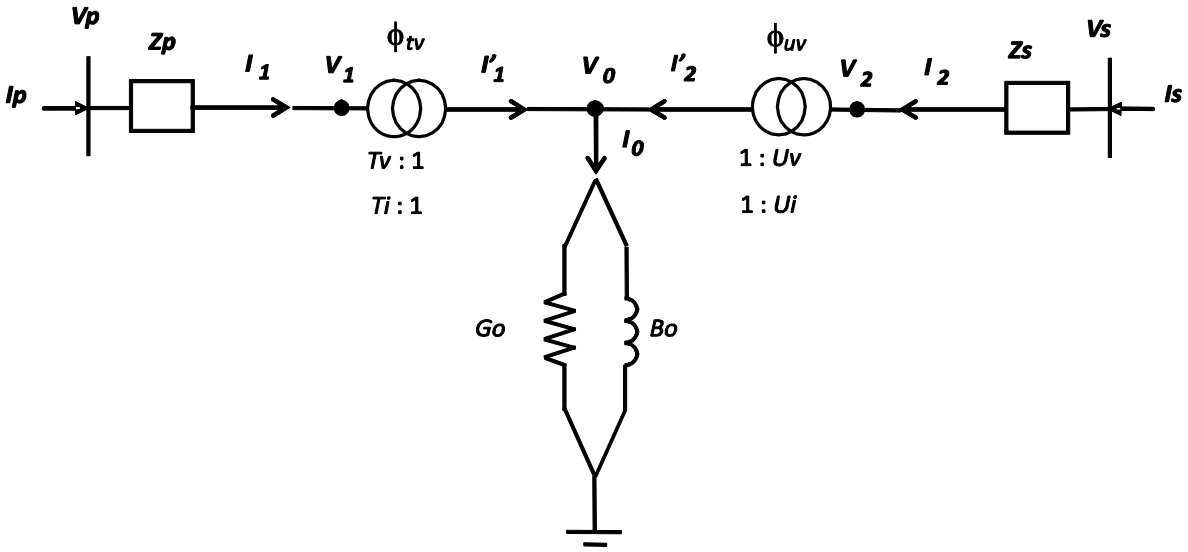

Figure 2.17: Equivalent circuit of a two-winding transformer.

The primary winding is represented as an ideal transformer having complex tap ratios $T_v:1$ and $T_i:1$ in series with the impedance Z_p where $T_v = T_i^* = T_v \angle \phi_{tv}$. The * denotes the conjugate operation. The secondary winding is also represented as an ideal transformer having complex tap ratios $U_v:1$ and $U_i:1$ in series with the impedance Z_s where $U_v = U_i^* = U_v \angle \phi_{tv}$.

The transfer admittance matrix relating the primary voltage V_p and current I_p to the secondary voltage V_s and current I_s in the two-winding transformer is determined by considering the current I_1 across the impedances Z_p and the current I_2 across the impedance Z_s [Fuerte-Esquivel, 1997]

$$\begin{bmatrix} I_p \\ I_s \end{bmatrix} = \frac{1}{T_v^2 Z_s + U_v^2 Z_p + Z_p Z_s Y_0} \begin{bmatrix} U_v^2 + Z_s Y_0 & -T_v U_v^* \\ -T_v^* U_v & T_v^2 + Z_p Y_0 \end{bmatrix} \begin{bmatrix} V_p \\ V_s \end{bmatrix}. \qquad (2.99)$$

where

$$Y_0 = G_0 + jB_0 \tag{2.100}$$

Equation (2.99) can be expressed as

$$\begin{bmatrix} I_p \\ I_s \end{bmatrix} = \left[\begin{bmatrix} G_{pp} & G_{ps} \\ G_{sp} & G_{ss} \end{bmatrix} + j \begin{bmatrix} B_{pp} & B_{ps} \\ B_{sp} & B_{ss} \end{bmatrix} \right] \begin{bmatrix} V_p \\ V_s \end{bmatrix} \tag{2.101}$$

where

$$G_{pp} = \frac{F1(U_v^2 + R1) + F2R2}{A2} \tag{2.102}$$

$$B_{pp} = \frac{F1R2 - F2(U_v^2 + R1)}{A2} \tag{2.103}$$

$$G_{ss} = \frac{F1(T_v^2 + R3) + F2R4}{A2} \tag{2.104}$$

$$B_{ss} = \frac{F1R4 - F2(T_v^2 + R3)}{A2} \tag{2.105}$$

$$G_{ps} = \frac{-T_v U_v \left(F1\cos(\phi 1) + F2\sin(\phi 1) \right)}{A2} \tag{2.106}$$

$$B_{ps} = \frac{T_v U_v \left(F2\cos(\phi 1) - F1\sin(\phi 1) \right)}{A2} \tag{2.107}$$

$$G_{sp} = \frac{-T_v U_v \left(F1\cos(\phi 2) + F2\sin(\phi 2) \right)}{A2} \tag{2.108}$$

$$B_{sp} = \frac{T_v U_v \left(F2\cos(\phi 2) - F1\sin(\phi 2) \right)}{A2} \tag{2.109}$$

$$F1 = T_v^2 R_s + U_v^2 R_p + R_{eq1} \tag{2.110}$$

$$F2 = T_v^2 X_s + U_v^2 X_p + X_{eq1} \tag{2.111}$$

$$A2 = F1^2 + F2^2 \tag{2.112}$$

$$R_{eq1} = \left(R_p R_s - X_p X_s \right) G_o - \left(R_p X_s + R_s X_p \right) B_o \tag{2.113}$$

$$X_{eq1} = \left(R_p R_s - X_p X_s\right) B_o + \left(R_p X_s + R_s X_p\right) G_o \tag{2.114}$$

$$R1 = R_s G_o - X_s B_o \tag{2.115}$$

$$R2 = R_s B_o + X_s G_o \tag{2.116}$$

$$R3 = R_p G_o - X_p B_o \tag{2.117}$$

$$R4 = R_p B_o + X_p G_o \tag{2.118}$$

$$\phi 1 = \phi_{tv} - \phi_{uv} \tag{2.119}$$

$$\phi 2 = \phi_{uv} - \phi_{tv}. \tag{2.120}$$

By changing the subscript (p=i and s=j), the active and reactive power injection equations of a two-winding transformer are equal to (2.89) and (2.90), respectively.

2.7.3 Bus types

The active and reactive power balance at each bus is given by (2.85)-(2.86), where both the generated and consumed power are computed according to the power system models presented in the previous Section, while the power flow injected at each bus only depends on the network variables (V_i, θ_i). Therefore, the power balance equations are consistent, and a unique solution can be found. Nevertheless, a bus classification is implemented according to the element embedded at bus and the reference frame used to perform the simulation.

- Load bus: no generator is connected to the bus, hence the active and reactive powers injected at bus are zero $\left(P_{g\,i} = Q_{g\,i} = 0\right)$. Furthermore, the active and reactive power drawn by the load $P_{L\,i}$ and $Q_{L\,i}$ are known as explained in Section 2.6.
- Generator bus: a generator is connected to the bus, and the active $P_{g\,i}$ and reactive $Q_{g\,i}$ power are computed with the generator model detailed in Section 2.3. Moreover, if there is a load embedded at the bus, the active and reactive power

demanded are computed as explained in Section 2.6; otherwise they are zero $\left(P_{L\,i} = Q_{L\,i} = 0\right)$.

- Infinite bus: one can represent a remote system by setting V_i and θ_i in a specified value. There is only one infinite bus in the power system, and it is not considered in the network's solution. Therefore, the number of network equations is 2(n-1) if there is an infinite bus.
- Fault bus: if a short-circuit or fault disturbance is applied at bus, the magnitude and angle voltage are then set to zero $\left(V_i = \theta_i = 0\right)$. Furthermore, this bus is considered an infinite bus during the time of perturbation because the nodal voltage is known.

2.8 Full-time scale reference frame

In a power system composed of m synchronous machines, it is convenient for analysis purposes referring the rotor position θ_r of each machine (see Figure 2.1) to a common frame of reference. Normally, the synchronous speed is used as a frame of reference, and the rotor position is expressed as [Van Cutsem and Vournas, 1998]

$$\theta_{ri} = \omega_0 t + \theta_{ri}^0 \tag{2.121}$$

where $i = 1, 2, \cdots, m$ and θ_{ri}^0 is the value of θ_{ri} at $t = 0$.

The rotor angle δ of each machine is then defined as the electrical angle between the machine quadrature axis and a synchronous rotating reference (see Figure 2.18) [Van Cutsem and Vournas, 1998]:

$$\delta_i = \theta_{ri} - \left(\omega_0 t + C\right). \tag{2.122}$$

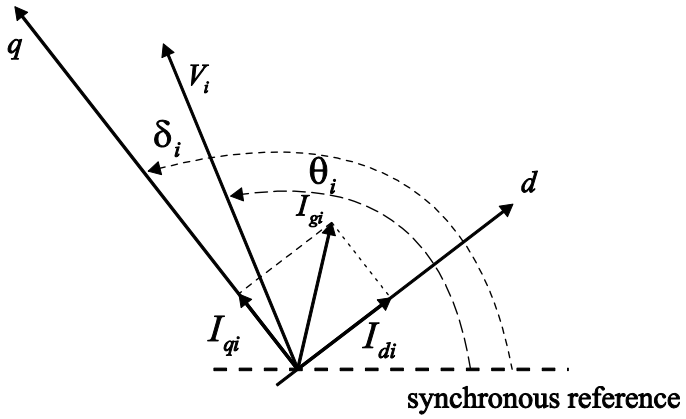

Figure 2.18: Phasor diagram of the stator variables of the *i*-th machine.

Since C is an arbitrary constant, the time derivative of rotor angle is given by (2.9), which is reproduced here:

$$\frac{d\delta_i}{dt} = \omega_i - \omega_0 \,. \tag{2.123}$$

FTS simulation (with the synchronous reference frame) is carried out for a disturbance that affects the power balance in the system. After a period of time, the system settles at a new equilibrium point (assuming a short-term and long-term stability) with the phase angles referring at a new angular frequency. Therefore, the δ_i variable linearly increases with time although the new equilibrium point is stable. This nonlinear behavior consumes unnecessary computational effort [Fabozzi and Van Cutsem, 2011].

The above difficulty can be solved by a change of the rotating reference frame. In transient stability analysis the Center-of-Inertia (COI) reference frame is commonly used [Sauer and Pai, 1998]. The COI angle and its time derivative are defined, respectively, as

$$\theta_{COI} = \frac{1}{M_T}\sum_{i=1}^{m} M_i\theta_i + K \tag{2.124}$$

$$\omega_{COI} = \frac{1}{M_T}\sum_{i=1}^{m} M_i\omega_i \tag{2.125}$$

where M_T is the total inertia, $M_i = 2H_i/\omega_0$ and K is an arbitrary constant. The rotor angle and its time derivative of the i-th generator are then given by [Fabozzi and Van Cutsem, 2011]:

$$\delta_i = \theta_i - \theta_{COI} \tag{2.126}$$

$$\frac{d\delta_i}{dt} = \omega_i - \omega_{COI} \,. \tag{2.127}$$

Therefore, (2.9) is replaced by (2.127) at the ω_{COI} rotating frame. Thus, (2.125) is added to the set of algebraic equations (2.2).

2.9 Full-time scale solution

Full-time scale dynamic studies consist of solving the DAE's mathematical model described by (2.1)-(2.3) during an interval of time $t \in [t_0, t_{end}]$. This can be achieved using either a Simultaneous Implicit (SI) or a Partitioned Explicit (PE) method [Van Cutsem and Vournas, 1998].

The SI method can handle stiff equations with no numerical problems and is more stable than the PE method [Sauer and Pai, 1998]. The SI method is widely used on commercial programs, where the DAE's system is solved in a unified frame work. In order to achieve this, the differential set (2.1) is transformed (algebraized) into a set of difference equations by using either the implicit Backward Euler (BE) method or the implicit Trapezoidal Rule (TR). The resulting equations are then added to the set of network algebraic equations (2.2), and both nonlinear algebraic sets are solved in a unified reference frame by using the Newton's method.

The SI method is used in the present work for the above-mentioned advantages. While both the BE and TR integration methods are adopted to solve the FTS model considering the structure preserving model of the power system, as explained in the following Sections.

2.9.1 Discretization of the differential equations

Numerical integration consists of discretizing the differential equation (2.1) by the following algebraized relationship [Van Cutsem and Vournas, 1998]:

$$x^{k+1} = x^k + h\left(\beta_0 f^{k+1} + \beta_1 f^k\right) \tag{2.128}$$

where β_i is a constant whose value depends on the integration method (see Table 2.1), and h is the integration time step ($h = t^{k+1} - t^k$). The superscript k is an index for the time instant t_k at which variables and functions are evaluated: $x^k = x\left(t_k\right)$ and $f^k = f\left(x^k, y^k\right)$. The dynamic state variables compose the vector x, while the vector y is composed of algebraic variables.

Equation (2.128) can be rewritten as

$$x^{k+1} - x^k - h\left(\beta_0 f^{k+1} + \beta_1 f^k\right) = 0\,. \tag{2.129}$$

Table 2.1: Fixed-step integration methods

Integration method	Formula
Backward Euler	$x^{k+1} = x^k + h\, f^{k+1} \quad \beta_0 = 1, \beta_1 = 0$
Trapezoidal Rule	$x^{k+1} = x^k + \frac{h}{2}\left(f^{k+1} + f^k\right) \quad \beta_0 = \beta_1 = 0.5$

2.9.2 Application of Newton-Raphson method to the FTS model

The set of algebraized equations (2.129) is added to the set of network algebraic equations (2.2). Thus, the set of DAEs are expressed as a set of algebraic-difference equations

$$F_1(\cdot) = x^{k+1} - x^k - h\left(\beta_0 f^{k+1} + \beta_1 f^k\right) = 0 \tag{2.130}$$

$$F_2\left(\cdot\right) = g^{k+1} = 0\,. \tag{2.131}$$

Both nonlinear algebraic sets (2.130) and (2.131) can be solved in a unified reference frame by using Newton's method to linearize with respect to x^{k+1} and y^{k+1} such that at the *i*-th iteration the following linear system is solved:

$$\underbrace{\begin{bmatrix} I - h\beta_0 f_x^{k+1} & -h\beta_0 f_y^{k+1} \\ g_x^{k+1} & g_y^{k+1} \end{bmatrix}^i}_{J} \begin{bmatrix} \Delta x^k \\ \Delta y^k \end{bmatrix}^i = -\begin{bmatrix} F_1(\cdot) \\ F_2(\cdot) \end{bmatrix}^i \tag{2.132}$$

where *J* is called the Jacobian matrix, and its submatrices are the partial derivative of $F_i,\ i=1,2$, with respect to x^{k+1} and y^{k+1}

$$\begin{aligned} f_x^{k+1} &= \frac{\partial f^{k+1}}{\partial x^{k+1}} \qquad f_y^{k+1} = \frac{\partial f^{k+1}}{\partial y^{k+1}} \\ g_x^{k+1} &= \frac{\partial F_2}{\partial x^{k+1}} \qquad g_y^{k+1} = \frac{\partial F_2}{\partial y^{k+1}} \end{aligned} . \tag{2.133}$$

For given values $\begin{bmatrix} x^k & y^k \end{bmatrix}^T$, the method starts from an initial guess $\begin{bmatrix} x_0^{k+1} = x^k & y_0^{k+1} = y^k \end{bmatrix}^T$ and updates the solution at each iteration *i* by (2.134), until a convergence criterion is satisfied. The process is repeated until $t^{k+1} \geq t_{end}$

$$\begin{bmatrix} x^{k+1} \\ y^{k+1} \end{bmatrix}^i = \begin{bmatrix} x^k \\ y^k \end{bmatrix}^i + \begin{bmatrix} \Delta x^k \\ \Delta y^k \end{bmatrix}^i . \tag{2.134}$$

For a power system composed by *n* buses (without infinite bus), *m* synchronous machines, *e* exciters, *f* feedback components, *ps* power system stabilizer, *o* OvereXcitation limiters, *r* governor-turbines, *d* load restoration dynamics and *a* induction motors, the FTS model at the synchronous rotating frame then has the following vectors of algebraic and state variables:

$$y = \begin{bmatrix} \left[\theta_1 \cdots \theta_n\right]^T \\ \left[V_1 \cdots V_n\right]^T \end{bmatrix} \tag{2.135}$$

$$x = \begin{bmatrix} \left[E'_{q1}, \psi_{1d1}, E'_{d1}, \psi_{2q1}, \delta_1, \omega_1 \ \cdots \ E'_{qm}, \psi_{1dm}, E'_{dm}, \psi_{2qm}, \delta_m, \omega_m\right]^T \\ \left[E_{fd1} \ \cdots \ E_{fde}\right]^T \\ \left[D_1 \ \cdots \ D_f\right]^T \\ \left[W'_1, P'_1, V'_1, \cdots, W'_{ps}, P'_{ps}, V'_{ps}\right]^T \\ \left[x_{t1}, x_{OXL1}, \cdots, x_{to}, x_{OXLo}\right]^T \\ \left[P_{GV1}, P_{HP1}, P_{IP1}, P_{LP1}, \cdots, P_{GVr}, P_{HPr}, P_{LPr}\right]^T \\ \left[z_{P1}, z_{Q1}, \cdots, z_{Pl}, z_{Ql}\right]^T \\ \left[e'_{q1}, e'_{d1}, \omega_{r1}, \cdots, e'_{qas}, e'_{das}, \omega_{ras}\right]^T \end{bmatrix}. \tag{2.136}$$

On the other hand, the algebraic vector is increased if the ω_{COI} rotating frame is used:

$$y = \begin{bmatrix} \left[\theta_1 \cdots \theta_n\right]^T \\ \left[V_1 \cdots V_n\right]^T \\ \omega_{COI} \end{bmatrix}. \tag{2.137}$$

2.10 Conclusions

This Chapter has presented the mathematical models of the power system components to be considered in this work. All models are developed (with the minimum of variables) based on the power-flow formulation.

Differential equations of the models have been algebraically represented using the BE or TR integration method. A set of nonlinear equations for the network elements and the generating plant components (e.g. generator, AVR, AGC, etc.) have been assembled in a unified frame of reference to study the dynamic behavior of large-scale power systems at the synchronous or ω_{COI} rotating frame.

Chapter 3

QUASI STEADY-STATE APPROXIMATION

3.1 Introduction

Despite that power system stability analysis using FTS simulation accomplishes results very close to the actual behavior of the power system during short-term (several seconds) and long-term (from minutes to hours) time frame, executing a FTS simulation is impractical when the long-term is the period of interest because the detailed models of electric power system components involve a very high computational effort due to the fast dynamic phenomena existing in the short-term. Therefore, a reduced model of the power system is more desirable, since it performs the long-term dynamic simulations more efficiently from a computational effort viewpoint.

The wide range of time scales inherent to the dynamics of a power system makes using the Quasi Steady-State (QSS) approximation possible to obtain reduced order models relevant to a particular time scale with the objective of simulating those reduced models much more efficiently. Herewith, the long-term dynamic simulation can be carried out using large time steps during numerical integration to capture slow transients.

In the present Chapter, the QSS models of the fundamental elements (shown in the previous Chapter) of the power system are exposed. The dynamic state variables are split up into fast and slow variables. Thus, the differential equations associated with fast variables are replaced by their equilibrium equations, and the resulting algebraic equations are added to the network equations. The new set of differential and algebraic equations

(DAEs) is then transformed to algebraic equations (AEs) using the TR or the BE integration method. Finally, the Newton-Raphson algorithm is used to solve the algebraized sets of equations in a single frame of reference.

3.2 Quasi steady-state formulation

Opposite to the approaches where the original set of DAEs is handled throughout the whole simulation, the QSS approximation of the long-term dynamics handles a reduced and simplified set of equations. The latter is obtained by considering a time scale decomposition of the dynamic state variables into fast and slow time-varying variables, respectively and by assuming that the former set of variables changes instantaneously with respect to variations of slow-state variables, replacing the corresponding differential equations by their equilibrium conditions. The set of differential equations (2.1) can then be decomposed according to the time scales of the state dynamics. In particular, in a two-time scale system, the simplified model can be expressed as [Van Cutsem and Mailhot, 1997]

$$\dot{x}_{sd} = f_{sd}(x_{sd}, x_{fd}, y, z) \qquad f_{sd} : \Re^{n_{sd}+m+p} \rightarrow \Re^{n_{sd}} \tag{3.1}$$

$$0 = f_{fd}(x_{sd}, x_{fd}, y, z) \qquad f_{fd} : \Re^{n_{fd}+m+p} \rightarrow \Re^{n_{fd}} \tag{3.2}$$

$$0 = g(x_{sd}, x_{fd}, y, z) \qquad g : \Re^{n_{sd}+n_{fd}+m+p} \rightarrow \Re^{m} \tag{3.3}$$

$$\begin{aligned} &z(t_k^+) = h(x_{sd}, x_{fd}, y, z(t_k^-)) \qquad h : \Re^{n_{sd}+n_{fd}+m+p} \rightarrow \Re^{p} \\ &x_{sd} \in X \subset \Re^{n_{sd}} \quad x_{fd} \in X \subset \Re^{n_{fd}} \quad t \in [t_0, t_{end}] \end{aligned} \tag{3.4}$$

where x_{sd} is a n_{sd}-dimensional vector with predominantly slow dynamics and initial conditions $x_{sd}(t_0) = x_{sd}^0$, while x_{fd} is a n_{fd}-dimensional vector of states that have fast dynamics superimposed on slow varying quasi steady-state responses with initial conditions $x_{fd}(t_0) = x_{fd}^0$.

In the following Sections the mathematical FTS models presented in Chapter 2 are transformed into QSS models. Note that according to the QSS formulation only the components represented by differential equations may be transformed while those represented by algebraic equations are kept without changes. The appropriate procedure to solve the equations associated with the simplified model, (3.1)-(3.4), is also developed.

3.3 Generator QSS modelling

In practically all well-designed two-axis single synchronous machine (presented in Section 2.3), the subtransient T''_{qo}, T''_{do} and transient T'_{qo} open-circuit time constants are quite small as shown in Table 3.1 [Kundur, 1994].

Table 3.1: Typical values of synchronous machine time constants

Open-circuit time constant	Salient-point machine (Hydraulic plant)	Round-rotor machine (Thermal plant)
T'_{do}	1.5 – 9 s	3 – 10 s
T'_{qo}	– – – – –	0.5 – 2 s
T''_{do}	0.01 – 0.05 s	0.02 – 0.05 s
T''_{qo}	0.01 – 0.09 s	0.02 – 0.05 s

Since the time constants associated with the damper winding at the *d*- and *q*-axis typically are small values (see Table 3.1), their corresponding flux linkages (ψ_{1d}, ψ_{2q}) and the voltage magnitude behind transient *d*-axis reactance (E'_d) can be considered fast-state variables. The voltage E'_q is then treated as a slow state variable. Therefore, the QSS generator model can be found by splitting (2.8) as

$$\frac{dE'_q}{dt} = \frac{K_1 E'_q + K_2 \psi_{1d} + K_3 V \cos(\delta - \theta) + E_{fd}}{T'_{do}} \tag{3.5}$$

$$\begin{bmatrix} 0 \\ 0 \\ 0 \end{bmatrix} = \begin{bmatrix} K_4 & K_5 & 0 & 0 \\ 0 & 0 & K_7 & K_8 \\ 0 & 0 & K_{10} & K_{11} \end{bmatrix} \begin{bmatrix} E'_q \\ \psi_{1d} \\ E'_d \\ \psi_{2q} \end{bmatrix} + \begin{bmatrix} K_6 & 0 \\ 0 & K_9 \\ 0 & K_{12} \end{bmatrix} \begin{bmatrix} V\cos(\delta-\theta) \\ V\sin(\delta-\theta) \end{bmatrix}. \tag{3.6}$$

Since the electromechanical oscillation is slower than the electrical dynamics, the rotor angle and the rotor speed can be assumed to be slow-state variables. Hence, the swing equation is

$$\frac{d\delta}{dt} = \omega - \omega_0 \tag{3.7}$$

$$\frac{d\omega}{dt} = \frac{\omega_0}{2H}\left(P_m - P_g - D(\omega-\omega_0)\right) \tag{3.8}$$

where the active and reactive power generated by the synchronous machine are only expressed in terms of the fast- and slow-state variables:

$$\begin{aligned} P_g = {} & K_{13}E'_dV\cos(\delta-\theta) + K_{14}\psi_{2q}V\cos(\delta-\theta) + K_{15}E'_qV\sin(\delta-\theta) \\ & + K_{16}\psi_{1d}V\sin(\delta-\theta) + K_{17}V^2\sin(2(\delta-\theta)) \end{aligned} \tag{3.9}$$

$$\begin{aligned} Q_g = {} & -K_{13}E'_dV\sin(\delta-\theta) - K_{14}\psi_{2q}V\sin(\delta-\theta) + K_{15}E'_qV\cos(\delta-\theta) \\ & + K_{16}\psi_{1d}V\cos(\delta-\theta) - V^2\left(K_{18}\cos(\delta-\theta)^2 + K_{19}\sin(\delta-\theta)^2\right). \end{aligned} \tag{3.10}$$

Finally, the initial condition of all state variables (E'_q, E'_d, ψ_{1d}, ψ_{2q}, δ, ω) and the fixed input (E_{fd}, P_m) are computed as detailed in Section 2.3.1.

3.4 Automatic voltage regulator QSS modelling

As mentioned in Section 2.4, the AVR control loop is composed of several devices acting at two-time scale. The feedback compensation and OvereXcitation limiter are considered

slow components, because their dynamic behavior is dominant during the slow transients [Van Cutsem and Vournas, 1998], [Kundur, 1994]. On the other hand, the exciter and the PSS are viewed as fast devices [Xu et al., 1998]. Therefore, the QSS models of the slow devices are those given for the FTS model, while the QSS models of the fast devices are developed in the following Sections.

3.4.1 Exciter QSS modelling

The electric field exciter control is generally fast, with a small time constant (0.01 – 0.05 seconds) in order to respond immediately when the terminal voltage is perturbed; this small time constant is one reason to use small integration time steps in FTS simulations. The QSS exciter model can then be represented by its steady-state response as shown in Figure 3.1.

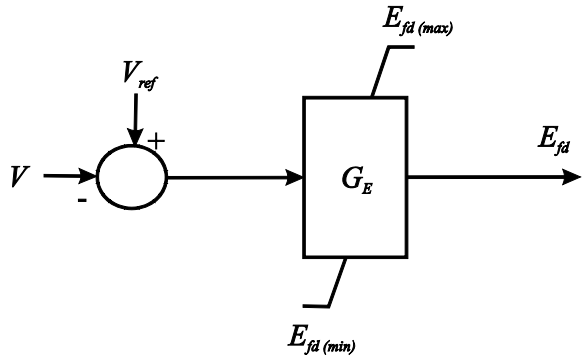

Figure 3.1: Block diagram of exciter steady-state.

From the block diagram of the model, the equilibrium equation of the exciter can be expressed as

$$0 = G_E \left(V_{ref} - V\right) - E_{fd} \qquad E_{fd\,(\min)} \le E_{fd} \le E_{fd\,(\max)} \tag{3.11}$$

where the voltage reference and the initial condition are calculated as in Section 2.4.1.

3.4.2 Power system stabilizer QSS modelling

Based on the time constants associated with the PSS, its dynamic can be split up into two-time scales. The phase-lead network has a fast response because of its small time constants T_1 and T_4, while the washout block acts slowly because its time constant is long enough $(1 \le T_w \le 20)$ to pass signals associated with oscillations at the frequency of unchanged interest [Xu et al., 1998], [Kundur, 1994].

Based on the mentioned above, the differential equations of the fast blocks can be replaced by their equilibrium equations, as shown in Figure 3.2.

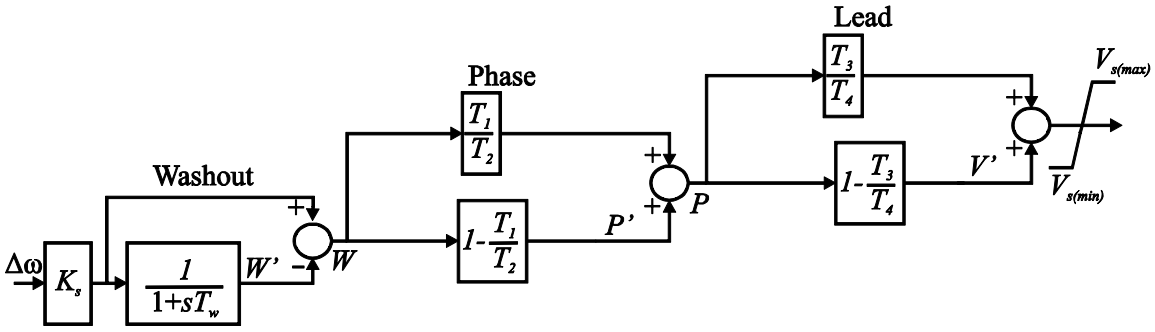

Figure 3.2: Block diagram of simplified model of PSS.

Thus, the QSS model of PSS is obtained from the block diagram as

$$T_w \frac{dW'}{dt} = K_S \Delta\omega - W' \tag{3.12}$$

$$0 = c_1 \left(K_S \Delta\omega - W' \right) - P' \tag{3.13}$$

$$0 = c_2 \left(K_S \Delta\omega - W' \right) - c_3 P' - V' \tag{3.14}$$

The compensation (V_s) of the PSS that is incorporated in the exciter is still given by (2.29), which is reproduced here:

$$V_s = c_4 \left(K_s \Delta\omega - W' \right) + c_5 P' + V' \tag{3.15}$$

where all gain c_i and the initial value of all variables are given in Section 2.4.3.

3.5 Speed governor and turbine QSS modelling

The AGC operation is more important in long-term simulations than in short-term simulations. However, some time constants of the governor and turbine may be relatively fast (see Table 3.2), and replacing the differential equations associated with these fast control elements by algebraic equations may be possible to produce a reduced order model for long-term simulations [IEEE Committee Report, 1973].

Table 3.2: Typical time constants of governor and turbine

Control device	Time constants	Typical value
Speed governor	T_{GV}	0.1 – 0.3 s
Turbine	T_{CH}	0.1 – 0.4 s
	T_{RH}	4 – 11 s
	T_{CO}	0.3 – 0.5 s

According to the typical time constants given in Table 3.2, the states associated with valve position (P_{GV}), as well as high (P_{HP}) and low (P_{LP}) pressure turbines, could be taken as relatively fast variables. The QSS model of speed governor and turbine is then obtained by transforming their differential equations into algebraic equations as follows:

$$0 = P_{ref} - \frac{1}{R}\frac{(\omega - \omega_0)}{\omega_0} - P_{GV} \qquad 0 \le P_{GV} \le P_{GV\,(\max)} \tag{3.16}$$

$$0 = P_{GV} - P_{HP} \tag{3.17}$$

$$0 = P_{IP} - P_{LP}\,. \tag{3.18}$$

The intermediate (P_{IP}) pressure turbine is considered slow state variable, and its dynamic is given by

$$\frac{dP_{IP}}{dt} = \frac{P_{HP} - P_{IP}}{T_{RH}}\,. \tag{3.19}$$

All state variables are initialized with the value of P_{set}, which is given by (2.39) in Section 2.5. Moreover, the QSS model of these controls can be represented by the block diagram shown in Figure 3.3. Note that the mechanical power injected to the generator P_m is still represented by (2.43).

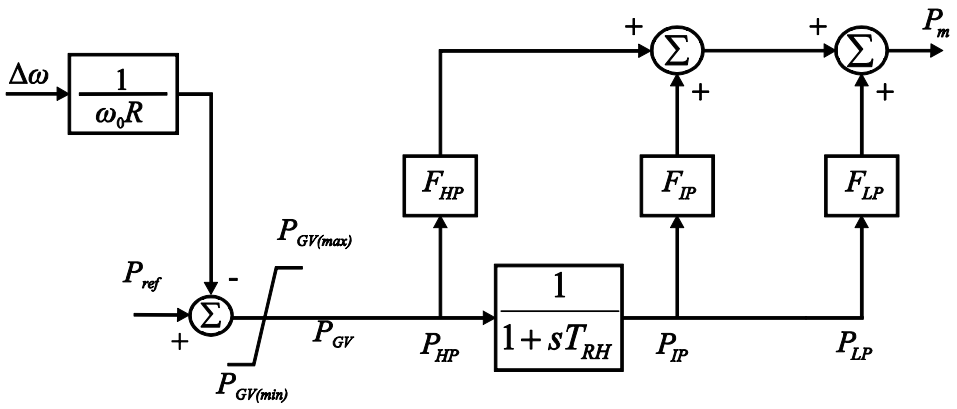

Figure 3.3: QSS model of the speed governor and steam turbine.

3.6 Load QSS modelling

The dynamic loads can be split up into two-time scales by examining the time constants associated with each differential equation. The response of a self-restoring load (see Section 2.6.2) is relatively slow due to its large active (T_P) and reactive (T_Q) time constants, such that its generic model is still given by (2.50)-(2.51), and its transient response has more effect during the long-term dynamics.

On the other hand, the induction motor rotor transients (see Section 2.6.4) are faster than the electromechanical transients associated with synchronous machines. Hence, the QSS model of the induction motor can be obtained by neglecting the rotor dynamics (T_o' is very small):

$$\begin{bmatrix} 0 \\ 0 \end{bmatrix} = \begin{bmatrix} M_3 & M_2 + M_1(1-\omega_r) \\ -M_2 + M_1(1-\omega_r) & M_3 \end{bmatrix} \begin{bmatrix} e_q' \\ e_d' \end{bmatrix} + \begin{bmatrix} -M_2 & M_4 \\ M_4 & M_2 \end{bmatrix} \begin{bmatrix} V\cos(\theta) \\ V\sin(\theta) \end{bmatrix}. \quad (3.20)$$

The rotor motion is still given by (2.60), which is repeated here for the sake of completeness:

$$\frac{d\omega_r}{dt} = \frac{1}{2H_m}\left(T_e - T_m\right) \tag{3.21}$$

where the T_e and T_m are represented by (2.61) and (2.62), respectively. The active and reactive power consumed by the QSS model of the induction motor are also given by (2.63) and (2.64), respectively. Finally, this model is initialized based on the same process described for the FTS model in Section 2.6.4.1.

3.7 QSS reference frame

A reference bus axis rotating at a synchronous speed is also adopted as a frame of reference to express the machine rotor dynamic in the QSS simulation. These equations are given by (3.22)-(3.23) so that each generator conserves its own rotating speed:

$$\frac{d\delta_i}{dt} = \omega_i - \omega_0 \tag{3.22}$$

$$\frac{d\omega_i}{dt} = \frac{\omega_0}{2H}\left(P_{mi} - P_{gi} - D_i\left(\omega_i - \omega_0\right)\right). \tag{3.23}$$

On the other hand, the limitation of the synchronous rotating reference (described in Section 2.8) is also avoided by changing to a ω_{COI} rotating reference in the QSS simulation as [Fabozzi and Van Cutsem, 2011]:

$$\frac{d\delta_i}{dt} = \omega_i - \omega_{COI} \tag{3.24}$$

$$\frac{d\omega_i}{dt} = \frac{\omega_0}{2H}\left(P_{mi} - P_{gi} - D_i\left(\omega_i - \omega_{COI}\right)\right) \tag{3.25}$$

where (3.22) is replaced by (3.24) at the ω_{COI} rotating frame. Thus, (2.125) is added to the set of algebraic equations (3.3).

Nevertheless, the QSS approximation is mainly used in long-term stability studies where the dynamics of interest consists of synchronous machine rotor oscillations with a large period of the order of 25 s [Van Cutsem et al., 2006], [Grenier et al., 2005], such that perfect coherency between all synchronous machines can be assumed for QSS simulation. Note that this assumption requires neglecting the oscillations between machines, which is valid only for long-term studies [Van Cutsem et al., 2006], [Grenier et al., 2005].

Under this assumptions and using ω_{COI} as the rotating reference, the system can be represented by the block diagram of Figure 3.4 [Van Cutsem et al., 2006], [Grenier et al., 2005)].

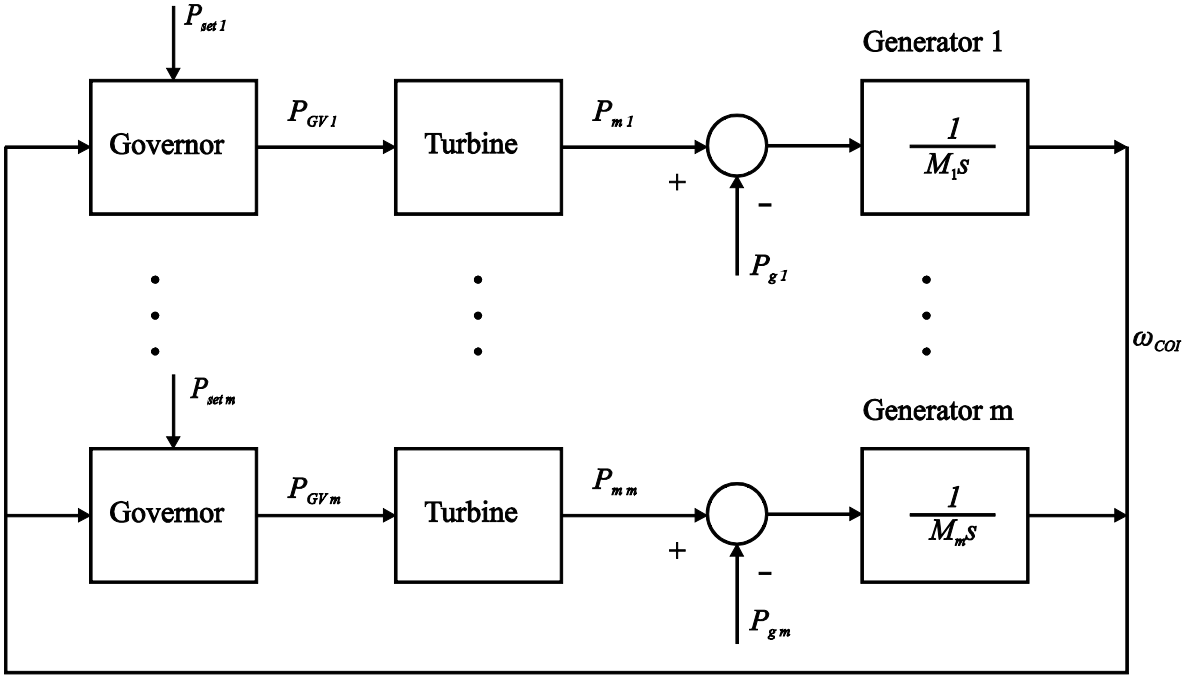

Figure 3.4: Common frequency model of the system.

Since all generators are rotating at ω_{COI}, the swing equation of the *i*-th generator takes the following form:

$$0 = \omega_i - \omega_{COI} \tag{3.26}$$

$$M_i \frac{d\omega_{COI}}{dt} = P_{mi} - P_{gi}, \quad i = 1, \cdots, m \tag{3.27}$$

where (3.27) is obtained by substituting (3.26) into (3.25). Note that the mechanical damping *D* cannot be considered under this common frequency reference frame.

A common differential equation of ω_{COI} for all generators is obtained by summing (3.27) over all them [Van Cutsem et al., 2006], [Grenier et al., 2005)]

$$\sum_{i=1}^{m} M_i \frac{d\omega_{COI}}{dt} = \sum_{i=1}^{m} P_{mi} - \sum_{i=1}^{m} P_{gi} \tag{3.28}$$

or

$$M_T \frac{\mathrm{d}\omega_{COI}}{\mathrm{dt}} = \eta \tag{3.29}$$

where $M_T = \sum_{i=1}^{m} M_i$, and η represents the total imbalance of mechanical and electrical powers given by

$$\eta = \sum_{i=1}^{m} P_{mi} - \sum_{i=1}^{m} P_{gi}\,. \tag{3.30}$$

Another limitation lies in that the rotor angle cannot be determined using (3.26) because this equation has to be removed from the generator model. In order to solve this problem, (3.27) and (3.29) are combined to obtain

$$P_{gi} = P_{mi} - \frac{M_i}{M_T}\eta \tag{3.31}$$

where P_{gi} is given by (3.9) which involves the rotor angle δ_i. Based on (3.9) the active power can be expressed as

$$K_{13}E'_d V\cos(\delta-\theta)+K_{14}\psi_{2q}V\cos(\delta-\theta)+K_{15}E'_q V\sin(\delta-\theta)$$
$$+K_{16}\psi_{1d}V\sin(\delta-\theta)+K_{17}V^2\sin(2(\delta-\theta))=P_{mi}-\frac{M_i}{M_T}\eta \quad (3.32)$$

Therefore, (3.26) is replaced by (3.32) and η is established as a new algebraic variable common to all generators; however, finding a unique solution is not possible because there are more variables than equations. This difficulty is solved by defining a new type of bus (called a reference bus), where the voltage phase angle should be kept as constant at θ_{ref}, and the common algebraic variable η takes the place of θ_{ref} [Van Cutsem et al., 2006], [Grenier et al., 2005]. Furthermore, the reference bus should have a connected generator.

Finally, another difference between the individual rotor speed and the common frequency reference frame appears when the network equations are solved. At this point, the active power P_{gi} injected by the *i*-th generator is given by (3.9) for the individual rotor speed reference frame and by (3.31) for the common frequency reference frame. The rest of the formulation presented in Section 2.7 continues without changes for both reference frames.

3.8 QSS solution

The QSS simulation consists of solving the power system reduced model represented by (3.1)-(3.4) for a specified period of time. To this purpose, the set of differential equations associated with the slow variables is algebraized by using one of the well-known integration formulas. In this work, the BE or the TR (as in FTS simulation) is used to transform (3.1) into the difference equation

$$x_{sd}^{k+1}=x_{sd}^{k}+h\left(\beta_0 f_{sd}^{k+1}+\beta_1 f_{sd}^{k}\right) \quad (3.33)$$

where constant β_i is given in Table 2.1, and its value depends on the integration formula, h is the integration time step ($h = t^{k+1} - t^k$) and the superscript k is an index for the time instant t_k at which variables and functions are evaluated: $x_{sd}^k = x_{sd}\left(t_k\right)$ and $f_{sd}^k = f_{sd}\left(x_{sd}^k, x_{fd}^k, y^k\right)$. The slow-state variables compose the vector x_{sd}, while the vectors x_{fd} and y represent the algebraic variables. The resultant set of difference equations is added to the set of algebraic equations (3.2)-(3.3), and all nonlinear algebraic equations are solved in an integrated way by using the Newton's method.

3.8.1 Application of Newton-Raphson method to the QSS model

The set of DAEs is easily rewritten as a set of algebraic-difference equations:

$$F_1(\cdot) = x_{sd}^{k+1} - x_{sd}^k - h\left(\beta_0 f_{sd}^{k+1} + \beta_1 f_{sd}^k\right) = 0 \tag{3.34}$$

$$F_2\left(\cdot\right) = f_{fd}^{k+1} = 0 \tag{3.35}$$

$$F_3\left(\cdot\right) = g^{k+1} = 0 \tag{3.36}$$

The above nonlinear algebraic equations (3.34)-(3.36) are solved by using the Newton´s method to linearize with respect to x_{sd}^{k+1}, x_{fd}^{k+1} and y^{k+1}, such that the linear system (3.37) is solved at the i-th iteration:

$$\underbrace{\begin{bmatrix} I - h\beta_0 A^{k+1} & -h\beta_0 B^{k+1} & -h\beta_0 C^{k+1} \\ D^{k+1} & E^{k+1} & F^{k+1} \\ L^{k+1} & M^{k+1} & N^{k+1} \end{bmatrix}}_{J}{}^{i} \begin{bmatrix} \Delta x_{sd}^k \\ \Delta x_{fd}^k \\ \Delta y^k \end{bmatrix}^i = -\begin{bmatrix} F_1\left(\cdot\right) \\ F_2\left(\cdot\right) \\ F_3\left(\cdot\right) \end{bmatrix}^i \tag{3.37}$$

where J is called the Jacobian matrix, and its submatrices are given by

$$A^{k+1} = \frac{\partial f_{sd}^{k+1}}{\partial x_{sd}^{k+1}} \qquad B^{k+1} = \frac{\partial f_{sd}^{k+1}}{\partial x_{fd}^{k+1}} \qquad C^{k+1} = \frac{\partial f_{sd}^{k+1}}{\partial y^{k+1}}$$
$$D^{k+1} = \frac{\partial F_2}{\partial x_{sd}^{k+1}} \qquad E^{k+1} = \frac{\partial F_2}{\partial x_{fd}^{k+1}} \qquad F^{k+1} = \frac{\partial F_2}{\partial y^{k+1}} . \tag{3.38}$$
$$L^{k+1} = \frac{\partial F_3}{\partial x_{sd}^{k+1}} \qquad M^{k+1} = \frac{\partial F_3}{\partial x_{fd}^{k+1}} \qquad N^{k+1} = \frac{\partial F_3}{\partial y^{k+1}}$$

The method starts from an initial guess point $\left[x_{sd}^{k+1} = x_{sd}^{0} \quad x_{fd}^{k+1} = x_{fd}^{0} \quad y^{k+1} = y^{0} \right]^T$ and updates the solution at each iteration *i* by

$$\begin{bmatrix} x_{sd}^{k+1} \\ x_{fd}^{k+1} \\ y^{k+1} \end{bmatrix}^i = \begin{bmatrix} x_{sd}^{k} \\ x_{fd}^{k} \\ y^{k} \end{bmatrix}^i + \begin{bmatrix} \Delta x_{sd}^{k} \\ \Delta x_{fd}^{k} \\ \Delta y^{k} \end{bmatrix}^i \tag{3.39}$$

where the correct solution is obtained until a convergence criterion is satisfied. This process is repeated until $t^{k+1} \geq t_{end}$.

Lastly, assuming that a power system is composed by *n* buses (without an infinite bus), *m* synchronous machines, *e* exciters, *f* feedback components, *ps* power system stabilizer, *o* OvereXcitation limiters, *r* governor-turbines, *d* load restoration dynamics and *a* induction motors, the QSS model at the synchronous rotating frame has the following variables vectors:

$$y = \begin{bmatrix} \left[\theta_1 \cdots \theta_n \right]^T \\ \left[V_1 \cdots V_n \right]^T \end{bmatrix} \tag{3.40}$$

$$x_{fd} = \begin{bmatrix} \left[\psi_{1d\,1}, E'_{d\,1}, \psi_{2q\,1}, \cdots, \psi_{1d\,m}, E'_{d\,m}, \psi_{2q\,m}\right]^T \\ \left[E_{fd\,1}, \cdots, E_{fd\,e}\right]^T \\ \left[P'_1, V'_1, \cdots, P'_{ps}, V'_{ps}\right]^T \\ \left[P_{GV\,1}, P_{HP\,1}, P_{LP\,1}, \cdots, P_{GV\,r}, P_{HP\,r}, P_{LP\,r}\right]^T \\ \left[e'_{q\,1}, e'_{d\,1}, \cdots, e'_{q\,as}, e'_{d\,as}\right]^T \end{bmatrix} \tag{3.41}$$

$$x_{sd} = \begin{bmatrix} \left[E'_{q1}, \delta_1, \omega_1, \cdots, E'_{q\,m}, \delta_m, \omega_m\right]^T \\ \left[D_1, \cdots, D_f\right]^T \\ \left[W'_1, \cdots, W'_{ps}\right]^T \\ \left[x_{t\,1}, x_{OXL\,1}, \cdots, x_{t\,o}, x_{OXL\,o}\right]^T \\ \left[P_{IP\,1}, \cdots, P_{IP\,r}\right]^T \\ \left[z_{P\,1}, z_{Q\,1}, \cdots, z_{P\,l}, z_{Q\,l}\right]^T \\ \left[\omega_{r\,1}, \cdots, \omega_{r\,as}\right]^T \end{bmatrix}. \tag{3.42}$$

On the other hand, the network algebraic vector is increased if the ω_{COI} rotating frame is used:

$$y = \begin{bmatrix} \left[\theta_1 \cdots \theta_n\right]^T \\ \left[V_1 \cdots V_n\right]^T \\ \omega_{COI} \end{bmatrix}. \tag{3.43}$$

Lastly, the dynamic and algebraic vectors take the following form when a perfect coherency between all generators and the ω_{COI} rotating frame are considered:

$$y = \begin{bmatrix} \left[\theta_1 \cdots \theta_{n-1}\right]^T \\ \eta \\ \left[V_1 \cdots V_n\right]^T \end{bmatrix} \tag{3.44}$$

$$x_{fd} = \begin{bmatrix} \left[\psi_{1d\,1}, E'_{d\,1}, \psi_{2q\,1}, \delta_1, \cdots, \psi_{1d\,m}, E'_{d\,m}, \psi_{2q\,m}, \delta_m\right]^T \\ \left[E_{fd\,1}, \cdots, E_{fd\,e}\right]^T \\ \left[P'_1, V'_1, \cdots, P'_{ps}, V'_{ps}\right]^T \\ \left[P_{GV\,1}, P_{HP\,1}, P_{LP\,1}, \cdots, P_{GV\,r}, P_{HP\,r}, P_{LP\,r}\right]^T \\ \left[e'_{q\,1}, e'_{d\,1}, \cdots, e'_{q\,as}, e'_{d\,as}\right]^T \end{bmatrix} \tag{3.45}$$

$$x_{sd} = \begin{bmatrix} \left[E'_{q\,1}, \cdots, E'_{q\,m}\right]^T \\ \left[D_1, \cdots, D_f\right]^T \\ \left[W'_1, \cdots, W'_{ps}\right]^T \\ \left[x_{t\,1}, x_{OXL\,1}, \cdots, x_{t\,o}, x_{OXL\,o}\right]^T \\ \left[P_{IP\,1}, \cdots, P_{IP\,r}\right]^T \\ \left[z_{P\,1}, z_{Q\,1}, \cdots, z_{P\,l}, z_{Q\,l}\right]^T \\ \left[\omega_{r\,1}, \cdots, \omega_{r\,as}\right]^T \\ \omega_{COI} \end{bmatrix} \tag{3.46}$$

where the *n*-th bus is assumed to be a reference bus, which implies that θ_n is constant. The rotor angle δ is included in the x_{fd} vector and a global variable ω_{COI} is added to x_{sd}. In this case, the rotor speed of each generator is given by

$$\omega_i = \omega_{COI} \qquad i = 1 \cdots m. \tag{3.47}$$

3.9 Conclusions

This Chapter has presented the mathematical formulation of the Quasi Steady-State approximation taking into account the rotor speed as dynamic variable. To this purpose two approaches were reported: i) Each generator conserves its own rotating speed by considering ether the synchronous speed or the ω_{COI} speed as rotating reference; ii) In the second approach, a perfect coherency is considered in all generators by neglecting the oscillations between them, and the ω_{COI} speed is used as the frame of reference.

Moreover, the set of DAEs that represents the QSS approximation is transformed into a set of algebraic-difference equations by using the BE or TR integration method. Lastly, the resulting set of algebraized equations is solved with the Newton-Raphson method to study the long-term dynamic stability of large-scale power systems.

Chapter 4

COMBINING SHORT- AND LONG-TERM MODELLING AND SIMULATION

4.1 Introduction

In this Chapter, the idea of combining FTS and QSS models is used to develop a single unified program for long-term dynamic simulation. An accurate criterion to determine the appropriate switching time between these models, preserving a uniform approximation of state and algebraic variables, is proposed based on the singular perturbation and two-time scale techniques. The main contributions of the proposed approach are: i) The time step size of integration is adjusted based on the direct monitoring of the damping associated with fast time-varying state variables instead of the truncation error of all state and algebraic variables; ii) The simulation efficiency is achieved with both, the time step size adjustment and the reduction of the power system model instead of by using only the former; and iii) Finally, the proposed criterion to automatically switch from FTS to QSS simulation allows the initialization of the state variables of the slow reduced model from the final system state provided by the full simulation.

4.2 Singular perturbation and two-time scale

Power system dynamics can be described by a mixed set of parameter-dependent differential and algebraic equations, as given by the FTS model

$$\dot{x} = f(x, y, z) \qquad f : \Re^{n+m+p} \rightarrow \Re^{n} \tag{4.1}$$

$$0 = g(x, y, z) \qquad g : \Re^{n+m+p} \to \Re^{m} \tag{4.2}$$

$$\begin{aligned} & z(t_k^+) = h(x, y, z(t_k^-)) \qquad h : \Re^{n+m+p} \to \Re^{p} \\ & x \in X \subset \Re^{n} \quad y \in Y \subset \Re^{m} \quad z \in Z \subset \Re^{p} \quad t \in \left[t_0, t_{end}\right] \end{aligned} \tag{4.3}$$

where t_0 and t_{end} are the initial and final times, respectively, of the study time period. x is a n-dimensional vector of dynamic state variables with initial conditions $x(t_0) = x_0$, y is a m-dimensional vector of instantaneous state (algebraic) variables with initial conditions $y(t_0) = y_0$ and z is a set of p discrete states which undergoes step changes from $z(t_k^-)$ to $z(t_k^+)$ at some instant t_k [Van Cutsem and Vournas, 1998]. Because transmission network dynamics are much faster than dynamics of the equipment or loads, the variables y are understood to change instantaneously with variations of the x states under the quasi-sinusoidal (or phasor) approximation. Hence, only the dynamics of the equipment, e.g. generators, controls and loads at buses, are explicitly modelled by the set of nonlinear ordinary differential equations (4.1). The set of nonlinear algebraic equations (4.2) represents the stator algebraic equations and mismatch power flow equations at each node. Lastly, the set of discrete-time equations (4.3) capture the discrete controls and protections acting on the system.

The set of differential equations (4.1) can be partitioned according to the time scales of the state dynamics. In particular, in a two-time scale system [Kokotovic et al., 1986],

$$\dot{x}_{sd} = f_{sd}(x_{sd}, x_{fd}, y, z) \qquad f_{sd} : \Re^{n_{sd}+m+p} \to \Re^{n_{sd}} \tag{4.4}$$

$$\dot{x}_{fd} = F_{fd}(x_{sd}, x_{fd}, y, z) \qquad F_{fd} : \Re^{n_{fd}+m+p} \to \Re^{n_{fd}} \tag{4.5}$$

where x_{sd} is a n_{sd}-dimensional vector with predominantly slow dynamics and initial conditions $x_{sd}(t_0) = x_{sd}^0$, while x_{fd} is a n_{fd}-dimensional vector of states that has fast dynamics

superimposed on slow varying quasi steady-state responses with initial conditions $x_{fd}(t_0) = x_{fd}^0$.

Since the dynamics of the states x_{fd} are faster than those of x_{sd}, that is $\dot{x}_{fd}$ is larger than $\dot{x}_{sd}$, F_{fd} must be scaled by introducing a scaling factor ε [Peponides et al., 1982], [Kokotovic et al., 1986]:

$$f_{fd} = \varepsilon F_{fd} \tag{4.6}$$

where ε represents the ratio of time scales associated with x_{sd} and x_{fd}: ratios of small and large time constants, subtransient and transient inductances or weak and strong connections [Xu et al., 1998].

Hence, when functions are scaled to have the same order of magnitude the FTS model (4.1)-(4.3) can be expressed as a standard form (also called the explicit form) of the singular perturbation problem [Peponides et al., 1982], [Kokotovic et al., 1986]:

$$\dot{x}_{sd} = f_{sd}(x_{sd}, x_{fd}, y, z) \qquad f_{sd} : \Re^{n_{sd}+m+p} \to \Re^{n_{sd}} \tag{4.7}$$

$$\varepsilon \dot{x}_{fd} = f_{fd}(x_{sd}, x_{fd}, y, z) \qquad f_{fd} : \Re^{n_{fd}+m+p} \to \Re^{n_{fd}} \tag{4.8}$$

$$0 = g(x_{sd}, x_{fd}, y, z) \qquad g : \Re^{n_{sd}+n_{fd}+m+p} \to \Re^{m} \tag{4.9}$$

$$\begin{aligned} &z(t_k^+) = h(x_{sd}, x_{fd}, y, z(t_k^-)) \qquad h : \Re^{n_{sd}+n_{fd}+m+p} \to \Re^{p} \\ &x_{sd} \in X \subset \Re^{n_{sd}} \quad x_{fd} \in X \subset \Re^{n_{fd}} \quad t \in [t_0, t_{end}] \end{aligned} . \tag{4.10}$$

One simple technique to reduce the order of the FTS model, thereby reducing the stiffness of the system, is to formally set $\varepsilon = 0$. In this case, dynamics of x_{fd} become infinitely faster than x_{sd} and instantaneously reach their equilibrium $f_{fd}(x_{sd}, x_{fd}, y, z) = 0$, such that the system approaches the solution of the n_{sd}-dimensional slow-reduced model if

the Jacobian $\partial f_{fd}(\cdot)/\partial x_{fd}$ is nonsingular [Kokotovic et al., 1986]. This model is often referred to as the Quasi Steady-State (QSS) model and is expressed by

$$\dot{x}_{sd}^{sm} = f_{sd}(x_{sd}^{sm}, x_{fd}^{sm}, \overline{y}, z) \tag{4.11}$$

$$0 = f_{fd}(x_{sd}^{sm}, x_{fd}^{sm}, \overline{y}, z) \tag{4.12}$$

$$0 = g(x_{sd}^{sm}, x_{fd}^{sm}, \overline{y}, z) \tag{4.13}$$

$$z(t_k^+) = h(x_{sd}^{sm}, x_{fd}^{sm}, \overline{y}, z(t_k^-)). \tag{4.14}$$

In this case, the solution $x_{sd}^{sm}(t)$ represents an approximation to the actual slow subsystem dynamics $x_{sd}(t)$, and $x_{fd}^{sm}(t)$ represents an approximation of the slow modes (hence the upperscript *sm*) of the fast subsystem dynamics $x_{fd}(t)$. This approximation is accurate for $t \in [t_{sw}, t_{end}]$ where t_{sw} is the time instant at which switching from the FTS model to the QSS model is appropriate. The values of algebraic variables associated with the slow dynamics are represented by $\overline{y}$.

A discrepancy between the responses computed by the QSS model and from the FTS model takes place during the interval $[t_0, t_{sw}]$ and is due to the fast dynamic response. However, the equivalence between both responses can be established by investigating the dynamics of the fast-reduced model, which can be derived from (4.7)-(4.10) by considering the so-called boundary layer correction [Kokotovic et al., 1986], [Peponides et al., 1982] in the fast time scale τ

$$x_{sd}(t) = x_{sd}^{sm}(t) + x_{sd}^{fm}(\tau) \tag{4.15}$$

$$x_{fd}(t) = x_{fd}^{sm}(t) + x_{fd}^{fm}(\tau) \tag{4.16}$$

where $x_{sd}^{fm}(\tau)$ and $x_{fd}^{fm}(\tau)$ are fast modes, and τ is given by [Kokotovic et al., 1986]

$$\tau = \frac{t}{\varepsilon} \,. \tag{4.17}$$

Applying the chain rule derivative to (4.15) and (4.16) yields

$$\frac{dx_{sd}(t)}{dt} = \frac{dx_{sd}^{sm}(t)}{dt} + \frac{x_{sd}^{fm}(\tau)}{d\tau}\frac{d\tau}{dt} \tag{4.18}$$

$$\frac{dx_{fd}(t)}{dt} = \frac{dx_{fd}^{sm}(t)}{dt} + \frac{x_{fd}^{fm}(\tau)}{d\tau}\frac{d\tau}{dt} \,. \tag{4.19}$$

Taking the derivative of τ with respect to time and substituting into (4.18) and (4.19)

$$\varepsilon\frac{dx_{sd}(t)}{dt} = \varepsilon\frac{dx_{sd}^{sm}(t)}{dt} + \frac{x_{sd}^{fm}(\tau)}{d\tau} \tag{4.20}$$

$$\varepsilon\frac{dx_{fd}(t)}{dt} = \varepsilon\frac{dx_{fd}^{sm}(t)}{dt} + \frac{x_{fd}^{fm}(\tau)}{d\tau} \,. \tag{4.21}$$

Moreover, substituting (4.7) into (4.20) and (4.8) into (4.21), the differential equations can be rewritten as

$$\varepsilon f_{sd}(x_{sd}^{sm}(t) + x_{sd}^{fm}(\tau), x_{fd}^{sm}(t) + x_{fd}^{fm}(\tau), y, z) = \varepsilon\frac{dx_{sd}^{sm}(t)}{dt} + \frac{x_{sd}^{fm}(\tau)}{d\tau} \tag{4.22}$$

$$f_{fd}(x_{sd}^{sm}(t) + x_{sd}^{fm}(\tau), x_{fd}^{sm}(t) + x_{fd}^{fm}(\tau), y, z) = \varepsilon\frac{dx_{fd}^{sm}(t)}{dt} + \frac{x_{fd}^{fm}(\tau)}{d\tau} \,. \tag{4.23}$$

Finally, the fast reduced model is then obtained by letting $\varepsilon \to 0$:

$$\frac{dx_{sd}^{fm}}{d\tau} = 0 \tag{4.24}$$

$$\frac{dx_{fd}^{fm}}{d\tau} = f_{fd}(x_{sd}^{sm}, x_{fd}^{sm} + x_{fd}^{fm}, y, z) \tag{4.25}$$

$$0 = g(x_{sd}^{sm}, x_{fd}^{sm} + x_{fd}^{fm}, y, z) \tag{4.26}$$

$$z(t_k^+) = h(x_{sd}^{sm}, x_{fd}^{sm} + x_{fd}^{fm}, y, z(t_k^-)). \tag{4.27}$$

The equation (4.24) implies that x_{sd}^{fm} is frozen at its initial value $x_{sd}^{fm}(t_0)$. Furthermore, as x_{sd} is predominantly slow, the quasi steady-state x_{sd}^{sm} can be constrained to start from the prescribed initial condition $x_{sd}^{sm}(t_0) = x_{sd}(t_0) = x_{sd}^0$, which implies that $x_{sd}^{fm}(t_0) = 0$. Based on this assumption, the approximation of x_{sd} by x_{sd}^{sm} is uniform for all $t \in [t_0, t_{end}]$ with errors on the order of ε, i.e. $x_{sd} = x_{sd}^{sm} + O(\varepsilon)$, and $x_{sd}^{fm}(\tau) = 0$ for all $t \in [t_0, t_{sw}]$ [Peponides et al., 1982] , [Kokotovic et al., 1986].

The fast modes x_{fd}^{fm} of x_{fd} are the states of the fast reduced model (4.25) which will damp out to their equilibrium $x_{fd}^{fm}(\tau = t_{sw}) = 0$ if they are asymptotically stable. In this case, a uniform approximation of the fast dynamics is given by $x_{fd} = x_{fd}^{sm} + x_{fd}^{fm} + O(\varepsilon)$ over $t \in [t_0, t_{sw}]$, and once the fast modes become small enough, $x_{fd}^{sm}(t)$ is a uniform approximation of $x_{fd}(t)$, $x_{fd} = x_{fd}^{sm} + O(\varepsilon)$, for $t \in [t_{sw}, t_{end}]$.

Based on the theory described above, Tikhonov's theorem [Kokotovic et al., 1986] guarantees that the solution given by the QSS model (4.11)-(4.14) uniformly approximates the true solution computed from the FTS model (4.1)-(4.3) after a time interval $t \in [t_0, t_{sw}]$ has elapsed.

4.3 Switching criterion

An appropriate criterion to determine when the fast modes x_{fd}^{fm} are small enough, which is the necessary condition to switch from the FTS model to the QSS model, can be determined using the singular perturbation technique as detailed hereafter.

The sets of ODEs in (4.7)-(4.10) associated with the dynamic models of power system components can be represented in their linearized form such that the singular perturbation model can be reformulated by considering $x_{sd}^{fm} \approx 0$ as

$$\dot{x}_{sd} = A_{21}\left(x_{fd}^{sm} + x_{fd}^{fm}\right) + A_{22}x_{sd}^{sm} + A_{23}y + B_2u \tag{4.28}$$

$$\varepsilon\dot{x}_{fd} = A_{11}\left(x_{fd}^{sm} + x_{fd}^{fm}\right) + A_{12}x_{sd}^{sm} + A_{13}y + B_1u \tag{4.29}$$

$$0 = g(x_{sd}^{sm}, x_{fd}^{sm} + x_{fd}^{fm}, y, z) \tag{4.30}$$

$$z(t_k^+) = h(x_{sd}^{sm}, x_{fd}^{sm} + x_{fd}^{fm}, y, z(t_k^-)) \tag{4.31}$$

where u_i is a vector with input variables. A_{ij} and B_i are constant matrices of appropriate dimensions.

Similarity, the QSS model (4.11)-(4.14) consists of neglecting x_{fd}^{fm} while setting $\varepsilon = 0$ which yields

$$\dot{x}_{sd}^{sm} = A_{21}x_{fd}^{sm} + A_{22}x_{sd}^{sm} + A_{23}\bar{y} + B_2u \tag{4.32}$$

$$0 = A_{11}x_{fd}^{sm} + A_{12}x_{sd}^{sm} + A_{13}\bar{y} + B_1u \tag{4.33}$$

$$0 = g(x_{sd}^{sm}, x_{fd}^{sm}, \bar{y}, z) \tag{4.34}$$

$$z(t_k^+) = h(x_{sd}^{sm}, x_{fd}^{sm}, \bar{y}, z(t_k^-)). \tag{4.35}$$

Thus, x_{fd}^{sm} can be obtained from (4.33):

$$x_{fd}^{sm} = -A_{11}^{-1}\left(A_{12}x_{sd}^{sm} + A_{13}\bar{y} + B_1u\right), \tag{4.36}$$

and the resulting expression can be substituted into (4.29) to obtain (4.37) that permits the computation of the fast modes

$$x_{fd}^{fm} = A_{11}^{-1}\left(\varepsilon\dot{x}_{fd} - A_{13}\left(y - \bar{y}\right)\right). \tag{4.37}$$

Since the change of x_{fd} will lag far behind the instantaneous change of algebraic variables, and considering that the difference $\left(y-\overline{y}\right)$ tends to zero faster than $\dot{x}_{fd}$, as numerically shown in Section 4.4.1, one can assume that a good approximation to compute x_{fd}^{fm} can be obtained by

$$x_{fd}^{fm} = A_{11}^{-1}\varepsilon\dot{x}_{fd} \tag{4.38}$$

where $\dot{x}_{fd}$ is computed by the integration of the full model at each time step. Therefore, (4.38) can be evaluated without additional computational cost.

Since the dynamics of x_{fd}^{fm} are associated with different fast-state variables, the normalized value of each component of x_{fd}^{fm} must be considered:

$$x_{fd\,i}^{nor} = \frac{x_{fd\,i}^{fm}}{x_{fd\,i}} \qquad i = 1,\ldots,n_{fd} \tag{4.39}$$

Therefore, the time of switching t_{sw} from the full model to the slow reduced model is determined when the maximum absolute value of x_{fd}^{nor} is smaller than a specified tolerance TOL_{sw}, $\max\left|x_{fd}^{nor}\right| \le TOL_{sw}$ continually for a fixed number of time steps h_{TOL}, which is given by

$$h_{Tol} = \frac{t_{TOL}}{h} \tag{4.40}$$

where t_{TOL} is a prespecified period of time which must be large enough to guarantee the correct determination of t_{sw}, but small enough to preserve computational efficiency.

4.4 Proposed approach for long-term stability analysis in power system

The proposed approach to tackle the complexity of long-term dynamic simulations consists of using the FTS model to simulate the dynamics associated with the short-time period

following a disturbance with a small step size, and once the fast dynamics are small enough, switching to the QSS model to perform the long-term simulation with a larger step size as shown in Figure 4.1. Owing to the fact that at the switching time there exists a uniform approximation between models, the state and algebraic variables of the slow reduced model are automatically initialized from the final system state provided by the full simulation. Lastly, the information required to determine the evolution of the discrete states z is directly transferred from the FTS simulation to the QSS model. This proposed procedure for long-term dynamic analysis using the switching criterion is as follows:

- **Step 1.-** Select the fast- and slow-state variables, $x = (x_{fd},\ x_{sd})$, to ensure that the system is state separable.
- **Step 2.-** Solve the FTS model (4.1)-(4.3) with a small time step of integration. For instance, the Backward Euler or Trapezoidal Rule can be applied to transform the differential equations into algebraic equations. The Newton-Raphson method is then applied to solve the set of algebraic-difference equations as explained in Section 2.9. A possible short-term instability associated with the loss of synchronism or voltage instability is checked, and if it occurs the simulation stops.
- **Step 3.-** The switching criterion is checked at each time instant t_k to determine the switching time. When this criterion is satisfied continuously during t_{TOL}, the algorithm proceeds with Step 4; otherwise, Step 2 and 3 are repeated.
- **Step 4.-** The simulation switches to the QSS model (4.11)-(4.14), which is solved as explained in Section 3.8 with a larger time step of integration. At the switching time, initial conditions of QSS variables x_{sd}^{sm}, x_{fd}^{sm} and $\overline{y}$ are set to values $x_{sd}^{t_{sw}}$, $x_{fd}^{t_{sw}}$ and $y^{t_{sw}}$, respectively.

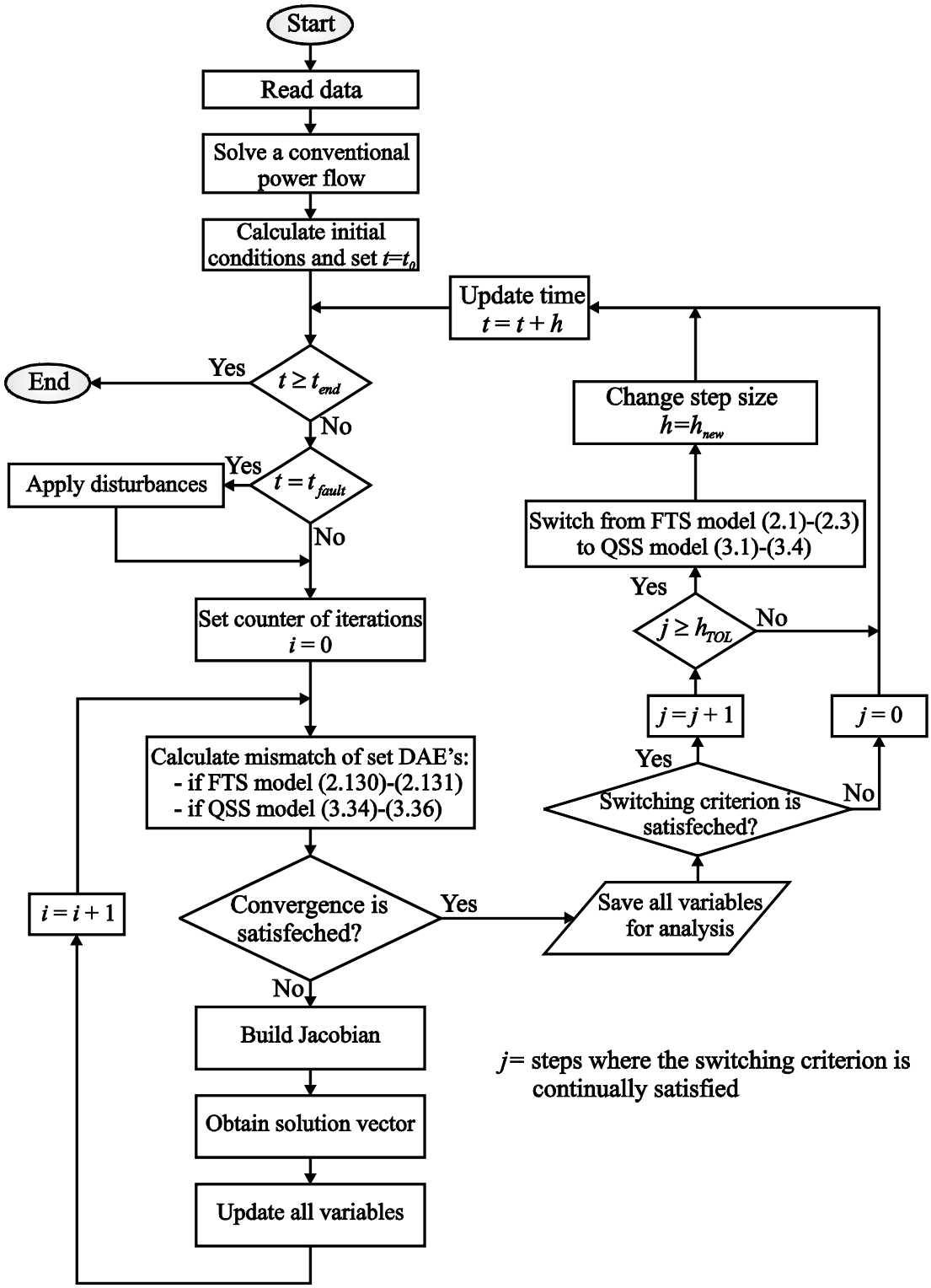

Figure 4.1: Combined FTS-QSS simulation algorithm.

4.4.1 Application of the switching criterion

In this section the well-known one-machine infinite-bus system is used to illustrate the application of the proposed methodology. The system is shown with single-line diagram in Figure 4.2. The transmission lines and generator data are given in Appendix D.1.

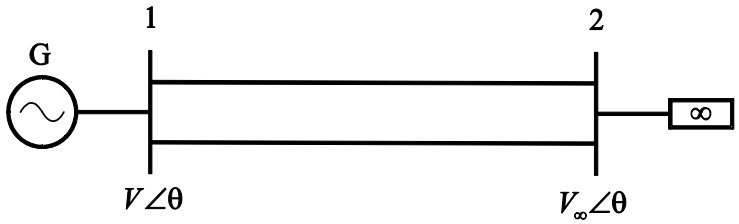

Figure 4.2: One-machine infinite-bus system.

The generator is represented by a two-axis model, as explained in Section 2.3, with the following set of equations [Pai, 1989]:

$$T'_{do}\dot{E}'_q = K_1 E'_q + K_2\psi_{1d} + K_3 V\cos(\delta-\theta) + E_{fd} \tag{4.41}$$

$$T''_{do}\dot{\psi}_{1d} = K_4 E'_q + K_5\psi_{1d} + K_6 V\cos(\delta-\theta) \tag{4.42}$$

$$T'_{qo}\dot{E}'_d = K_7 E'_d + K_8\psi_{2q} + K_9 V\sin(\delta-\theta) \tag{4.43}$$

$$T''_{qo}\dot{\psi}_{2q} = K_{10}\psi_{1q} + K_{11}\psi_{2q} + K_{12} V\sin(\delta-\theta) \tag{4.44}$$

$$\dot{\delta} = \omega - \omega_s \tag{4.45}$$

$$\dot{\omega} = \frac{\omega_s}{2H}\left[P_g - P_m - D(\omega-\omega_s)\right] \tag{4.46}$$

The network equations are written in terms of active and reactive power mismatch equations [Sauer and Pai, 1998]:

$$0 = P_g - \left[V^2 G_{11} + VV_\infty\left(G_{1\infty}\cos(\theta) + B_{1\infty}\sin(\theta)\right)\right] \tag{4.47}$$

$$0 = Q_g - \left[V^2 B_{11} + VV_\infty\left(G_{1\infty}\sin(\theta) - B_{1\infty}\cos(\theta)\right)\right] \tag{4.48}$$

where

$$P_g = K_{13}E'_d V\cos(\delta-\theta) + K_{14}\psi_{2q}V\cos(\delta-\theta) + K_{15}E'_q V\sin(\delta-\theta) + K_{16}\psi_{1d}V\sin(\delta-\theta) + K_{17}V^2\sin(2(\delta-\theta)) \tag{4.49}$$

$$Q_g = -K_{13}E'_d V\sin(\delta-\theta) - K_{14}\psi_{2q}V\sin(\delta-\theta) + K_{15}E'_q V\cos(\delta-\theta) + K_{16}\psi_{1d}V\cos(\delta-\theta) - V^2\left(K_{18}\cos(\delta-\theta)^2 + K_{19}\sin(\delta-\theta)^2\right). \tag{4.50}$$

The time constants T'_{do}, T'_{qo} and T''_{qo} are generally small as explained in Section 3.3. Hence, ψ_{1d} , E'_d and ψ_{2q} can be considered fast time-varying variables, while E'_q, δ and ω can be assumed to be slow time-varying variables. Therefore, the FTS model has the following state vectors using the synchronous speed rotating reference:

$$y = \begin{bmatrix}\theta & V\end{bmatrix}^T \tag{4.51}$$

$$x_{fd} = x_{fd}^{sm} + x_{fd}^{fm} = \begin{bmatrix}\psi_{1d} & E'_d & \psi_{2q}\end{bmatrix}^T \tag{4.52}$$

$$x_{sd} = \begin{bmatrix}E'_q & \delta & \omega\end{bmatrix}^T \tag{4.53}$$

while the slow-reduced model is represented by

$$\bar{y} = \begin{bmatrix}\bar{\theta} & \bar{V}\end{bmatrix}^T \tag{4.54}$$

$$x_{fd}^{sm} = \begin{bmatrix}\psi_{1d}^{sm} & E'^{sm}_d & \psi_{2q}^{sm}\end{bmatrix}^T \tag{4.55}$$

$$x_{sd}^{sm} = \begin{bmatrix}E'_q & \delta & \omega\end{bmatrix}^T. \tag{4.56}$$

The proposed switching criterion relies on computing x_{fd}^{nor} given by

$$x_{fd}^{nor} = \left[\frac{T''_{do}}{K_8}\frac{\dot{\psi}_{1d}}{\psi_{1d}} \quad \frac{1}{K_{11}K_7 - K_{10}K_8}\left(\frac{K_{11}T'_{qo}\dot{E}'_d - K_8T''_{qo}\dot{\psi}_{2q}}{E'_d}\right) \quad \frac{1}{K_{11}K_7 - K_{10}K_8}\left(\frac{-K_{10}T'_{qo}\dot{E}'_d + K_7T''_{qo}\dot{\psi}_{2q}}{\psi_{2q}}\right)\right]^T \tag{4.57}$$

such that the switching time is obtained when the condition $\max\left|x_{fd}^{nor}\right| \le TOL_{sw}$ has been satisfied continuously for a fixed number of time steps h_{TOL} which is computed by (4.40) for a prespecified t_{TOL}.

In order to numerically validate the proposed switching criterion, a single contingency scenario is defined by removing one transmission line at time *t*=1s. Following the disturbance, a FTS simulation and a QSS simulation are performed with an integration time step of *h*=0.01s. Figure 4.3 shows the evolution of the voltage magnitude *V* and flux linkage ψ_{1q} as a function of time computed by both simulations. Note that flux linkage ψ_{1q} is proportional to E'_d (see Appendix A).

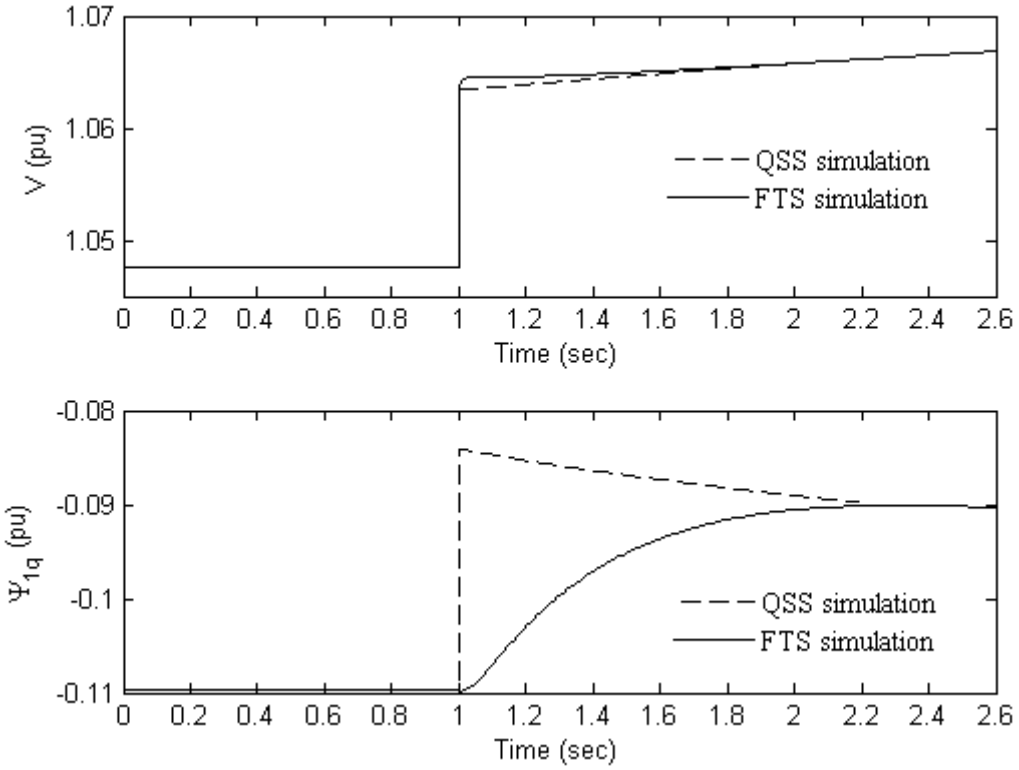

Figure 4.3: Terminal voltages and flux linkage at bus 1.

At the instant of the disturbance application both active and reactive power flows from bus 1 to bus 2 are reduced instantaneously, thus that the terminal voltage magnitude *V*

is increased. The generation of both active and reactive powers is also reduced in order to satisfy the power balance. After this instant, the generator variables are changing until the active generated power achieves the mechanical power.

A comparison of these evolutions shows that the existing difference of the algebraic variable's value V computed by both FTS and QSS simulations, $\left[V - \bar{V}\right]$, is much smaller than the difference between the values of the fast-state variable ψ_{1q}, $\left[\psi_{1q} - \psi_{1q}^{sm}\right]$, computed by each simulation. Therefore, the proposed criterion can be considered a suitable method to determine the switching time. The system survives the short-term period, and the switching criterion is satisfied at t=2.2 s with $TOL_{sw} = 0.1$ and t_{TOL}=0.1 s. At this instant of time t_{sw}, the values of state and algebraic variables computed by FTS and QSS simulations are very close to each other, indicating that fast dynamics have died out and long-term responses can be assessed by the simpler QSS model.

4.5 Methodology to applying disturbance

In order to perform short-term and long-term dynamic simulation, a digital program has to be able to compute the disturbance and post-disturbance condition of the algebraic system variables. At the instant of either application (t_{ap}) or clearing (t_{cl}) of a disturbance, the dynamic variables cannot change instantaneously, as shown in Figure 4.4. Therefore, at these two instants of time such variables keep constant and their corresponding changes with respect to time are considered zero, while the algebraic variables suddenly change with respect to the dynamics. This phenomena can be numerically represented by setting the step size of integration to zero ($h = 0$), such that the set of algebraic equations must be solved considering the dynamic variables as fixed input at the instant of a disturbance.

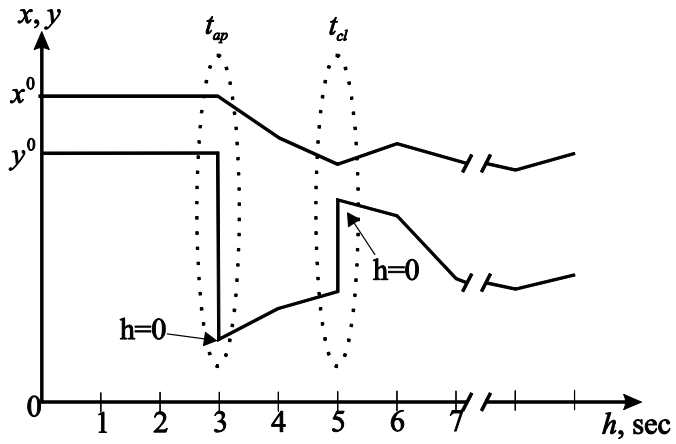

Figure 4.4: Representation of discontinuity condition.

In case of the FTS simulation, the set of algebraic equations (2.131) is linearized with respect to *y* by using the Newton method, such that at *i*-th iteration the following linear system is solved

$$\underbrace{\left[\frac{\partial F_2(\cdot)}{\partial y}\right]^i}_{J}\left[\Delta y\right]^i = -\left[F_2(\cdot)\right]^i. \tag{4.58}$$

By starting with a initial value of *y*, the method updates the solution at each iteration $y = y + \Delta y$ until a convergence criterion is satisfied. The initial value of *y* is obtained previously by the normal solution (see Section 2.9.2).

On the other hand, the network variables *y* and the fast variables x_{fd} have to be computed in the case of the QSS simulation. Therefore, the set of algebraic equations (3.35)-(3.36) are linearized with respect to x_{fd} and y as

$$\underbrace{\begin{bmatrix} \frac{\partial F_2}{\partial x_{fd}} & \frac{\partial F_2}{\partial y} \\ \frac{\partial F_3}{\partial x_{fd}} & \frac{\partial F_3}{\partial y} \end{bmatrix}^i}_{J}\begin{bmatrix} \Delta x_{fd} \\ \Delta y_{fd} \end{bmatrix}^i = -\begin{bmatrix} F_2(\cdot) \\ F_3(\cdot) \end{bmatrix}^i. \tag{4.59}$$

The method starts from an initial value of y and x_{fd} and updates the solution at each iteration i by

$$\begin{bmatrix} x_{fd} \\ y \end{bmatrix}^i = \begin{bmatrix} x_{fd} \\ y \end{bmatrix}^i + \begin{bmatrix} \Delta x_{fd} \\ \Delta y \end{bmatrix}^i \tag{4.60}$$

where the correct solution is obtained until a convergence criterion is satisfied. The initial value of y and x_{fd} are obtained previously by the normal solution (see Section 3.8.1).

4.6 Conclusions

A new and simple criterion to accurately determine when a QSS model of a power system can be considered as a uniform approximation of the system FTS model, has been proposed in this work, inspired of singular perturbation and two-time scale theories.

On the basis of the suitability of this criterion, an integrated simulation method that combines the reliability of FTS simulation and the efficiency of the QSS simulation has been proposed to speed up the long-term dynamical analysis of power systems considering the presence of discrete events. The method is capable of assessing instability problems during the short-term period through the FTS simulation. If the fast modes are damped out, a model reduction is automatically carried out to analyze the long-term dynamics by the QSS simulation with larger integration time step sizes.

Chapter 5

STUDY CASES

5.1 Introduction

A combination of the FTS simulation in the short-term period and QSS approximation for the long-term time frame was proposed in [Loud et al., 2001] and [Van Cutsem et al., 2006]. Each mode of simulation is carried out by different programs which are coupled through load flow and dynamic data files, as well as the initial conditions for the QSS simulation. The time to switch from FTS to QSS simulation is chosen once the dynamics of frequency are below a specified value [Loud et al., 2001]. In this case, the QSS model is initialized by setting the continuous long-term variables and the algebraic variables to the values computed by FTS simulation at the switching time t_{sw}. The short-term variables are initialized at the values associated with the equilibrium point of the set of differential equations at t_{sw}. Lastly, the operation and waiting state of discrete events have to be considered to determine their initial conditions at t_{sw} and to establish the sequence of discrete controls during the QSS simulation with reasonable accuracy. The initialization process is avoided in [Van Cutsem et al., 2006] by performing an off-line coupling of both approaches based on the discrete events taking place during the detailed simulation. The FTS simulation is executed until the switching time t_{sw} is detected as proposed in [Loud et al., 2001], and the sequence of discrete events that have occurred over this interval are identified. The QSS simulation is then performed from the initial time with those discrete events imposed as external disturbances, without allowing the discrete devices to act by themselves until the simulation arrives at t_{sw}. From there on, the study proceeds with the usual QSS approximation.

In this Chapter, the exposed idea of combine FTS and QSS models in a single unified program for long-term dynamic simulation is tested on several systems: a simple system, the WSCC system, the New England system and an equivalent model of the Mexican power system. All the simulations are run on a laptop with the following characteristics: Intel processor dual cores at 1.728 GHz, total RAM Memory of 2.00 GB and operating system Windows XP.

5.2 2-machine, 4-bus system

This system is composed of one load embedded at bus 3 whose demanded power is supplied through a LTC transformer, thus the LTC keeps the voltage magnitude at 1 p.u. with a half-deadband of ± 0.01 p.u. A remote system (bus 1) supplies most of the power through a long double-circuit transmission line, while the rest of the power is provided by the generator connected to bus 2. The system single-line diagram is presented in Figure 5.1 [Van Cutsem and Vournas, 1998], [Vournas et al, 2004].

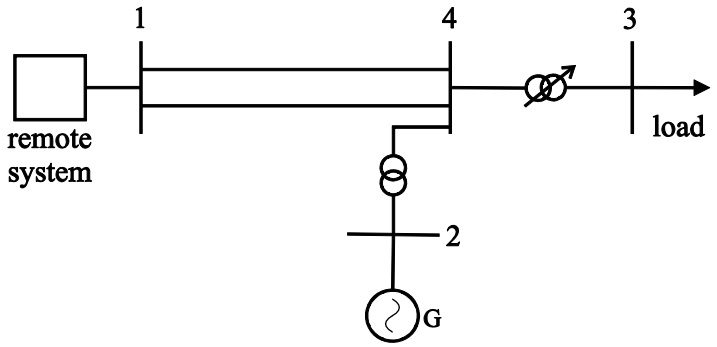

Figure 5.1: Simple electric system.

The system connected at bus 1 is considered as slack generator. Each transmission line is regarded as ideal with a serial reactance of $X_L = 0.055$ p.u. Similarly, each transformer is modelled by its reactance in series with an ideal on-nominal transformer, $X_T = 0.016$ p.u. Each generator is equipped with an exciter and a governor-turbine system. The load is composed of a generic self-restoring load and an induction motor that consumes

40% of the total demanded power with a constant mechanical torque. All system data are given in Appendix D.2.

Even though this is a simple system, the motivation of its analysis is supported by the dynamics presented at both short-term and long-term simulations [Van Cutsem and Vournas, 1998]. In order to perform the simulation by the proposed approach, the parameters for the switching criterion are TOL_{sw}=0.1 and $t_{TOL} = 0.1s$.

5.2.1 Case 1

To illustrate the dynamic behavior in short-term, the system load is represented by the generic models of self-restoring load and an induction motor whose initial demand is $P_L^0 = 6$ p.u. and $Q_L^0 = 1.5$ p.u. The generator at bus 2 produces an initial generation equal to $P_g^0 = 4$ p.u. and $Q_g^0 = -0.708$ p.u. Prior to any perturbation the system is operating in the steady-state equilibrium point reported in Table 5.1.

Table 5.1: Nodal complex voltages of system (Case 1)

Complex voltages	System buses			
	B1	B2	B3	B4
V (p.u.)	1.05	1	1	0.974
θ (degree)	0	0.539	-4.448	-3.082

Generator 1 is tripped at time $t = 1s$, and the system is supplied completely for generator 2. The system dynamics are assessed by using FTS, FTS-QSS and QSS simulations. The former two simulations are performed with each generator having its own rotor speed and ω_s as the rotating frame, while perfect coherency is assumed for the latter simulation. All simulations are performed for a time period of 15 s with an integration step size of 0.01 s. The perturbation causes a short-term instability such that the QSS simulation cannot accomplish the convergence to a solution because the Jacobian matrix becomes singular. In contrast, the FTS-QSS simulation obtains the same results given by the FTS simulation because the switching criterion is never satisfied, and therefore the whole simulation is carried out with the detailed model.

Figure 5.2 shows the voltage magnitude behavior at bus 3, which decays for a few seconds, but it is recovered by the fast action of the AVR control. This control is achieved by increasing the generation of reactive power, as shown in Figure 5.3.

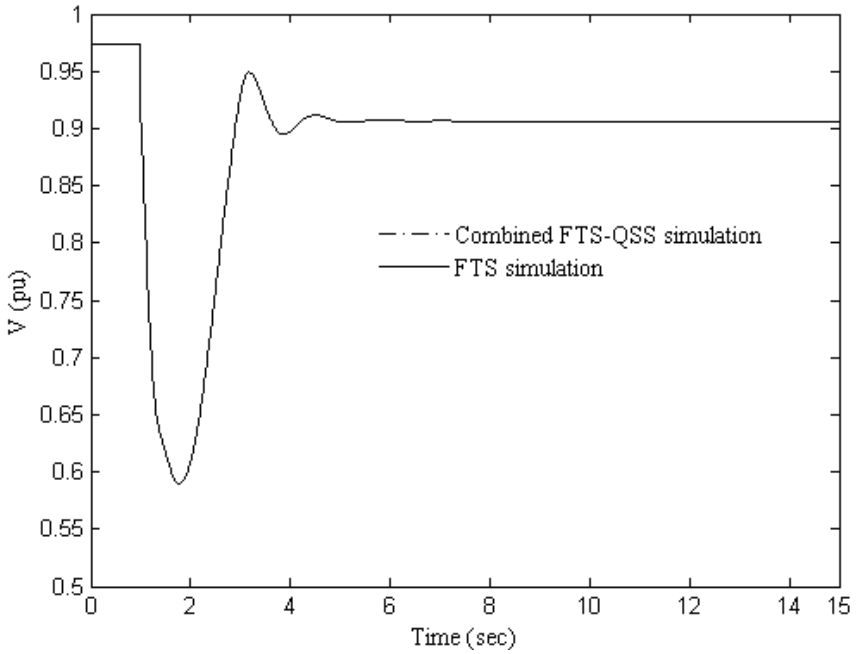

Figure 5.2: Voltage evolution of bus 3 (Case 1).

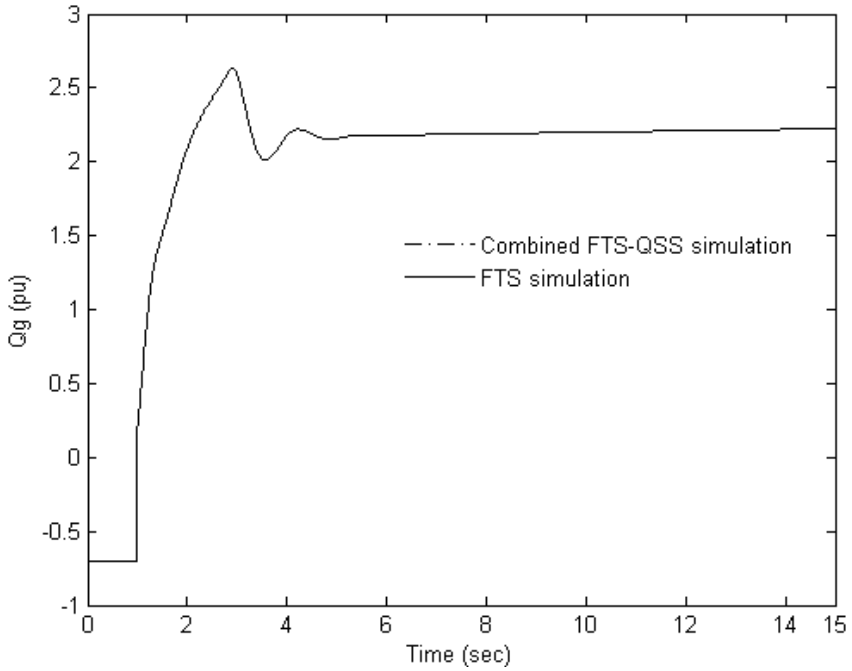

Figure 5.3: Reactive power generation (Case 1).

On the other hand, the active power consumed by the load is almost restored at its initial value 600 MW which is larger than the generator capacity of 450 MW. Thus, the governor is unable to restore the frequency to its nominal value because the mechanical power reaches its nominal value, and the generator cannot provide the demanded power. Therefore, the rotor speed decays as shown in Figure 5.4, and the system presents frequency instability of the short-term.

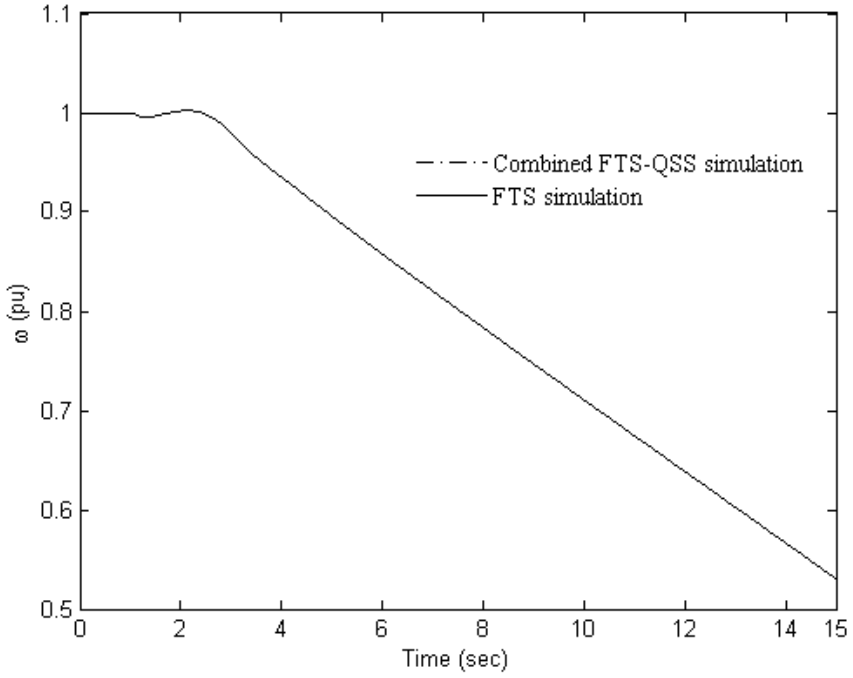

Figure 5.4: Rotor speed evolution (Case 1).

5.2.2 Case 2

The purpose of this case is to demonstrate the advantages of using both the QSS simulation and the combined FTS-QSS simulation in long-term dynamic stability when the system survives the short-term period. For this purpose, the active power demanded at bus 3 is increased to $P_L^0 = 13.7$ p.u. The steady-state initial equilibrium point is computed by a conventional power flow and is given in Table 5.2.

Table 5.2: Nodal complex voltages of system (Case 2)

Complex voltages	System buses			
	B1	B2	B3	B4
V (p.u.)	1.05	1	1	0.955
θ (degree)	0	-11.73	-18.54	-15.24

The system is perturbed at time $t = 1\,s$ by a sudden change in the network topology: one of the lines between buses 1 and 4 is tripped. The three types of simulations are carried out with the following characteristics: i)The FTS simulation uses a step size of integration of 0.01 s, and the ω_s is adopted as the rotating frame; ii) the QSS simulation is performed with h=0.1 s, and a perfect coherency between all generators is assumed; and iii) The FTS-QSS simulation uses ω_s as the rotating frame for the whole simulation, and the step size of integration takes the value of the corresponding simulation. Hence, the combined FTS-QSS simulation allows the increasing of the step size from 0.01 s to 0.1 s at the switching time. The fast-state variables monitored to enable the switching from the FTS to QSS model are those associated with the exciters (E_{fd}), generators (ψ_{1d}, E'_d, ψ_{2q}), turbines (P_{HP}, P_{LP}) and the induction motor (e'_q, e'_d). Considering a TOL_{sw}=0.1 and $t_{TOL} = 0.1\,s$, the fast variables of generators, induction motor, exciters and turbines satisfy the switching criterion at 1.1 s, 1.23 s, 2.18 s and 4.17 s, respectively, such that the switching of models occurs at $t_{sw} = 4.17$ s.

The evolution of voltage magnitude at bus 3 is depicted in Figure 5.5. The short-term dynamics remain stable because the fast transients are damped out. However, the voltage magnitude at bus 3 decays from its schedule value, such that the LTC acts to restore the voltage within the deadband. The control of the LTC starts after an initial time delay of 20 s; hereafter the tap changes every 10 s until the control target is achieved or until the tap ratio limit is encountered, as shown in Figure 5.6. The LTC restores the voltage close to its schedule after the perturbation, but the generator's field current at bus 2 is increased during this process such that the OXL is triggered at about t=180 s which causes the reduction of the generation of reactive power. Therefore, the voltage at bus 3 decays at this time, and the

LTC tries to restore the voltage again but without success. Finally, the voltage at bus 3 starts to collapse when the LTC reaches its lower limit tap ratio.

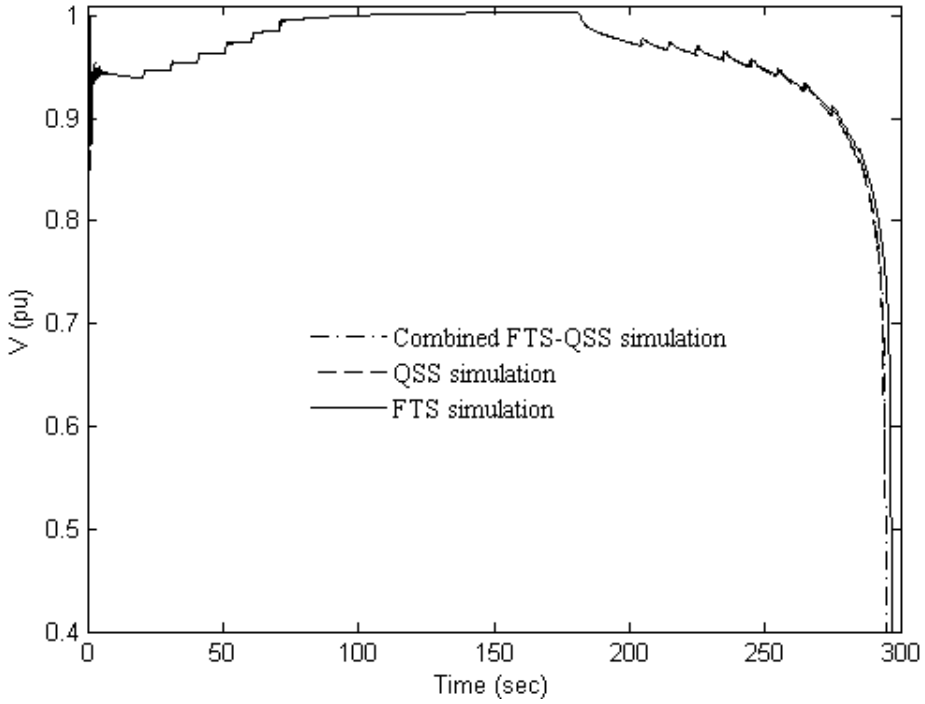

Figure 5.5: Voltage evolution of bus 3 (Case 2).

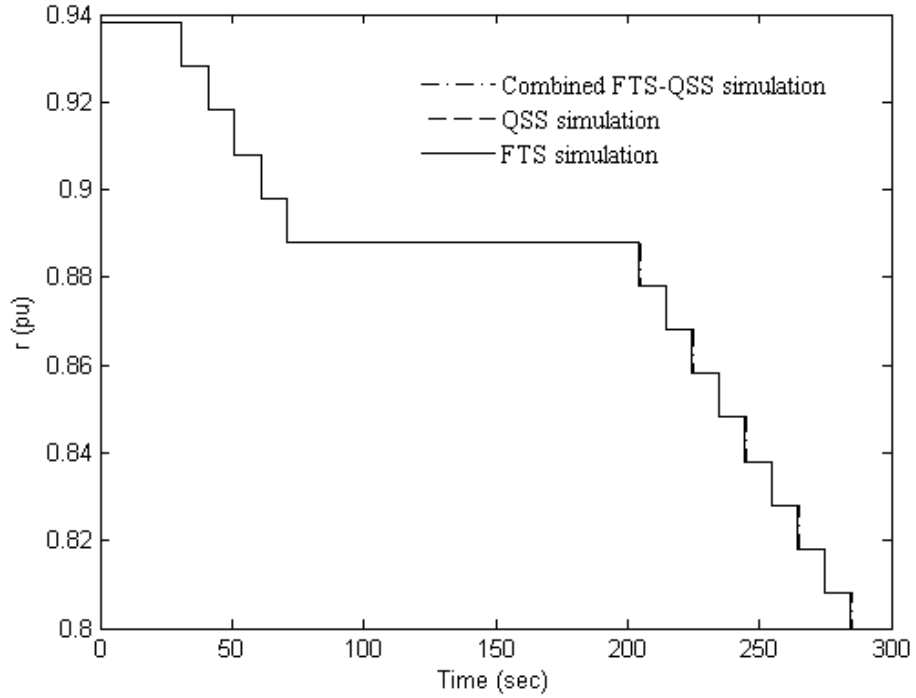

Figure 5.6: Tap ratio evolution of the LTC (Case 2).

The field current of the generator connected at bus 2 reaches values larger than its limit, ($I_{fd}^{\lim} = 2.825$ p.u.), as shown in Figure 5.7. This initiates the inverse time mechanism x_t of the OXL, such that x_t starts increasing from its lower value -20 and becomes positive at t=180.77 s as depicted in Figure 5.8. Therefore, the OXL is triggered at t=180.77 s and its output x_{OXL} (see Figure 5.9) is subtracted from the AVR input which causes the limitation of the field current. The OXL activation time computed for the three simulations are reported in Table 5.3.

Table 5.3: Activation of OXL control

Simulation	Time (in seconds)
FTS	180.77
QSS	181.1
Combined FTS-QSS	181.3

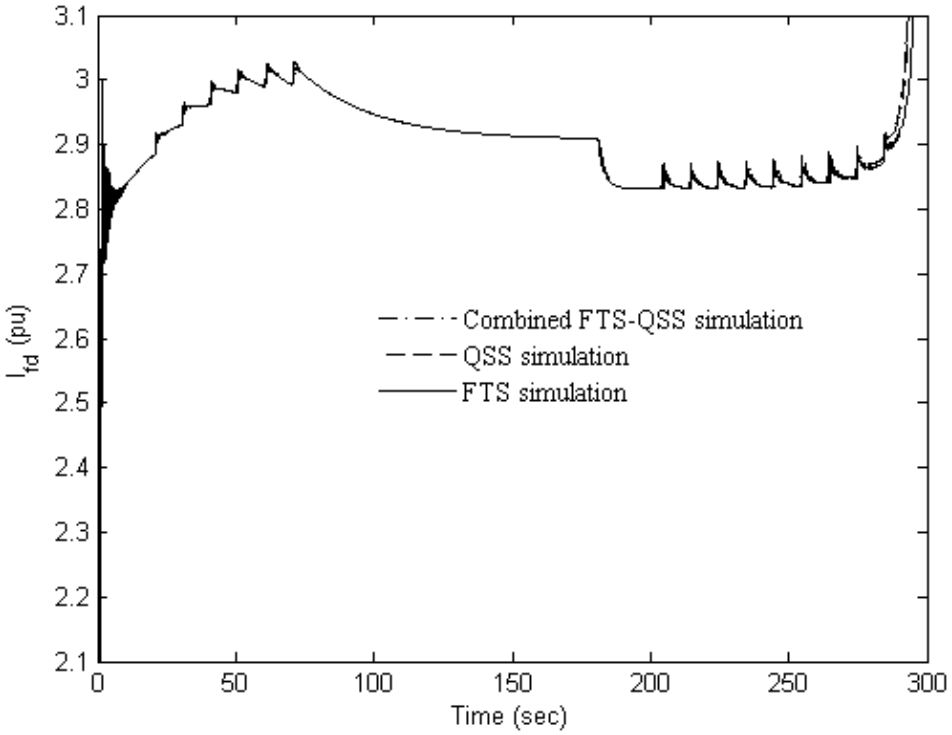

Figure 5.7: Field current evolution of generator 2 (Case 2).

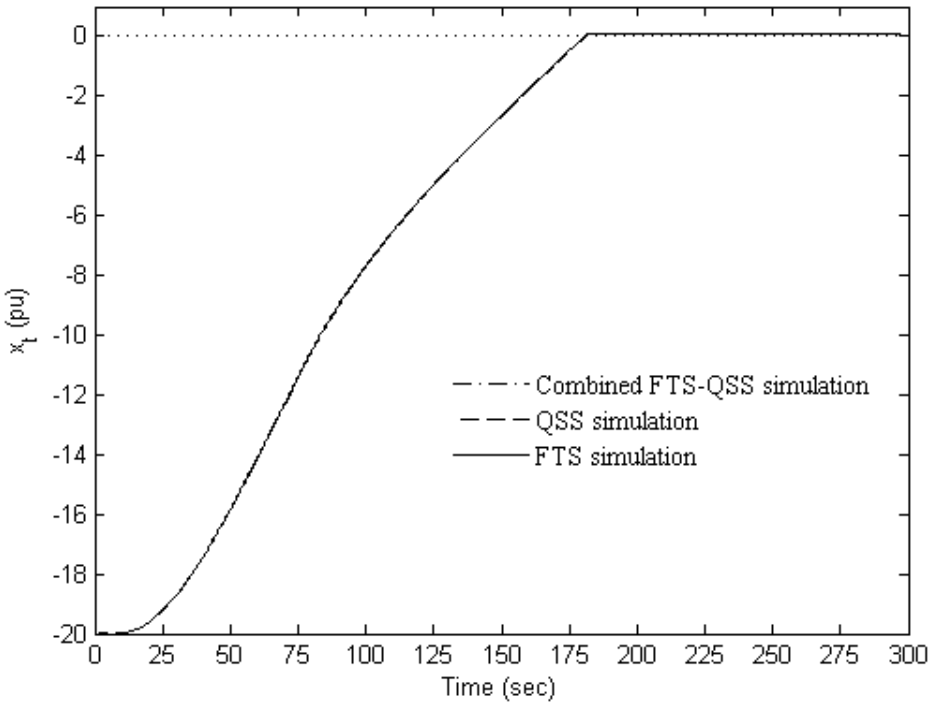

Figure 5.8: Inverse time mechanism x_t evolution (Case 2).

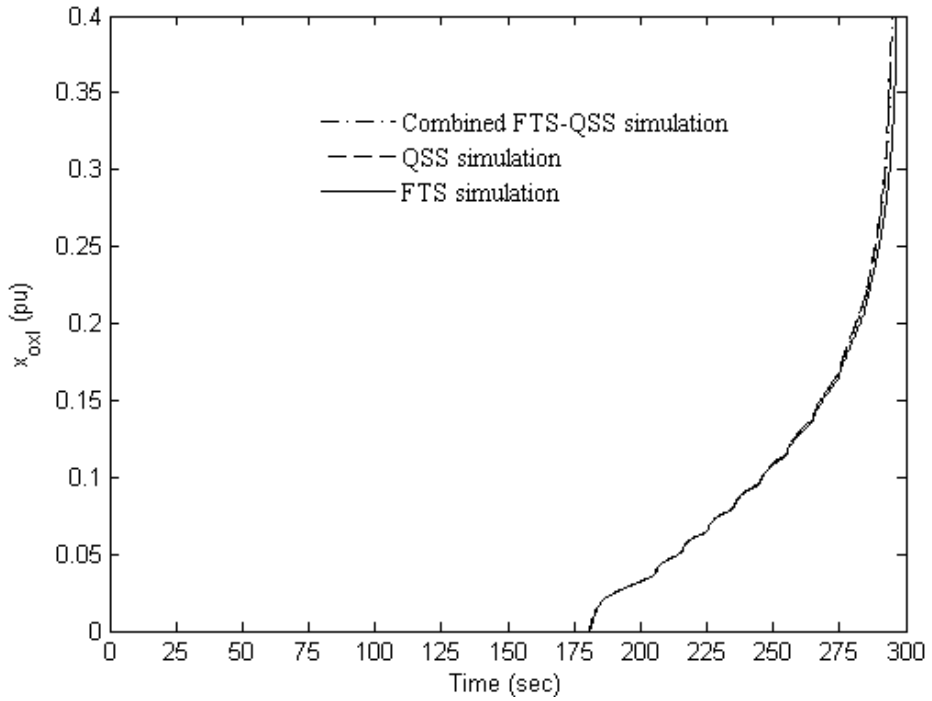

Figure 5.9: x_{OXL} evolution (Case 2).

The curves show that the QSS and FTS-QSS simulation provide quite acceptable results, but the LTC control and OXL control occur slightly later w.r.t those computed by the FTS simulation. However, the computing time required by the FTS simulation is 14.531 s while the QSS and the FTS-QSS simulation consume 1.438 s and 1.781 s, respectively. This saves considerable computational time for the study under analysis.

On the other hand, there are no significant differences between the QSS and the combined simulation. This is because the switching is given early at $t_{sw} = 4.17s$ since the fast transient damped out very soon, but large differences may arise in a contrary case (see Section 5.4).

5.3 3-machine, 9-bus WSCC system

One of the most important issues in the stability problem is the rotor angle stability; it is frequently studied when the system is subjected to large disturbance (e.g. a solid three-phase fault) [Kundur et al., 2004]. In order to apply the proposed approach in this stability problem, the WSCC power system is considered in this case of study. The system consists of 9 buses, 3 generators and 3 loads with the network shown in Figure 5.10. All system data were taken from [Sauer and Pai, 1998] and are given in Appendix D.3.

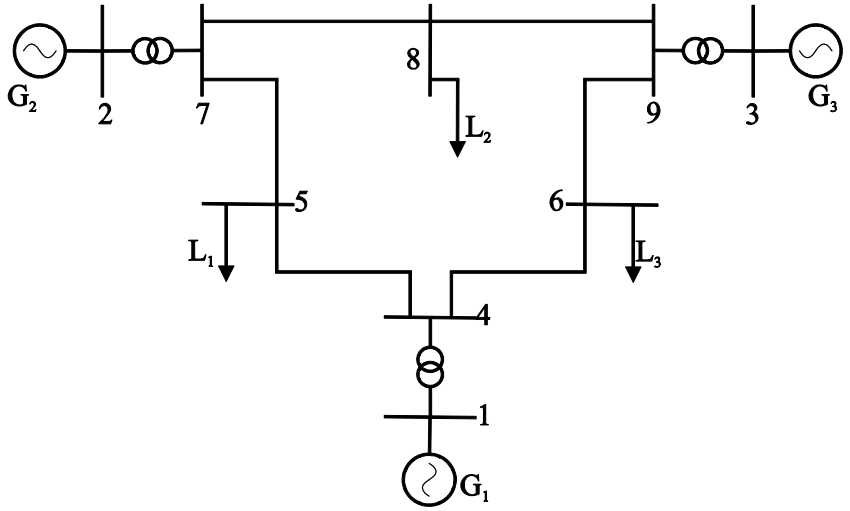

Figure 5.10: WSCC power system.

A solid three-phase fault is applied at t = 0 s at bus 7, and it is cleared by opening the transmission line between buses 5 and 7 at t = 0.135 s. The analysis is performed with both FTS and FTS-QSS simulations. The former uses an integration step size of 0.001s, while the proposed FTS-QSS simulation is performed with the same step size because the switching criterion is never satisfied (as explained below) when considering a switching tolerance of 0.1 and $t_{TOL} = 0.1s$. All simulations are carried out considering ω_{COI} as the rotating frame of reference.

The disturbance lasts for 0.135 s, while the critical clearing time to preserve transient stability is 0.131 s, such that generators 2 and 3 lose angular stability, as shown in Figure 5.11.

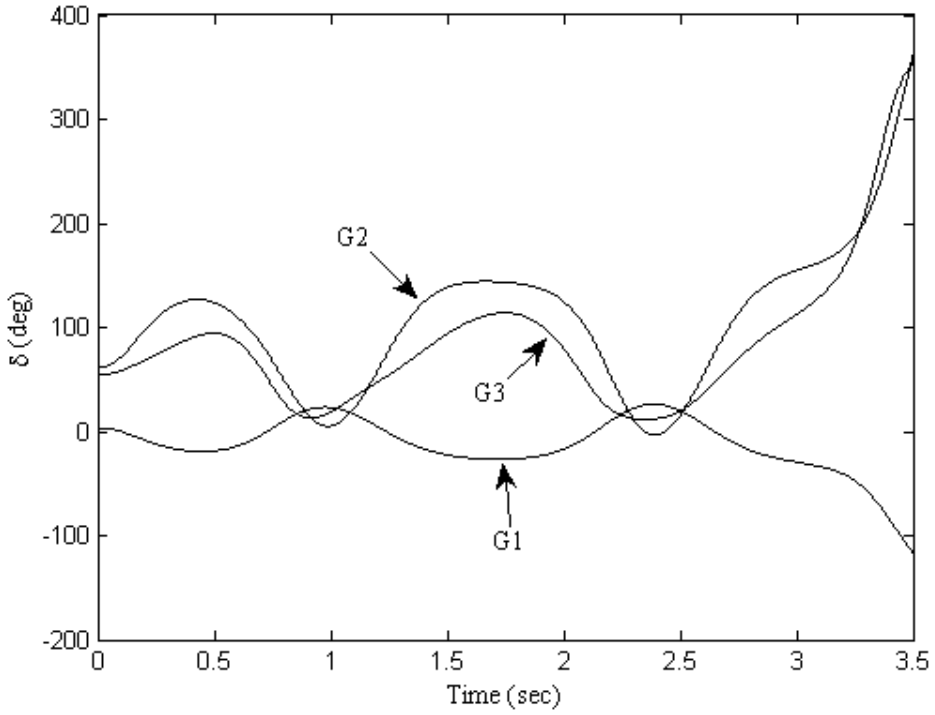

Figure 5.11: Rotor angles of the WSCC power system.

The switching criterion is never satisfied, and the FTS simulation is always performed because the fast modes never disappear. Similarly to Case 1 of Section 5.2.1, the QSS simulation cannot be applied because the system is unstable in the short-term period.

5.4 10-machine, 39-bus New England system

For the purpose of this test case the generators were selected to be steam power plants. Generating plants were assumed to be equipped with an exciter, an automatic voltage regulator, a speed governor and a steam turbine. All exciters include derivative feedback compensation [Kundur, 1994]. Likewise, three LTCs were installed on transformers to keep the voltage magnitudes at buses 12 and 20 at 1 p.u. with a half-deadband of ± 0.01 p.u., as shown in Figure 5.12. All loads are represented with the exponential model [Van Cutsem and Vournas, 1998]. For the specified disturbance, long-term dynamics come from the LTCs' control actions [Van Cutsem and Vournas, 1998]. In this case, the LTCs' delay is 20 s on the first tap change and 10 s on subsequent tap changes, resulting in a 0.01 p.u. change of ratios for each. Additionally, steam turbines and governors act in the long-term to avoid large excursions of frequency. The data of this system were taken from [Pai, 1989]; however, gains and time constants were adjusted to make rotor oscillations last longer. All system data are given in Appendix D.4.

At time $t = 1\,s$, the system is suddenly perturbed by completely disconnecting the loads at buses 4, 20 and 29. A long-term simulation is performed with the full model, the combined FTS-QSS model and the QSS model, respectively. The FTS simulation and FTS-QSS simulation are performed considering ω_s as the rotating frame. On the other hand, a perfect coherency between all generators is assumed in the QSS simulation [Grenier et al., 2005]. Integration step sizes are defined according to the model being used in the analysis: the FTS model is integrated using a time step of 0.01s, while the QSS simulation is accomplished with an integration time step of 1s. Hence, the combined FTS-QSS simulation allows the increasing of the step size from 0.01s to 1s at the switching time. The fast-state variables monitored to perform the switching from the FTS to QSS model are those associated with the exciters (E_{fd}), generators (ψ_{1d}, E'_d, ψ_{2q}) and turbines (P_{HP}, P_{LP}). Considering a switching tolerance of 0.1 and t_{TOL}=0.1s, the fast variables of exciters,

generators and turbines satisfy the switching criterion at 1.61s, 13.15s and 13.48s, respectively, such that the switching of models occurs at t=13.48s.

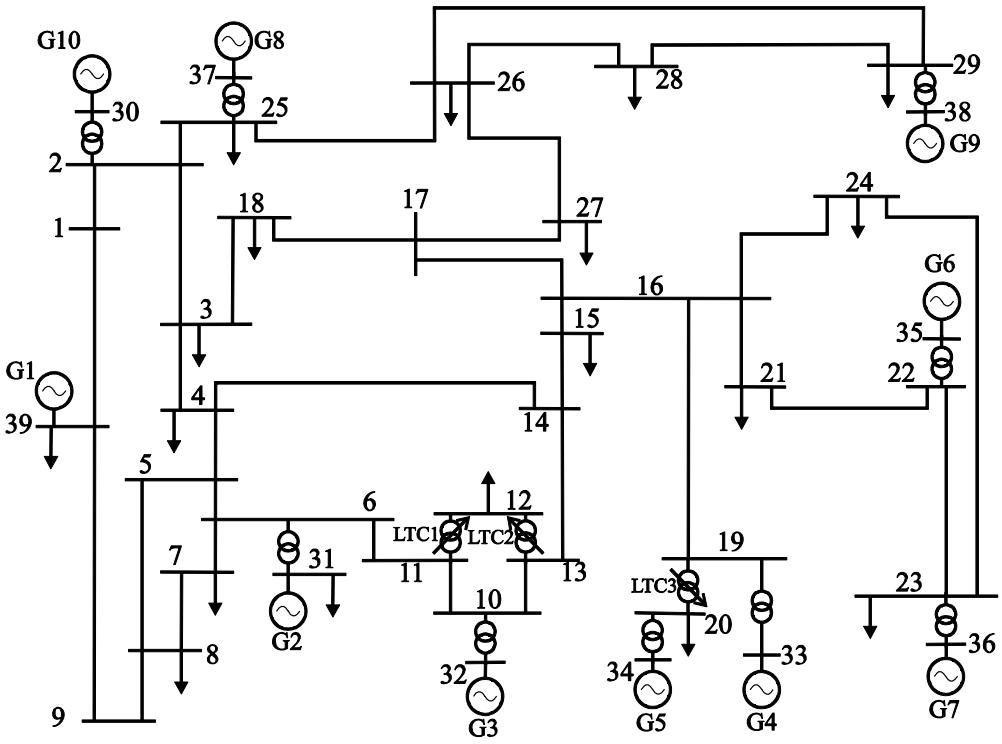

Figure 5.12: New England power system.

The electromechanical oscillations that follow the load shedding are damped out, indicating stable short-term dynamics. Figure 5.13 shows the rotor speed associated with the most critical generator, which is connected at node 34. Note that all the simulations tend to the same equilibrium point after the fast dynamics have been damped out. This demonstrates the suitability of the switching criterion, in the sense that the switching between models is done once the short-term dynamics are small enough, as shown in Figure 5.14, for the field voltage E_{fd} behavior of the generator at bus 34.

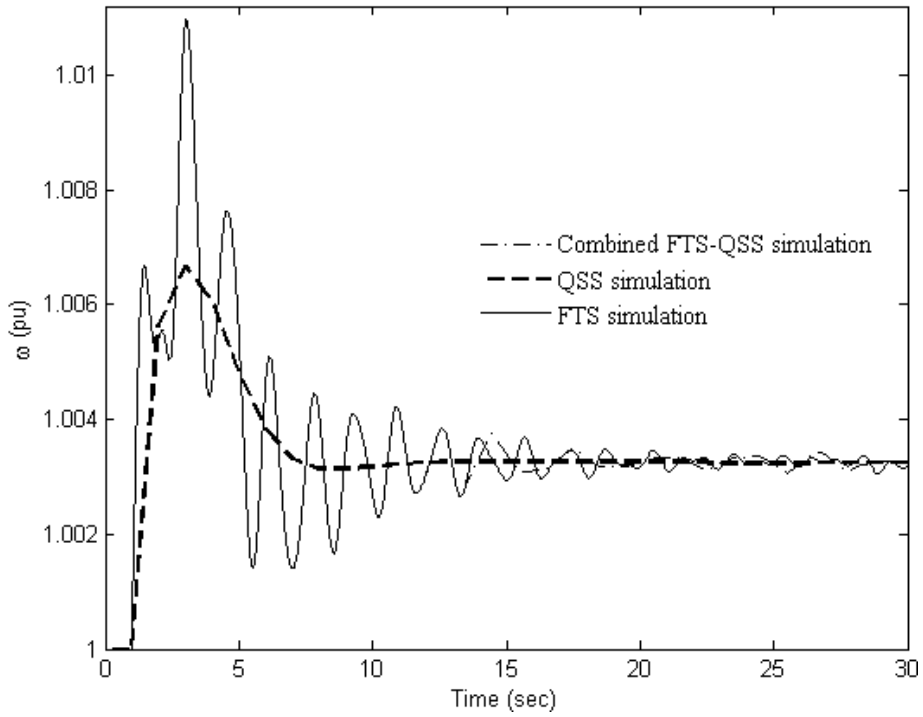

Figure 5.13: Angular speed of the generator connected at bus 34.

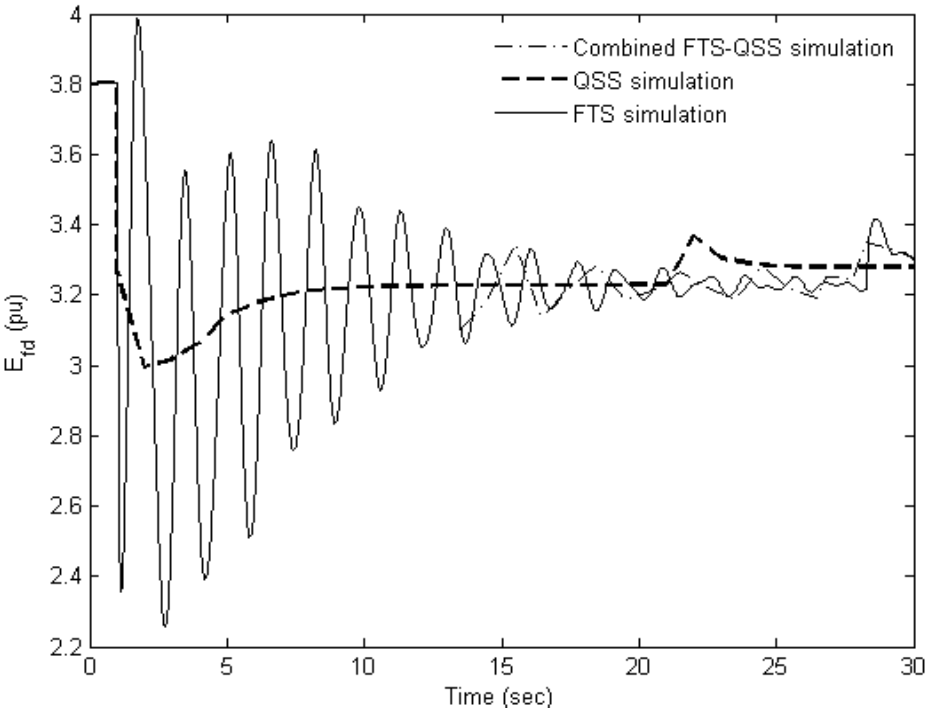

Figure 5.14: Field voltage of the generator connected at bus 34.

As expected, the evolutions of ω and E_{fd} obtained by the FTS and FTS-QSS simulations are overlapped during the short-term period and present small differences after the switching of the simulation models takes place. The numerical Relative Error Magnitude (REM) of the evolutions obtained by the FTS-QSS and QSS simulations with respect to the evolution computed by the FTS simulation are shown in Figures 5.15 and 5.16 for the rotor angular speed and the field voltage of the generator connected at bus 34.

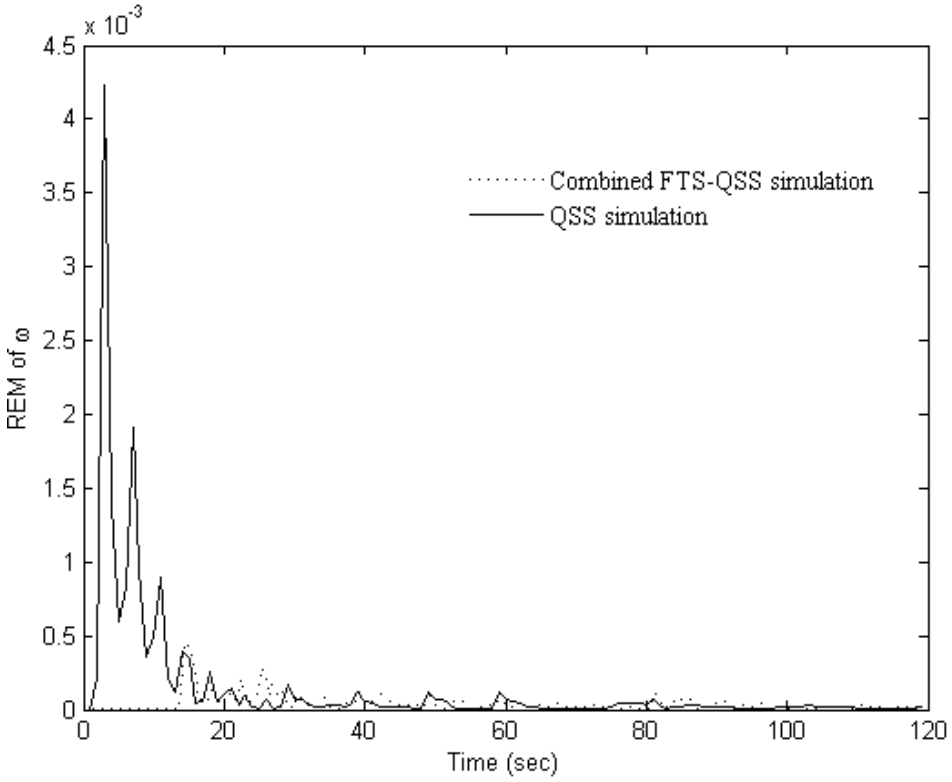

Figure 5.15: REM of the generator's angular speed connected at bus 34.

The REM of ω is quite small for the FTS-QSS and QSS simulations during the whole period of analysis because the disturbance does not cause large excursions of the generator's angular speed connected at bus 34 as shown in Figure 5.13. However, the REM of the field voltage presents large values for the QSS simulation during the short-term but for the long-term these values are small and progressively extinguishes. The peaks presented during the long-term period are due to the changes on the tap ratio of each LTC.

On the other hand, the REM of E_{fd} computed by the FTS-QSS simulation is zero until the switching of the simulation models occurs at t_{sw}, and starts with a small value after t_{sw} but soon decays. Furthermore, the REM obtained by the FTS-QSS simulation can be considered smaller than the REM computed by the QSS simulation during almost the whole period of study.

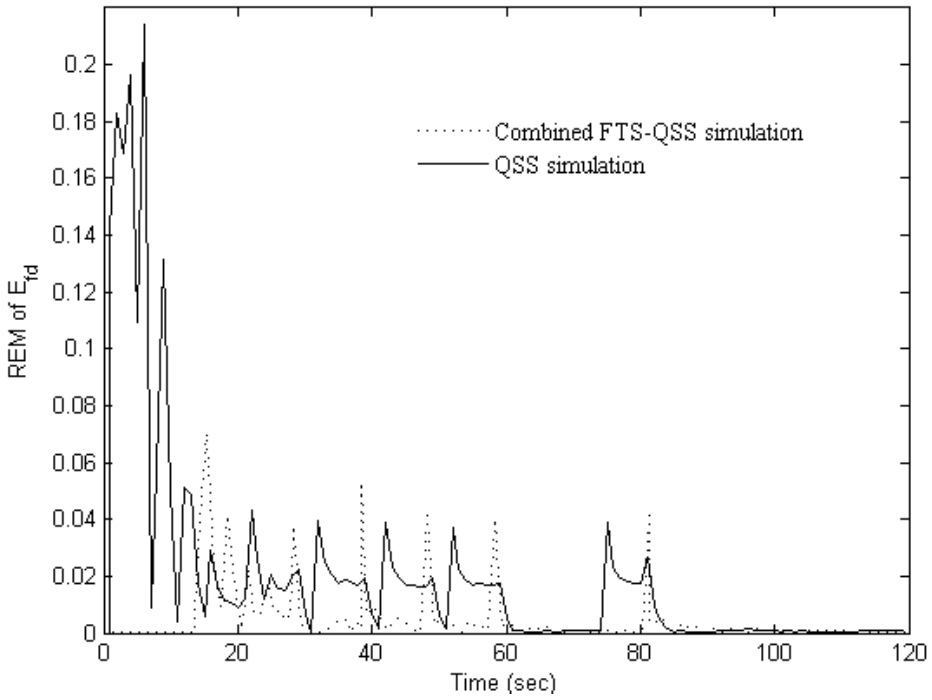

Figure 5.16: REM of the generator's field voltage connected at bus 34.

The evolutions of voltage magnitudes at buses 12 and 20 over a longer time interval are shown in Figures 5.17 and 5.18, respectively, and clearly demonstrate that the proposed approach provides very similar results to those obtained by the FTS simulation. At the instant of the disturbance, an unbalance of reactive power is presented with more generation than that demanded in the system. Therefore, the voltage magnitudes at buses 12 and 20 are increased from their scheduled values. Since the LTC-controlled voltages are deviated from scheduled values, the tap changers are activated with delays. Times at which the LTCs' control takes place are reported in Table 5.4 for each simulation. The control actions occur almost at the same time for the FTS and FTS-QSS simulations. On the other

hand, since the sequence of controls depends on the system dynamics, the LTCs' responses computed by the QSS simulation differ, given that the voltage oscillations at short-term are not captured by this simulation.

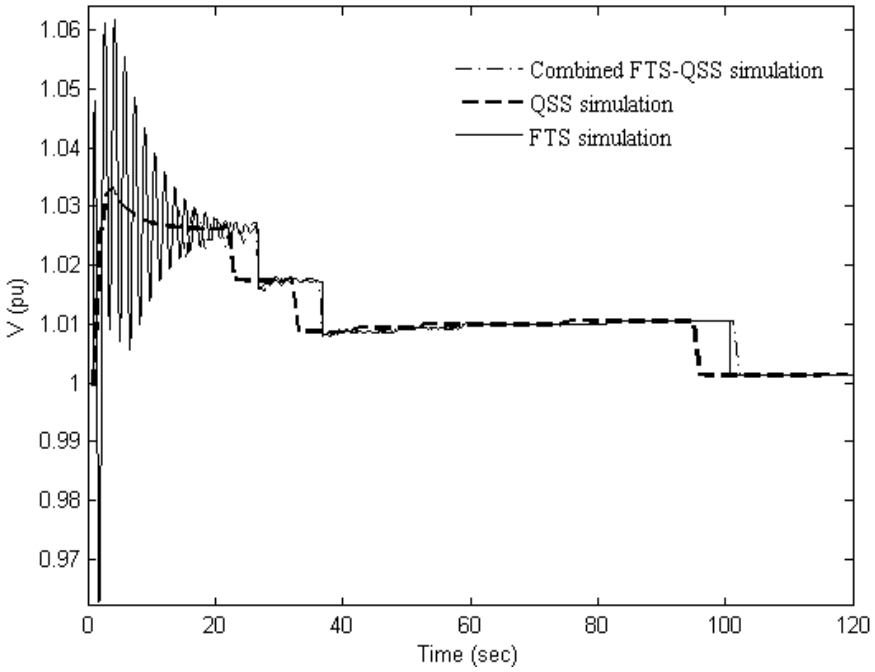

Figure 5.17: Voltage magnitude at bus 12.

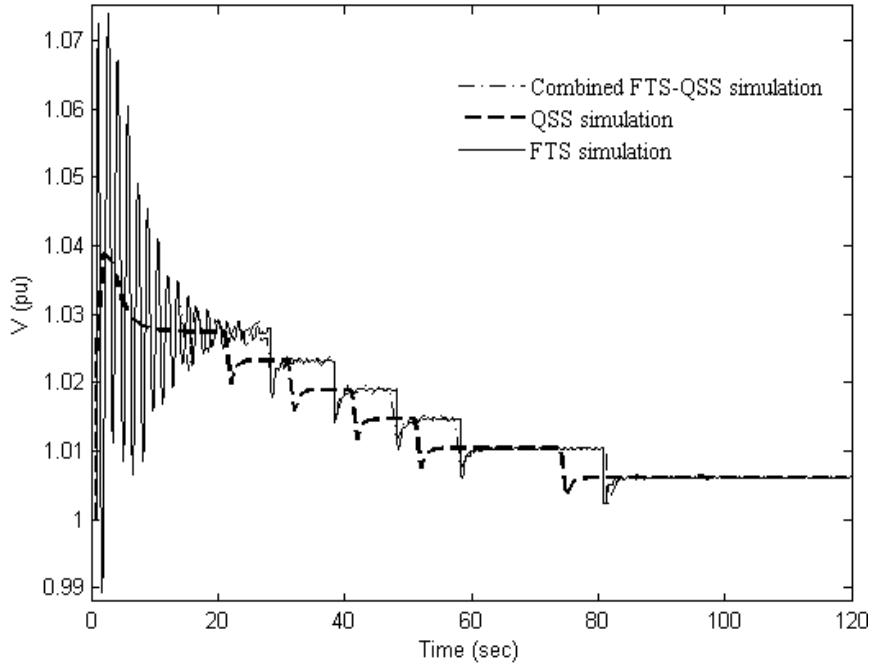

Figure 5.18: Voltage magnitude at bus 20.

Table 5.4: Activation of LTCs control in New England system

LTC1 and LTC2			LTC3		
FTS	QSS	Combined	FTS	QSS	Combined
26.79 s	23 s	26.79 s	28.29 s	22 s	28.29 s
36.79 s	33 s	36.79 s	38.29 s	32 s	38.29 s
100.80 s	96 s	102.29 s	48.29 s	42 s	48.29 s
			58.29 s	52 s	58.29 s
			80.79 s	75 s	81.29 s

Large voltage oscillations are presented during the short-term, causing the LTCs to be initialized at t=6.79 s and t=8.29 s for the control at bus 12 and 20, respectively. This discrete event is correctly captured by the FTS and FTS-QSS simulations while the QSS approximation does not detect the voltage oscillations, and the LTCs are initialized very early for the QSS simulation at t=3 s y t=2 s for the control at bus 12 and 20, respectively. Therefore, the evolution of the voltage magnitudes presents large differences between the results obtained by the QSS simulation and those given by the FTS and FTS-QSS simulations. The numerical REM of the evolutions obtained by the FTS-QSS and QSS simulations with respect to the evolution computed by the FTS simulation are shown in Figures 5.19 and 5.20 for the voltage magnitudes at buses 12 and 20.

The REM of the voltage magnitudes at buses 12 and 20 present large values for the QSS simulation during the short-term; however, for the long-term these values are decreased while the FTS-QSS simulation computes small values of the REM at the switching time. After this instant, the FTS-QSS simulation presents a quickly decay of the REM. Note that the REM obtained by the proposed approach can be considered smaller than the REM computed by the QSS simulation during almost the whole period of analysis, which demonstrates the suitability of the FTS-QSS simulation.

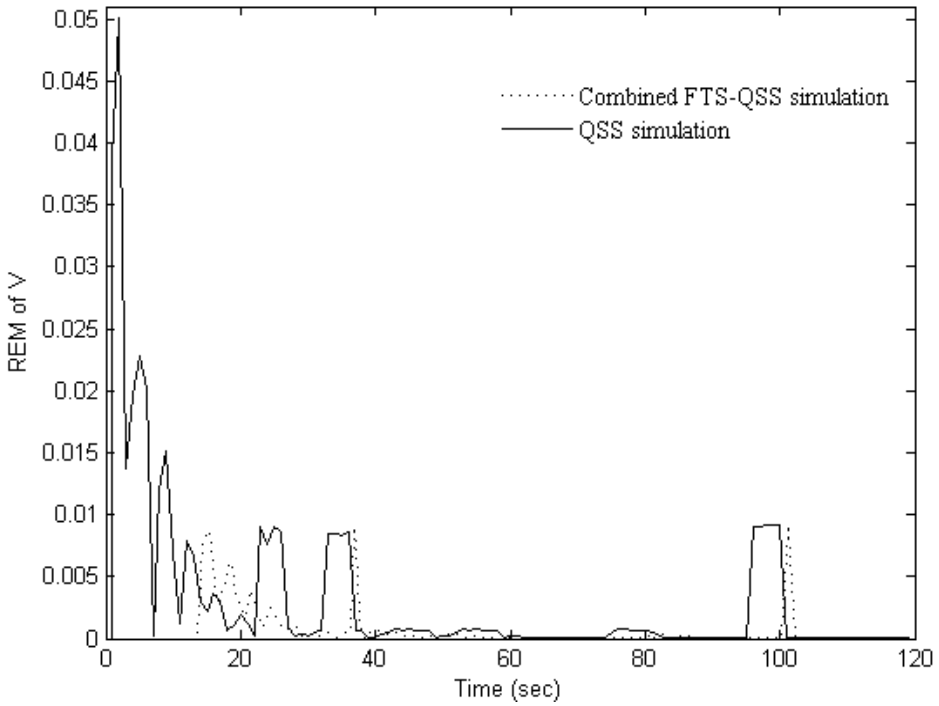

Figure 5.19: REM of voltage magnitude at bus 12.

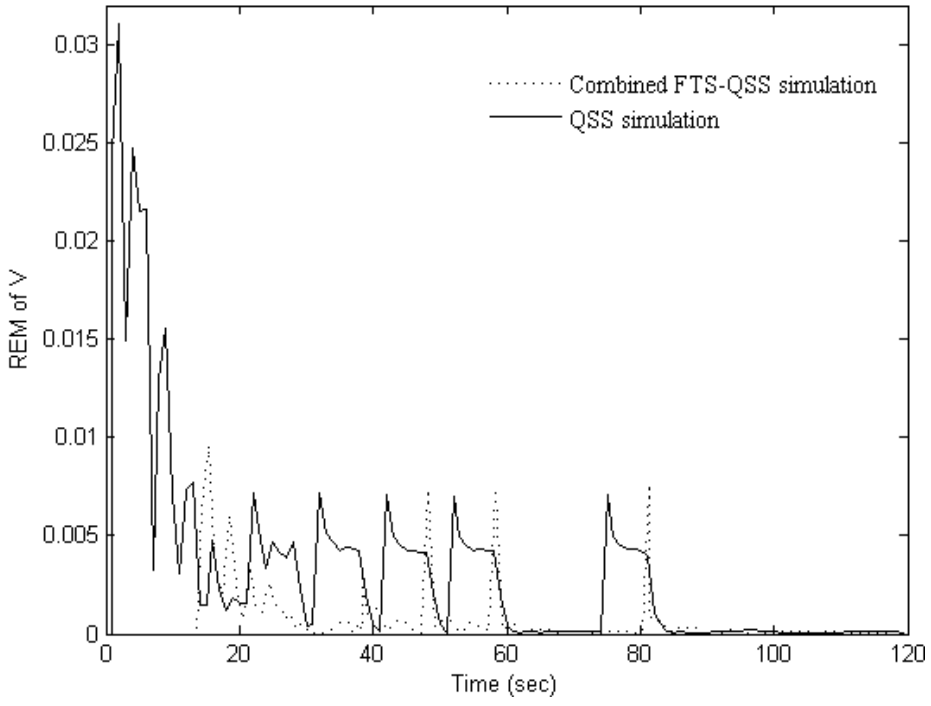

Figure 5.20: REM of voltage magnitude at bus 20.

On the other hand, the angular speed ω_{COI} of the Center-of-Inertia is shown in Figure 5.21. As expected, the frequency transient behavior computed by the QSS model quickly tends to the equilibrium value reached by the other two models. The resulting frequency deviation after the perturbation is very small due to the fast operation of the speed governor of each generator.

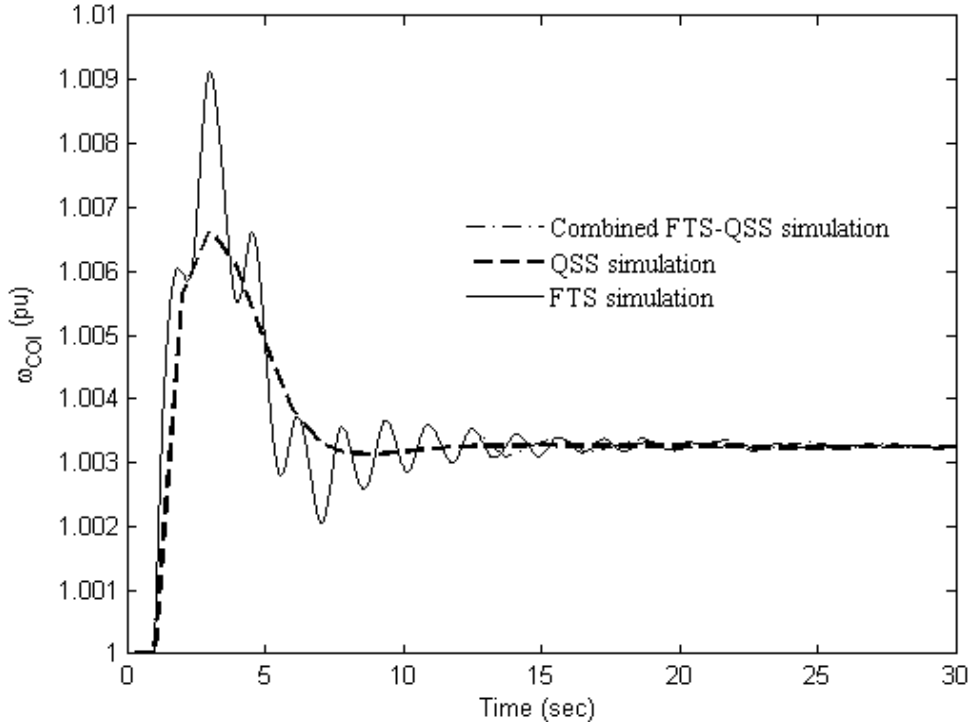

Figure 5.21: Angular speed in COI coordinates.

Lastly, the evolution of the angular speed of all generators computed by the FTS, FTS-QSS and QSS simulations are shown in Figures 5.22, 5.23 and 5.24, respectively. Note that the FTS and FTS-QSS simulations are performed considering that each generator conserves its own angular speed while a perfect coherence is assumed for the QSS simulation. However, the equilibrium point achieved by the three simulations is very close.

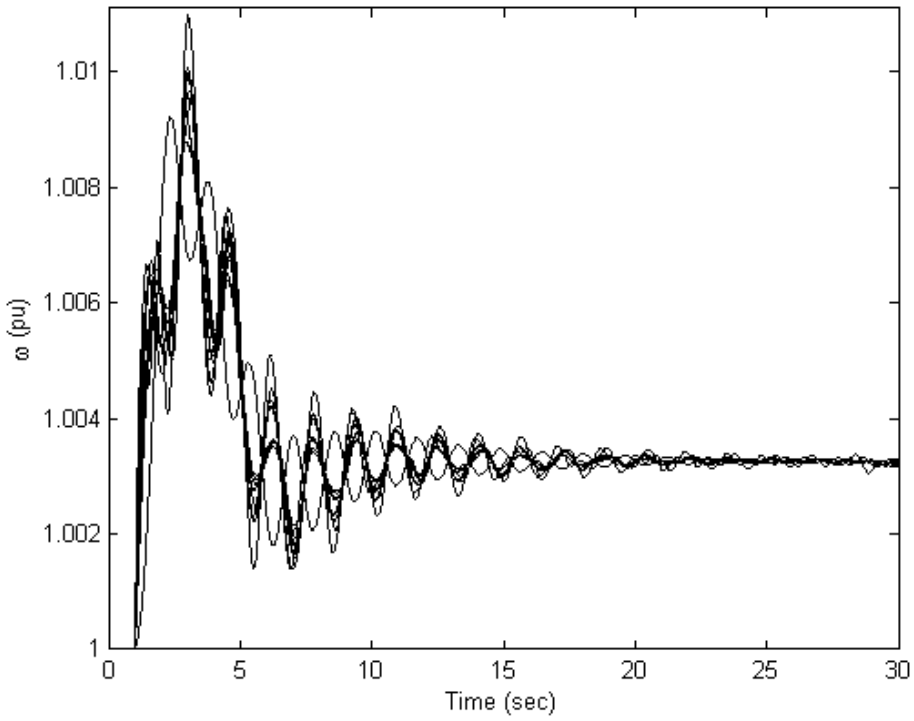

Figure 5.22: Individual angular speed computed by the FTS simulation.

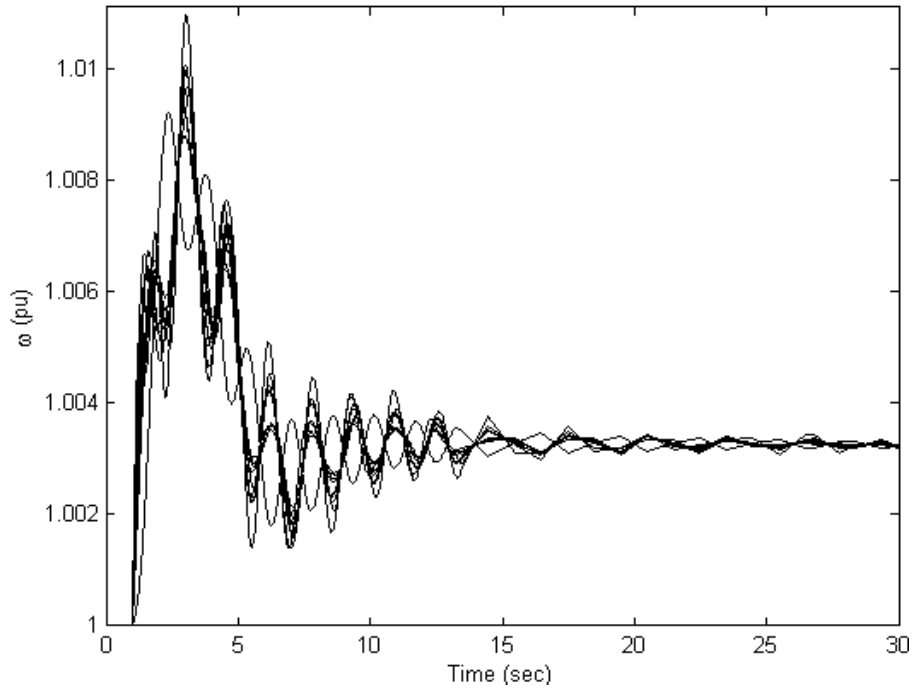

Figure 5.23: Individual angular speed computed by the FTS-QSS simulation.

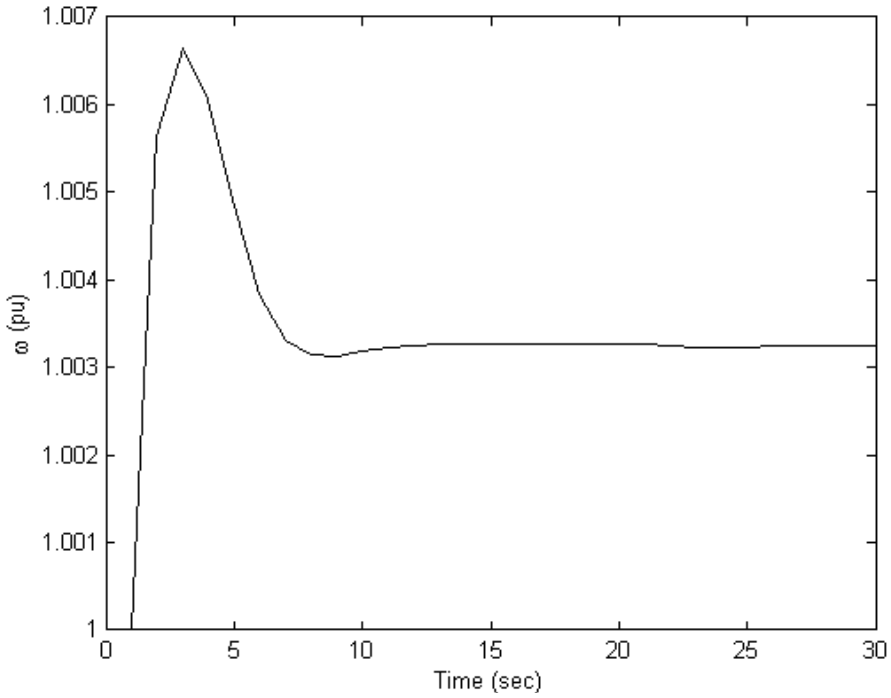

Figure 5.24: Individual angular speed computed by the QSS simulation.

5.5 46-machine, 190-bus Mexican power system

The proposed approach has been applied to a reduced model of the Mexican Interconnected System including the northern, north-eastern, western, central and south-eastern areas, as shown in Figure 5.25 [González et al., 2009]. This equivalent consists of 190 buses, 46 generators, 90 loads and 265 transmission lines operating at voltage levels ranging from 400 kV to 115 kV. Voltage problems are acute and of prime importance due to the longitudinal structure of the system, such that the loads connected at buses 182, 183 and 184 have been equipped with LTCs to maintain their voltage magnitude at 1 p.u. with a half-deadband of ± 0.01 p.u. The operation of the LTCs start after a first delay of 20 s, and subsequently after each 10 s, until the voltage target or the tap ratio limit is achieved. All system data are taken from [Messina and Vittal, 2005], while the LTCs data are given in Appendix D.5.

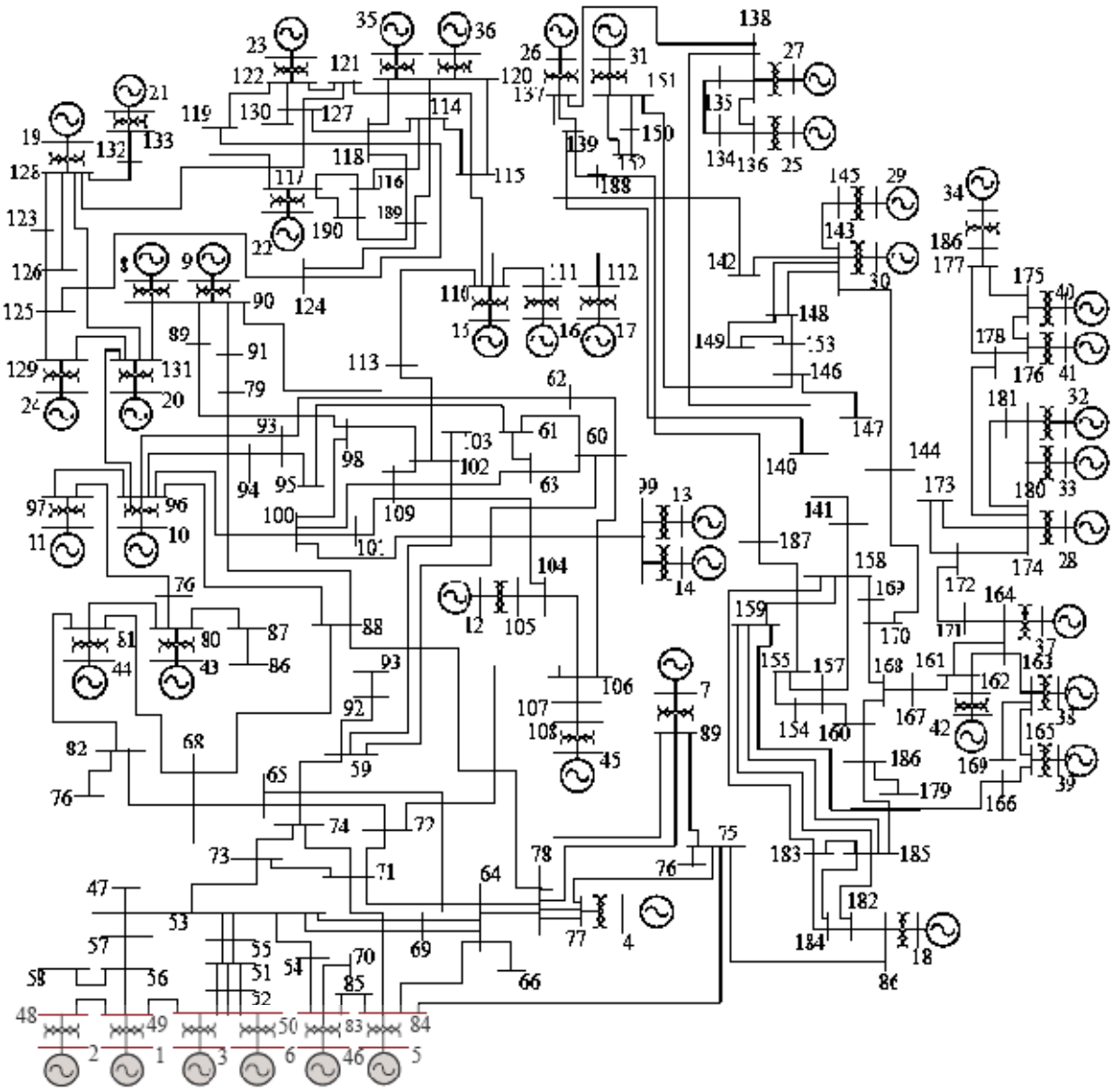

Figure 5.25: Schematic diagram of the Mexican power system.

The long-term study scope is to compute the system's dynamic responses caused by the following sequence of disturbances: i) a solid three-phase fault is applied at bus 185 at 1 s and cleared by tripping the line connecting the buses 185-159 at t = 1.12 s, and ii) the

generator 18 is tripped at 6 s. The analysis is performed for the integration interval $T=[0,280]\,s$ with both FTS and FTS-QSS simulations considering ω_s as the rotating frame of reference and assuming that each generator conserves its own rotating speed (i.e. coherency between all generators is not assumed). The FTS simulation uses an integration step size of 0.01 s, while the proposed FTS-QSS simulation permits the use of a time step of 1 s after the switching time which is satisfied at *t*=13.36 s, considering a switching tolerance of 0.1 and $t_{TOL}=1s$. At this time the fast modes x_{fd}^{sm} have died out, and the system behavior is determined by the slow variables. The fast-state variables monitored to carry out the switching from the FTS to the QSS model are those associated with the exciters (E_{fd}), generators (ψ_{1d}, E'_d, ψ_{2q}) and turbines (P_{HP}, P_{LP}), such that the fast variables of generators, exciters and turbines satisfy the switching criterion at 3.96 s, 8.42 s and 13.36 s, respectively.

As a result of the first perturbation, the angular speed ω_{COI} presents large oscillations due to the existing unbalance of mechanical and electrical powers; however, the fault's clearing time allows the preserving of the short-term stability, and the system tries to find a new state of operation. However, the second disturbance causes a large deviation of the ω_{COI} from the nominal speed ω_0, such that the speed governors act to restore the frequency close to its nominal value as shown in Figure 5.26. For clarity, the ω_{COI} evolution is plotted for a period of only 30 s; after this time the frequency is almost at its new steady-state value. As expected, the evolution of the variables obtained by the FTS and FTS-QSS simulations are overlapped before the switching of simulation takes place. After this time, small differences are present during the long-term frame.

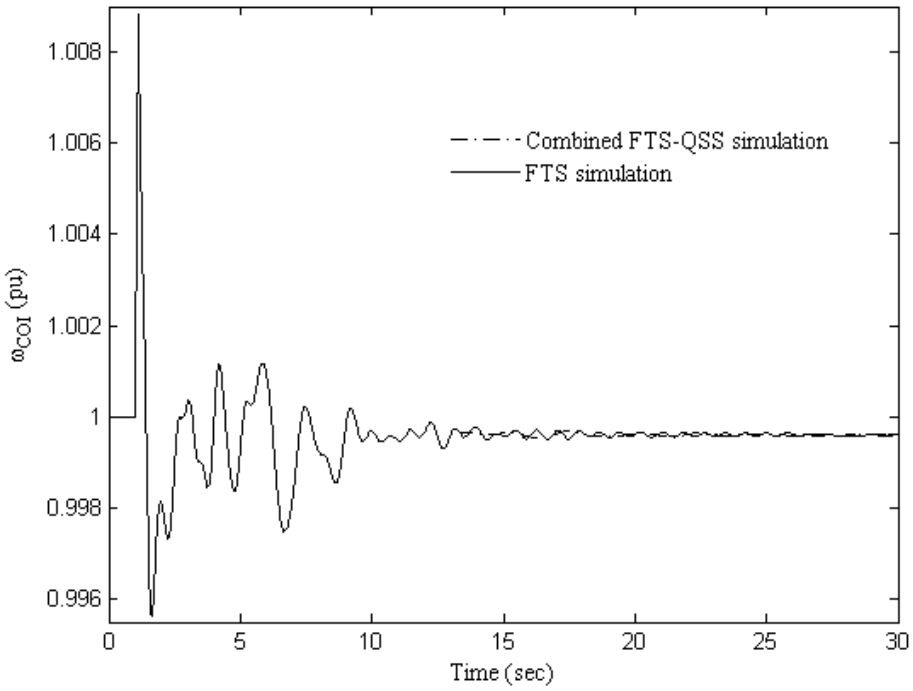

Figure 5.26: Angular speed of the Mexican system.

On the other hand, the voltage magnitude at buses 182, 183 and 184 are kept inside of their deadband after the first disturbance. However, at the instant of the application of the second disturbance these voltage magnitudes decay from their scheduled values because of the existing unbalance of generation and demand reactive powers, such that the LTCs should act to restore the voltage magnitude at their respective bus within the deadband.

The LTC installed at bus 182 tries to restore the voltage magnitude but without success because its tap lower limit of 0.8 p.u. is reached as shown in Figure 5.27. Therefore, the voltage magnitude at bus 182 cannot be controlled after the second perturbation as depicted in Figure 5.28. A similar evolution at bus 183 is presented due to its LTC reaches also the tap lower limit of 0.8 p.u. (see Figure 5.29) and the voltage magnitude cannot be restored as shown in Figure 5.30.

The operation of the LTCs installed at buses 182 and 184 is contrary to the control of the LTC installed at bus 184 because the voltage magnitude at bus 184 is returned to its schedule value, but the changes of the other LTCs causes a degradation on the voltage. Therefore, the LTC installed at bus 184 keeps the voltage magnitude in the schedule value

until the other LTCs reach their tap lower limits. The evolution of the voltage magnitude at bus 184 is shown in Figure 5.31 while the changes on the tap ratio of its LTC are depicted in Figure 5.32.

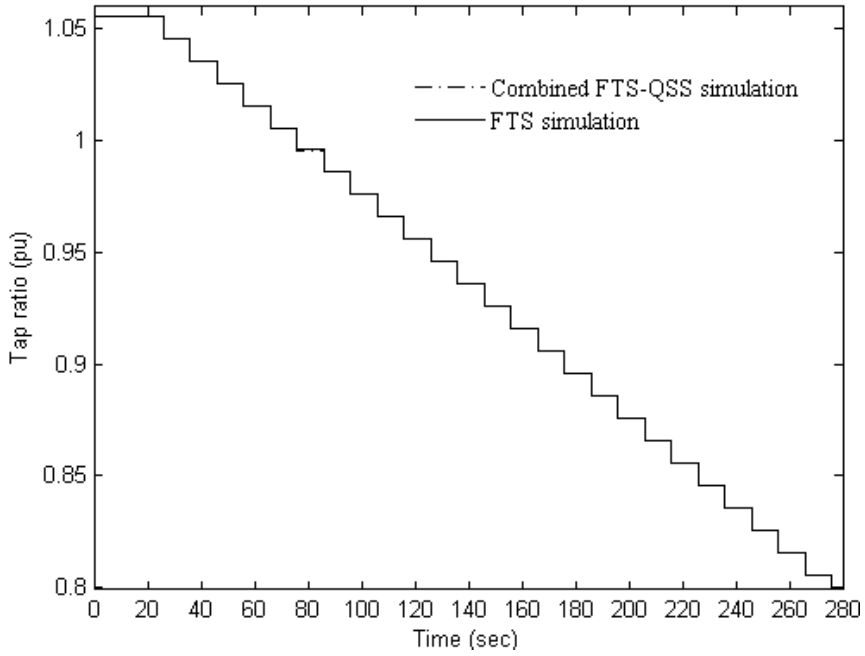

Figure 5.27: Tap ratio evolution of the LTC at bus 182.

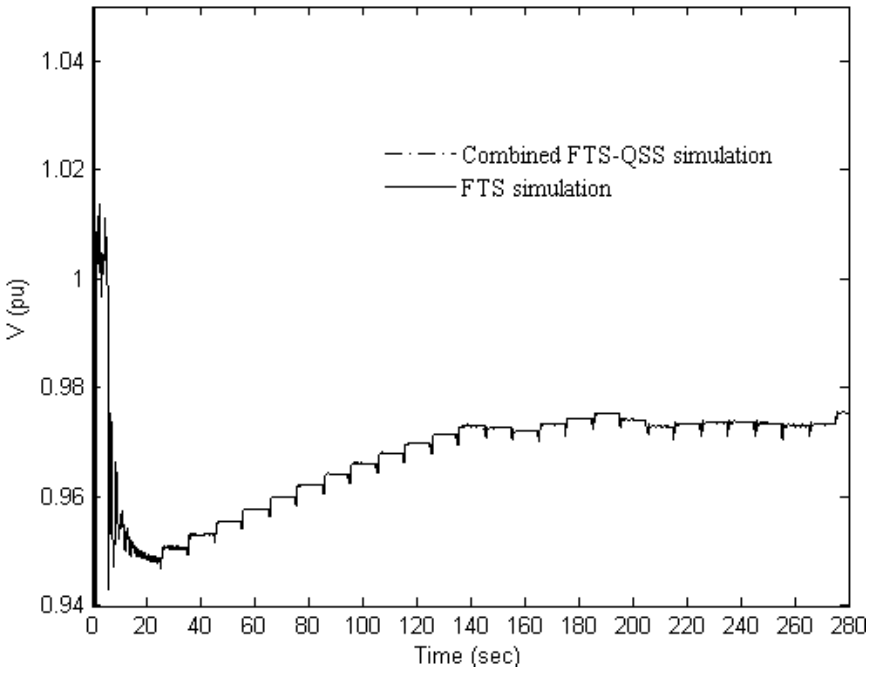

Figure 5.28: Voltage magnitude at bus 182.

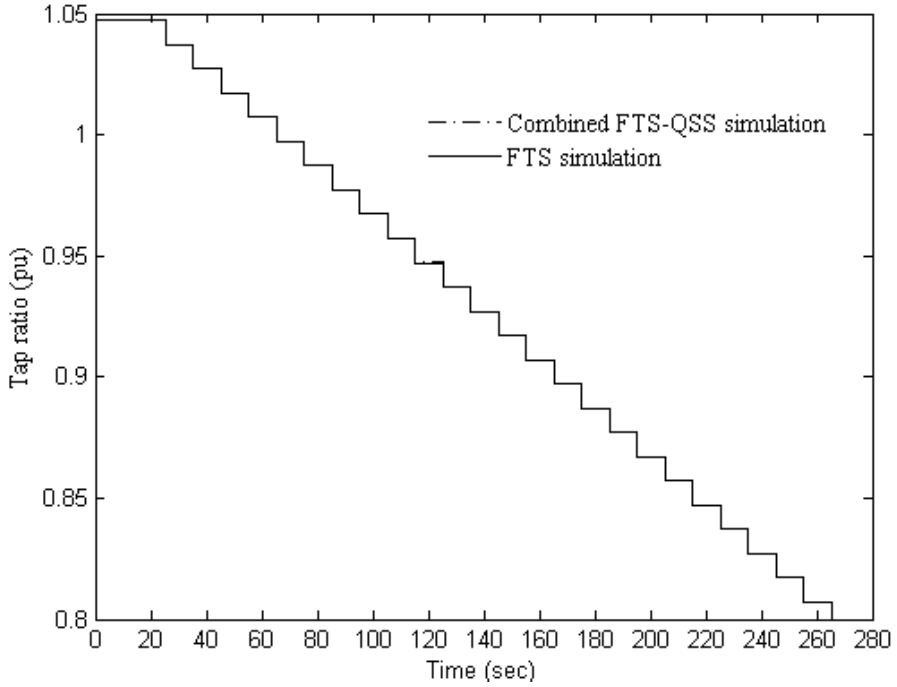

Figure 5.29: Tap ratio evolution of the LTC at bus 183.

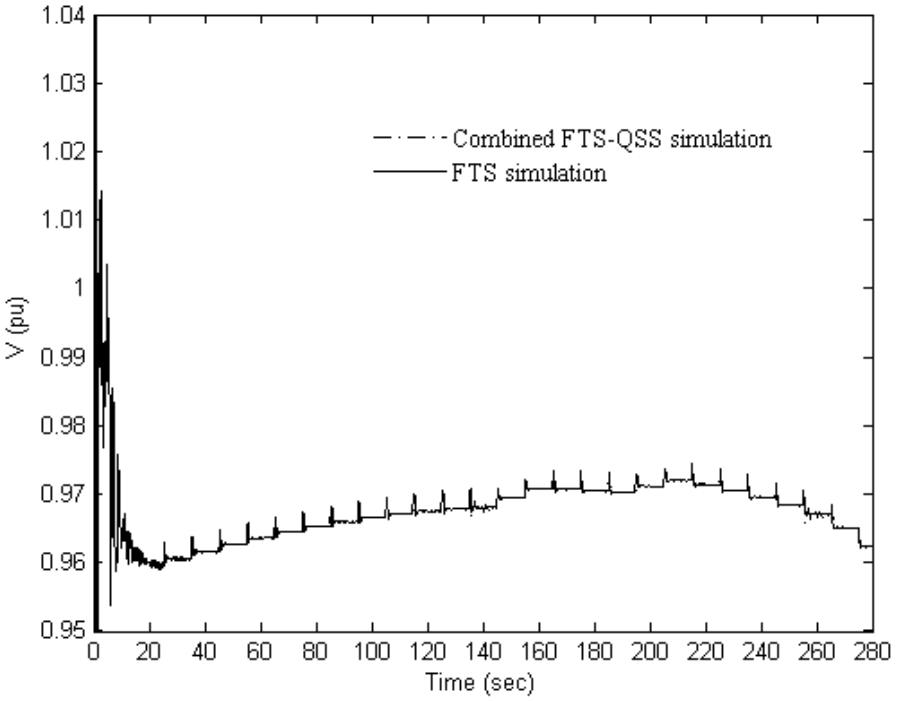

Figure 5.30: Voltage magnitude at bus 183.

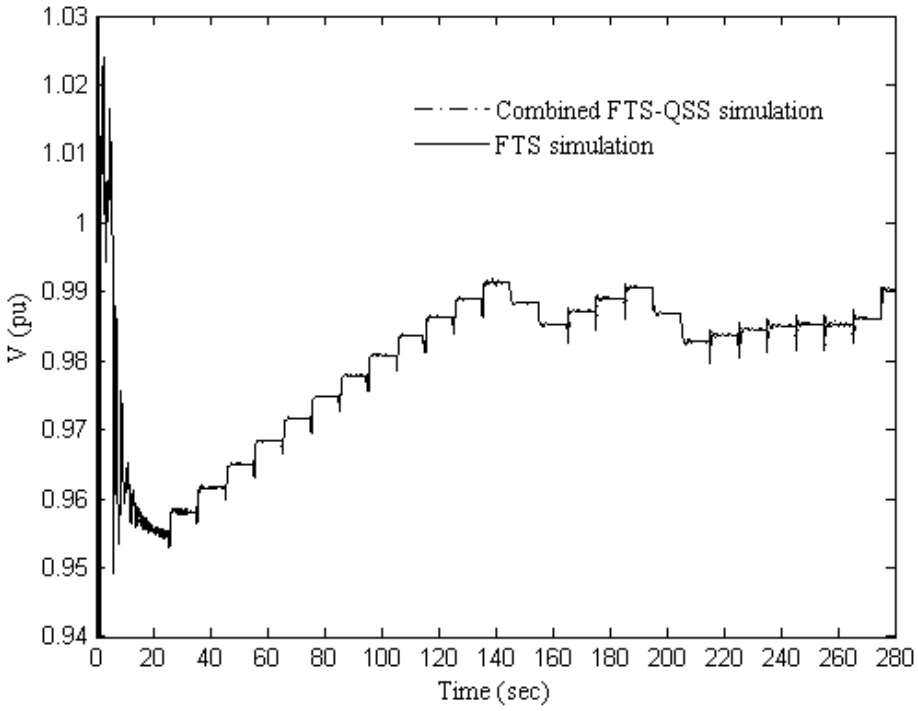

Figure 5.31: Voltage magnitude at bus 184.

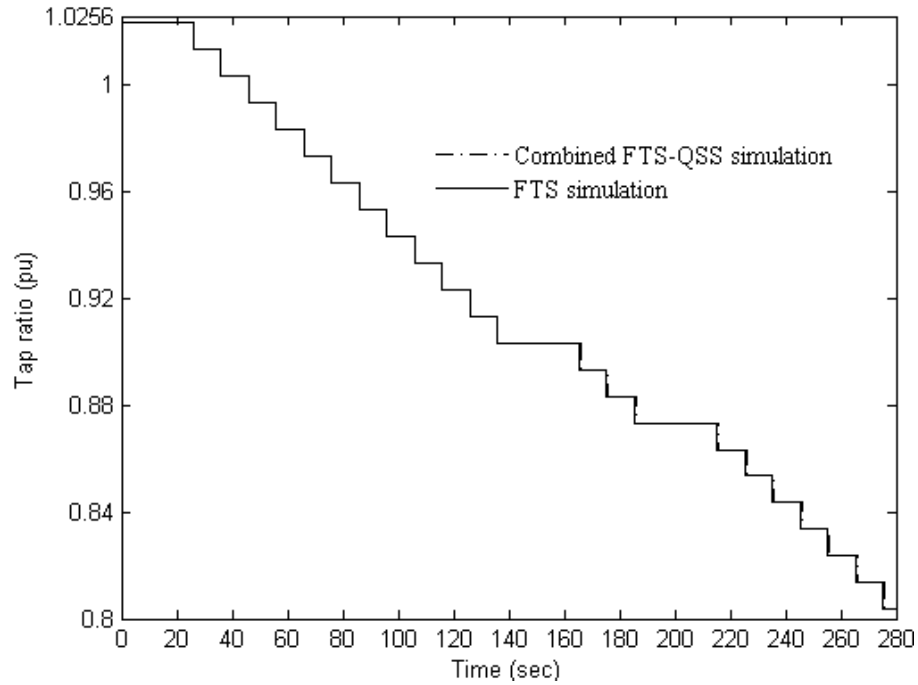

Figure 5.32: Tap ratio evolution of the LTC at bus 184.

The numerical REM of the evolution obtained by the FTS-QSS simulation with respect to the evolution computed by the FTS simulation are shown in Figure 5.33 for the voltage magnitude at bus 184 in order to illustrate the discrepancy between the FTS-QSS and FTS simulations.

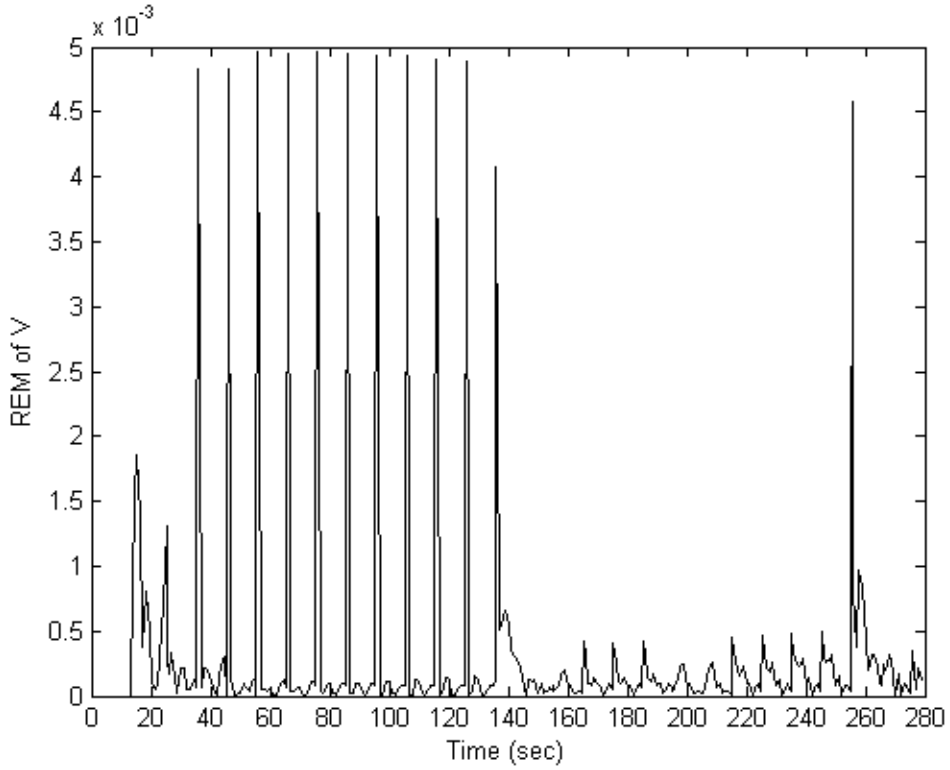

Figure 5.33: REM of voltage magnitude at bus 184.

The REM of the voltage magnitude at bus 184 is quite small after the switching of simulations occurs while the peaks presented during the long-term are due to the changes on the tap ratio of each LTC. As can be seen, the FTS-QSS evolution is a very good approximation of the FTS one, such that from a practical viewpoint the proposed method is suitable for the simulation of long-term dynamics including discrete events. Both FTS and combined FTS-QSS simulation tend to the same equilibrium point.

Lastly, the computing times required by the FTS and FTS-QSS simulations were 200.86 s and 17.937 s, respectively, being the proposed method 11.2 times faster than the

FTS simulation. For these cases, the number of iterations required by the Newton-Raphson method to reach the solution of the linearized set of equations at each time step of both types of dynamic simulations is shown in Figure 5.34. The convergence criterion was 10^{-6} p.u. These results indicate that the algorithms retain the quadratic convergence of the full Newton-Raphson method and that after a switching takes place, the maximum number of iterations for both simulations is 3 after the perturbation. This clearly demonstrates the suitability of the proposed approach to perform long-term dynamic studies.

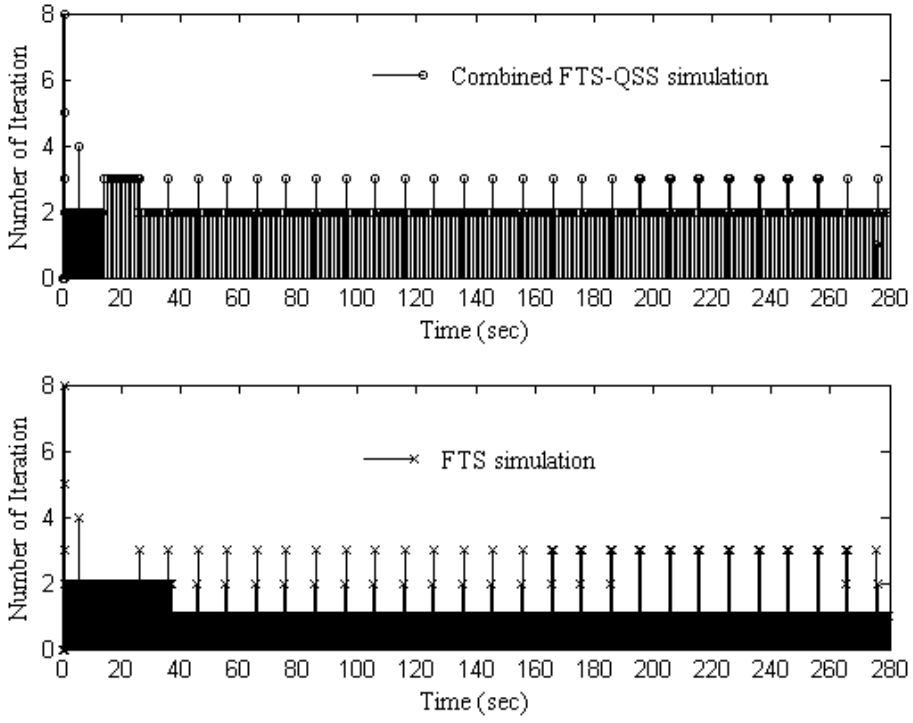

Figure 5.34: Newton iterations for each integration time step.

5.6 Conclusions

In this Chapter the proposed approach to carry out the long-term dynamic simulation of power systems has been tested to demonstrate its suitability to reduce the huge computational burden associated with FTS simulation.

Comparisons between the proposed approach, FTS and QSS methods clearly show the main advantages of the FTS-QSS simulation in terms of the accuracy of the results in both short-term and long-term periods and of the reduction of simulation time required to compute the long-term system dynamics.

Chapter 6

GENERAL CONCLUSIONS AND SUGGESTIONS FOR FUTURE RESEARCH WORK

6.1 General conclusions

A new and simple criterion to accurately determine when a QSS model of a power system can be considered as a uniform approximation of the system's FTS model has been proposed in this thesis based on the singular perturbation and the two-time scales theories. The proposed switching criterion is easily computed (with very low computational overhead) from the FTS simulation by monitoring the rate of change of the fast time-varying state variables.

On the basis of the suitability of this criterion, an integrated simulation method that combines the reliability of FTS simulation and the efficiency of the QSS simulation has been proposed to speed up the long-term stability analysis of power systems considering the presence of discrete events. The method is capable of assessing instability problems during the short-term period through the FTS simulation. If the fast modes of oscillation are damped out, a model reduction is automatically carried out to analyze the long-term dynamics by the QSS simulation with a larger time step size of integration. Therefore the proposed approach allows the long-term dynamic stability analysis of power system efficiently by both time step size adjustment and model reduction. In this context, initial conditions for the QSS simulation are given by the values of the state and algebraic variables provided by the FTS simulation at the switching time.

The proposed approach avoids the following limitations associated with a pure QSS simulation: i) after a large disturbance, the system may lose stability in the short-term time frame in terms of the loss of synchronism or voltage instability. In this case, the QSS model meets a singularity. On the other hand, the switching criterion is never satisfied (i.e. the simulation stops) in the proposed approach, such that the switching from FTS to QSS simulation does not takes places; ii) the activation of control schemes (e.g. load tap changer, overextension limiters, shunt compensation switching, etc.), which have great impact on the system long-term evolution, depends on the system short-term dynamics. These dynamics are incorrectly identified from the simplified QSS model, producing an erroneous activation of discrete controllers during the long-term simulation. Hence, the long-term dynamics computed by a QSS simulation will be different with respect to the dynamic trajectories computed by the proposed approach; and iii) finally, the proposed approach allows to perform a dynamic simulation considering that each generator conserves its own rotating speed instead of assuming a perfect coherency between all generators, as considered in the pure QSS simulation.

The effectiveness of the proposed method has been fully validated by a numerical example on the following: 2-machine, 4-bus system; 3-machine, 9-bus WSCC system; and 10-machine, 39-bus New England system. Simulation results from a test on a reduced 46-machine, 190-bus Mexican interconnected system have also shown the applicability of the proposal to efficiently analyze long-term dynamics of a real-life power system.

6.2 Suggestions for future research work

The proposed approach of power system simulation has demonstrated its correct operation. However, interesting suggestions for future research work can be derived from the work presented in this thesis in order to enhance and improve the computational efficiency of the long-term simulation:

- As already mentioned, FTS simulation should be performed with a small step size when the Trapezoidal Rule is used [Yang and Ajjarapu, 2006] while the Backward Euler method allows a significant increase in the step size, and it saves a lot of computational effort for the long-term dynamic simulation [Van Cutsem and Vournas, 1998]. However, the TR gives more accurate results w.r.t. the BE method. Therefore, the proposed approach can be used to combine both the TR and the BE integration method for long-term dynamic studies preserving the power system detailed model (i.e. FTS are solved during the whole simulation).

- The Area Interchange Control (AIC) of an interconnected power system is very important in studies of long-term simulation. Thus, the methodology and digital program can be adjusted to include AIC.

- Another interesting application is to modify the digital program in order to develop a variable step size integration method using the proposed switching criterion.

- Singular perturbation technique can be used to develop reduced models that can replace the detailed models during the FTS simulation to save even more computational time to perform the long-term simulation.

- It is necessary to find a switching criterion from the QSS simulation to the FTS simulation if the fast variables are excited during the long-term period.

- It is important the inclusion of a static load model that considers frequency dependence into the digital program for long-term analysis. The bus frequency can be computed by taking the numerical derivative of the bus voltage angle since it is not an inherent variable in the dynamic simulation.

BIBLIOGRAPHY

[Acha et al., 2004]

E. Acha, C. Fuerte-Esquivel, H. Hambriz-Pérez and C. Ángeles-Camacho, "FACTS: Modelling and Simulation in Power Networks", London, England: John Wiley & Sons Ltd, 2004.

[Anderson and Fouad, 1994]

M. P. Anderson and A. Fouad, "Power System Control and Stability", IEEE Press, 1994.

[Astic et al., 1994]

J. Y. Astic, A. Bihain and M. Jerosolimski, "The mixed Adams-BDF variable step size algorithm to simulate transient and long term phenomena in power systems", *IEEE Trans. on Power Syst.*, Vol. 9, No. 2, pp. 929-935, May 1994.

[Cate et al., 1984]

E. G. Cate, K. Hemmaplardh, J. W. Manke and D. P. Gelopulos, "Time frame notion and time response of the models in transient, mid-term and long term stability programs", *IEEE Trans. on Power App. and Syst.*, Vol. PAS-103, No.1, pp. 143-151, Jan. 1984.

[Chen, 1996]

M.-S. Chen, "Modeling and Analysis of Modern Power System: The Fundamental of GenCo TransCo DistCo & PoolCo", 1996.

[Chow, 1982]

J. H. Chow, "Time-scale modeling of dynamic networks with applications to power systems", Berlin:Springer-Verlag, 1982.

[de Mello et al., 1992]

F. P. de Mello, J. W. Feltes, T. F. Laskowski and L. J. Oppel, “Simulating fast and slow dynamic effects in power systems”, *IEEE Computer Applications in Power*, Vol. 5, No. 3, pp. 33-38, July 1992.

[Elgerd and Van der Puije, 1998]

O. I. Elgerd and P. D. Van der Puije, “Electric Power Engeneering”, New York: Chapman & Hall, 1998.

[Fabozzi ans Van Cutsem, 2011]

D. Fabozzi and T. Van Cutsem, “On Angle References in Long-Term Time-Domain Simulations” *IEEE Trans. on Power Syst.*, Vol. 26, No. 1, pp. 483-484, Feb. 2011.

[Frowd et al., 1982]

R. J. Frowd, J. C. Giri and R. Podmore, “Transient stability and long-term dynamics unified”, *IEEE Trans. on Power. App. and Syst.*, Vol. PAS-101, No.10, pp. 3841-3850, Oct. 1982.

[Fuerte-Esquivel, 1997]

C. R. Fuerte-Esquivel, “Steady State Modelling and Analysis of Flexible AC Transmission Systems”, PhD Thesis, Glasgow Scotland: Department of Electronics and Electrical Engineering, 1997.

[González et al., 2009]

M. J. González, A. Cañizares and J. M. Ramírez, “Stability modeling and comparative study of series vectorial compensators”, *IEEE Trans. Power Delivery*, Vol. 25, No. 2, pp. 1093-1103, Dec. 2009.

[Grenier et al., 2005]

M.-E. Grenier, D. Lefebvre and T. Van Cutsem, “Quasi steady-state models for long-term voltage and frequency dynamics simulation”, *in: Proc. IEEE Power Tech Conf.*, pp.1-8. St Petersburg, June 2005.

[IEEE Committee Report, 1973]

IEEE Committee Report, “Dynamic models for steam and hydro turbines in power system studies”, *IEEE Trans. On Power App. and Syst.*, Vol. 96, No. 5, pp. 1904-1915, Feb. 1973.

[IEEE Task Force, 1993]

IEEE Task Force., “Load Representation for Dynamic Performance Analysis”, *IEEE Trans. on Power Syst.*, Vol. 8, No. 2, pp. 472-482, May 1993.

[IEEE Task Force, 1995]

IEEE Task Force, “Standard Load Models for Power Flow and Dynamic Performance Simulation”, *IEEE Trans. on Power Syst.*, Vol. 10, No. 3, pp. 1302-1313, Aug. 1995.

[Kokotovic et al., 1986]

P. Kokotovic, H. K. Khalil and J. O´Reilly, “Singular Perturbation Methods in Control: Analysis and Design”, London: Academic Press, 1986.

[Krause et al., 2002]

P. C. Krause, O. Wasynczuk and S. D. Sudhoff, “Analysis of Electric Machinery and Drive Systems”, New York: IEEE Press, 2002.

[Khaitan et al., 2008]

S. K. Khaitan, J. D. McCalley and Q. Chen, “Multifrontal Solver for Online Power System Time-Domain Simulation”, *IEEE Trans. on Power Syst.*, Vol. 23, No. 4, pp. 1727-1737, Nov. 2008.

[Kundur, 1994]

P. Kundur, “Power System Stability and Control”, New York: McGraw-Hill, 1994.

[Kundur et al., 2004]

P. Kundur, J. Paserba, V. Ajjarapu, G. Andersson, A. Bose, C. Canizares, N. Hatziargyriou, D. Hill, A. Stankovic, C. Taylor, T. Van Cutsem and V. Vittal, “Definition and Classification on Power System Stability”, *IEEE Trans. on Power Syst.*, Vol. 19, No. 2, May 2004.

[Lesieutre et al., 1995]

B. Lesieutre, P. W. Saure and M. A. Pai, “Development and Comparative Study of Induction Machine Based Dynamic P, Q Load Models”, *IEEE Trans. on Power Syst.*, Vol. 10, No. 1, pp. 182-191, Feb. 1995.

[Lima Lopes and Zambroni de Souza, 2010]

B. I. Lima Lopes and A. C. Zambroni de Souza, “A Newton approach for long term stability studies in power systems”, *Applied Mathematics and Computation*, Vol. 215, No. 9, pp. 3327-3334, Oct. 2010.

[Loud et al., 2001]

L. Loud, P. Rousseaux, D. Lefebvre and T. Van Cutsem, “A time-scale decomposition-based simulation tool for voltage stability analysis”, *in: Proc. IEEE Power Tech Conf.*, Vol. 2, pp. 1-6, Porto, Portugal, Sep.2001.

[Machowski et al., 2008]

J. Machowski, J. W. Bialek and J. R. Bumby, “Power System Dynamics: Stability and Control”, UK: John Wiley & Sons, 2008.

[Messina and Vittal, 2005]

A. R. Messina, and V. Vittal, “Assessment of nonlinear interaction between nonlinearly coupled modes using higher order spectra”, *IEEE Trans. on Power Syst.*, Vol. 20, No. 1, pp. 375-383, Feb. 2005.

[Pai, 1989]

M. A. Pai, “Energy function analysis for power system stability”, Kluwer, 1989.

[Peponides et al., 1982]

G. Peponides, P. Kokotovic and J. Chow, “Singular perturbations and time scales in nonlinear models of power systems”, *IEEE Trans. on Circuits Syst.*, Vol. CAS-29, No. 11, pp. 758- 767, Nov. 1982.

[Rafian et al., 1987]

M. Rafian, M. Sterling and M. Irving, "Real Time Power System Simulation", *IEE Proceedings*, Vol. 134, No. 3, pp. 206-223, May 1987.

[Ruiz et al., 1999]

D. Ruiz, T. Asiaín and D. Olguín, “A Method for Initializing Induction Motors Modeling During Power System Transient Stability Studies”, *Electric Machines and Drives, International Conference IEMD '99*, pp. 177-179, Seattle, WA, USA, May 1999.

[Ruiz-Vega et al., 2002]

D. Ruiz-Vega, T.I. Asiaín Olivares and D. Olguín Salinas, “An Approach to the Initialization of Dynamic Induction Motor Models”, *IEEE Trans. on Power Syst.*, Vol. 17, No. 3, pp. 747-751, Aug. 2002.

[Sanchez-Gasca et al., 1995]

J. J. Sanchez-Gasca, R. D'Aquila, W. W. Price and J. J. Paserba, “Variable time step, implicit integration for extended-term power system dynamic simulation”, in: Proc. IEEE Power Industry Computer Application Conf., pp. 183-189, May 1995.

[Sauer and Pai, 1998]

P. W. Sauer and M. A. Pai, “Power System Dynamics and Stability”, New Jersey: Prentice Hall, Upper Saddle River, 1998.

[Stubbe et al., 1989]

M. Stubbe, A. Bihain, J. Deude and J. C. Baader, “STAG - A new unified software program for the study of the dynamic behavior of electric power systems”, *IEEE Trans. On Power App. and Syst.*, Vol. 4. No. 1, pp. 129-138 , Feb. 1989.

[Van Cutsem and Mailhot, 1997]

T. Van Cutsem and R. Mailhot, “Validation of a fast voltage stability analysis method on the Hydro-Québec system”, *IEEE Trans. on Power Syst.*, Vol. 12, No. 1, pp. 282-292, Feb. 1997.

[Van Cutsem and Vournas, 1998]

T. Van Cutsem and C. Vournas, “Voltage Stability of Electric Power Systems”, Massachusetts: Kluwer Academic Publishers, 1998.

[Van Cutsem et al., 2006]

T. Van Cutsem, M. E. Grenier and D. Lefebvre, “Combined detailed and quasi steady-state time simulation for large-disturbance analysis”, Electrical Power and Energy Systems, Vol. 28, No. 9, pp. 634-642, Mar. 2006.

[Vournas et al., 2004]

C. D. Vournas, E. G. Potamianakis, C. Moors and T. Van Cutsem, “An Educational Simulation Tool for Power System Control and Stability”, *IEEE Trans. on Power Syst.*, Vol. 19, No. 1, pp. 48-55, Feb. 2004.

[Xu et al., 1998]

X. Xu, R. M. Mathur, J. Jiang, G. J. Rogers and P. Kundur, “Modeling of Generators and Their Controls in Power System Simulations Using Singular Perturbations”, *IEEE Trans. on Power Syst.*, Vol. 13, No. 1, pp. 109-114, Feb. 1998.

[Yang and Ajjarapu, 2006]

D. Yang and V. Ajjarapu, “A decoupled time-domain simulation method via invariant subspace partition for power system analysis”, *IEEE Trans. on Power Syst.*, Vol. 21, No. 1, pp. 11-18, Feb. 2006.

Appendix A

Synchronous machine model

A.1 Generator model of order VI

The generator model used in power system analysis is based on a two-axis formulation of the machine equations considered in Figure A.1. The stator circuit is composed of three identical sinusoidally distributed armature winding, displaced 120°. The rotor circuits comprise a field winding (denoted by *fd*) and three amortisseur windings (denoted by 1*d*, 1*q* and 2*q*). The *1d* winding has the same magnetic axis as the field winding, while the magnetic axis of the *1q* winding (called the quadrature axis) is displaced 90° ahead of the direct axis. Furthermore, eddy currents are represented by the second winding (denoted by *2q*) on the quadrature axis [Van Cutsem, 2005], [Krause et al., 2002].

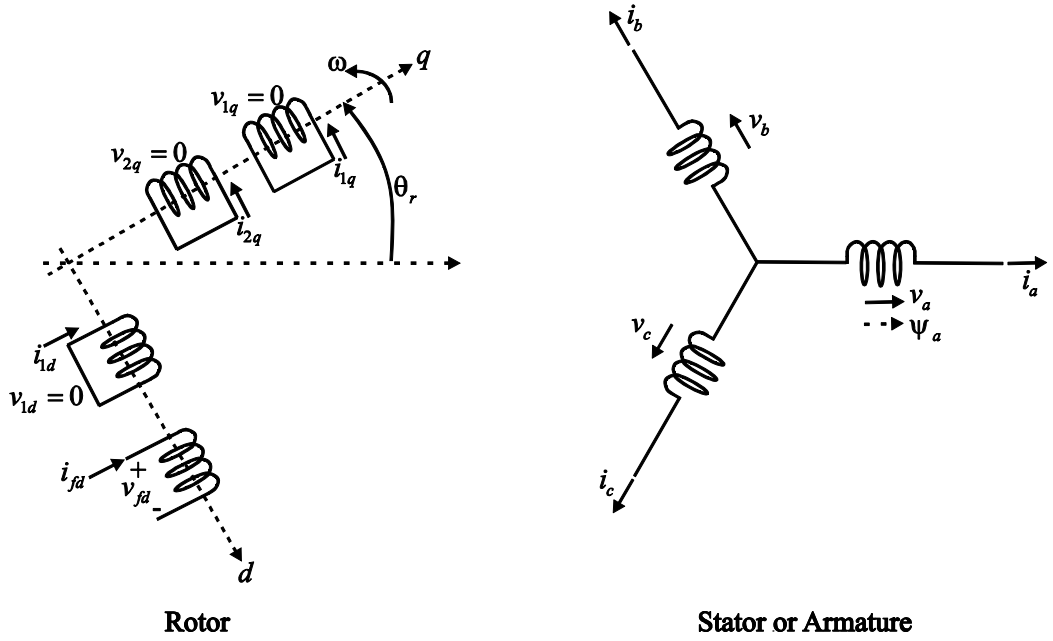

Figure A.1: Schematic diagram of the synchronous machine.

The stator and rotor voltage equations are obtained by applying the fundamental Kirchhoff's and Faraday's laws as well as the Park transformation [Sauer and Pai, 1998], [Krause et al., 2002],

$$V_d = -R_a I_d - \frac{\omega}{\omega_0}\psi_q + \frac{1}{\omega_0}\frac{d\psi_d}{dt} \tag{A.1}$$

$$V_q = -R_a I_q + \frac{\omega}{\omega_0}\psi_d + \frac{1}{\omega_0}\frac{d\psi_q}{dt} \tag{A.2}$$

$$V_{fd} = R_{fd} I_{fd} + \frac{1}{\omega_0}\frac{d\psi_{fd}}{dt} \tag{A.3}$$

$$0 = R_{1d} I_{1d} + \frac{1}{\omega_0}\frac{d\psi_{1d}}{dt} \tag{A.4}$$

$$0 = R_{1q} I_{1q} + \frac{1}{\omega_0}\frac{d\psi_{1q}}{dt} \tag{A.5}$$

$$0 = R_{2q} I_{2q} + \frac{1}{\omega_0}\frac{d\psi_{2q}}{dt}; \tag{A.6}$$

in addition the flux linkages per second are expressed as

$$\psi_d = -X_d I_d + X_{md} I_{fd} + X_{md} I_{1d} \tag{A.7}$$

$$\psi_q = -X_q I_q + X_{mq} I_{1q} + X_{mq} I_{1q} \tag{A.8}$$

$$\psi_{fd} = -X_{md} I_d + X_{fd} I_{fd} + X_{md} I_{1d} \tag{A.9}$$

$$\psi_{1d} = -X_{md} I_d + X_{md} I_{fd} + X_{1d1d} I_{1d} \tag{A.10}$$

$$\psi_{1q} = -X_{mq} I_q + X_{1q1q} I_{1q} + X_{mq} I_{2q} \tag{A.11}$$

$$\psi_{2q} = -X_{mq} I_q + X_{mq} I_{1q} + X_{2q2q} I_{2q} \tag{A.12}$$

where ω_0 is the synchronous speed, and ω is the actual rotor speed. X_{md} and X_{mq} are the d and q magnetizing reactances, respectively, R_s is the stator resistance, V_d is the d winding

voltage, I_d is the *d* winding current and X_d is the *d* leakage reactance. Appropiate variables are also associated with the *q* axis and the rotor circuit.

In accordance with dynamics of interest in the present work, the generator model considered in this work relies on the following assumption [Van Cutsem and Vournas, 1998]:

- The transformer voltages are neglected $(\dot{\psi}_d = \dot{\psi}_q = 0)$.
- The usual speed deviations are small compared to synchronous speed, $(\omega \approx \omega_0)$.
- The armature resistance (which is very small) is neglected.
- Magnetic saturation is neglected for convenience in analysis.

Therefore, under these assumptions the set of equations (A.1)-(A.5) take the following form:

$$V_d = -\psi_q \tag{A.13}$$

$$V_q = \psi_d \tag{A.14}$$

$$\frac{1}{\omega_0}\frac{d\psi_{fd}}{dt} = -R_{fd}I_{fd} + V_{fd} \tag{A.15}$$

$$\frac{1}{\omega_0}\frac{d\psi_{1d}}{dt} = -R_{1d}I_{1d} \tag{A.16}$$

$$\frac{1}{\omega_0}\frac{d\psi_{1q}}{dt} = -R_{1q}I_{1q} \tag{A.17}$$

$$\frac{1}{\omega_0}\frac{d\psi_{2q}}{dt} = -R_{2q}I_{2q}. \tag{A.18}$$

The synchronous machine model can be obtained using the definition of standard synchronous reactances, new state variables and standard time constants [Krause et al., 2002], [Sauer and Pai, 1998], then

$$X_d = X_{ls} + X_{md} \tag{A.19}$$

$$X_q = X_{ls} + X_{mq} \tag{A.20}$$

$$X_{fd} = X_{lfd} + X_{md} \tag{A.21}$$

$$X_{1d} = X_{l1d} + X_{md} \tag{A.22}$$

$$X_{1q} = X_{l1q} + X_{mq} \tag{A.23}$$

$$X_{2q} = X_{l2q} + X_{mq} \tag{5.1}$$

$$X'_d = X_{ls} + \frac{1}{\frac{1}{X_{md}} + \frac{1}{X_{lfd}}} = X_d - \frac{X_{md}^2}{X_{fd}} \tag{A.25}$$

$$X'_q = X_{ls} + \frac{1}{\frac{1}{X_{mq}} + \frac{1}{X_{l1q}}} = X_q - \frac{X_{mq}^2}{X_{1q}} \tag{A.26}$$

$$X''_d = X_{ls} + \frac{1}{\frac{1}{X_{md}} + \frac{1}{X_{lfd}} + \frac{1}{X_{l1d}}} \tag{A.27}$$

$$X''_q = X_{ls} + \frac{1}{\frac{1}{X_{mq}} + \frac{1}{X_{l1q}} + \frac{1}{X_{l2q}}} \tag{A.28}$$

$$E'_q = \frac{X_{md}}{X_{fd}} \psi_{fd} \tag{A.29}$$

$$E'_d = -\frac{X_{mq}}{X_{1q}} \psi_{1q} \tag{A.30}$$

$$E_{fd} = \frac{X_{md}}{R_{fd}} V_{fd} \tag{A.31}$$

$$T'_{do} = \frac{X_{fd}}{\omega_s R_{fd}} \tag{A.32}$$

$$T'_{qo} = \frac{X_{1q}}{\omega_s R_{1d}} \tag{A.33}$$

$$T''_{do} = \frac{1}{\omega_s R_{1d}} \left(X_{ls} + \frac{1}{\frac{1}{X_{md}} + \frac{1}{X_{lfd}}} \right) \tag{A.34}$$

$$T''_{qo} = \frac{1}{\omega_s R_{2q}} \left(X_{ls} + \frac{1}{\frac{1}{X_{mq}} + \frac{1}{X_{l1q}}} \right) \tag{A.35}$$

where E_{fd} can be defined as voltage proportional to the field voltage determined by exciters or as a constant value. The voltage magnitudes behind synchronous *q*- and *d*-axis reactances are E'_q and E'_d. Flux linkages per second related to the damping windings are given by ψ_{1d} and ψ_{2q}. T'_{qo}, T'_{do} and T''_{qo}, T''_{do} are the *q*-, *d*-axis transient and subtransient open-circuit time constant, respectively.

Based on the definitions (A.15)-(A.30) into (A.9)-(A.12), the rotor currents are

$$I_{fd} = \frac{E'_q + (X_d - X'_d)(I_d - I_{1d})}{X_{md}} \tag{A.36}$$

$$I_{1d} = \frac{\left((X'_d - X_{ls})I_d - E'_q\right)\left(X'_d - X''_d\right) + \psi_{1d}}{\left(X'_d - X_{ls}\right)^2} \tag{A.37}$$

$$I_{1q} = \frac{-E'_d + (X_q - X'_q)(I_q - I_{2q})}{X_{mq}} \tag{A.38}$$

$$I_{2q} = \frac{\left((X'_q - X_{ls})I_q + E'_d\right)\left(X'_q - X''_q\right) + \psi_{2q}}{\left(X'_q - X_{ls}\right)^2}. \tag{A.39}$$

On the other hand, the stator currents can be found by substituting the rotor currents equations into (A.7)-(A.8) and the resulting equation into (A.13)-(A.14):

$$I_d = \frac{(X_d'' - X_{ls})}{X_d''(X_d' - X_{ls})} E_q' + \frac{\left(X_d' - X_d''\right)}{X_d''(X_d' - X_{ls})} \psi_{1d} - \frac{V_d}{X_d''} \tag{A.40}$$

$$I_q = -\frac{(X_q'' - X_{ls})}{X_q''(X'_q - X_{ls})} E_d' + \frac{\left(X_q' - X_q''\right)}{X_q''(X_q' - X_{ls})} \psi_{2q} + \frac{V_q}{X_q''}. \tag{A.41}$$

Moreover, the stator voltages can be represented in a complex form as [Sauer and Pai, 1998], [Krause et al., 2002],

$$\left(V_d + jV_q\right) e^{j\left(\delta - \frac{\pi}{2}\right)} = Ve^{j\theta} \tag{A.42}$$

and manipulating (A.42) yields

$$\begin{aligned} V_d &= V \sin\left(\delta - \theta\right) \\ V_q &= V \cos\left(\delta - \theta\right) \end{aligned} \tag{A.43}$$

where V and θ are the magnitude and phase angle of the voltage measured at bus terminal. δ is the generator's rotor angle relative to a certain rotating reference with respect to the quadrature axis, which is defined below.

Therefore, the stator currents can be represented in terms of terminal voltage as

$$I_d = \frac{(X_d'' - X_{ls})}{X_d''(X_d' - X_{ls})} E_q' + \frac{\left(X_d' - X_d''\right)}{X_d''(X_d' - X_{ls})} \psi_{1d} - \frac{V\cos\left(\delta - \theta\right)}{X_d''} \tag{A.44}$$

$$I_q = -\frac{(X_q'' - X_{ls})}{X_q''(X_q' - X_{ls})} E_d' + \frac{\left(X_q' - X_q''\right)}{X_q''(X_q' - X_{ls})} \psi_{2q} + \frac{V\sin\left(\delta - \theta\right)}{X_q''}. \tag{A.45}$$

Hence, the synchronous machine model can be expressed only in terms of meaningful variables and with the least number of equations by introducing the rotor and stator currents equations into (A.15)-(A.18):

$$T_{do}' \frac{dE_q'}{dt} = K_1 E_q' + K_2 \psi_{1d} + K_3 V \cos\left(\delta - \theta\right) + E_{fd} \tag{A.46}$$

$$T''_{do}\frac{d\psi_{1d}}{dt} = K_4 E'_q + K_5\psi_{1d} + K_6 V\cos\left(\delta-\theta\right) \tag{A.47}$$

$$T'_{qo}\frac{dE'_d}{dt} = K_7 E'_d + K_8\psi_{2q} + K_9 V\sin\left(\delta-\theta\right) \tag{A.48}$$

$$T''_{qo}\frac{d\psi_{2q}}{dt} = K_{10} E'_d + K_{11}\psi_{2q} + K_{12} V\sin\left(\delta-\theta\right) \tag{A.49}$$

where

$$K_1 = -1-\frac{\left(X_d - X'_d\right)\left(X'_d - X''_d\right)}{\left(X'_d - X_{ls}\right)^2} - \frac{\left(X_d - X'_d\right)\left(X''_d - X_{ls}\right)^2}{X''_d\left(X'_d - X_{ls}\right)^2} \tag{A.50}$$

$$K_2 = \frac{\left(X_d - X'_d\right)\left(X'_d - X''_d\right)X_{ls}}{X''_d\left(X'_d - X_{ls}\right)^2} \tag{A.51}$$

$$K_3 = \frac{\left(X_d - X'_d\right)\left(X''_d - X_{ls}\right)}{X''_d\left(X'_d - X_{ls}\right)} \tag{A.52}$$

$$K_4 = \frac{X_{ls}}{X''_d} \tag{A.53}$$

$$K_5 = -\frac{X'_d}{X''_d} \tag{A.54}$$

$$K_6 = \frac{X'_d - X_{ls}}{X''_d} \tag{A.55}$$

$$K_7 = -1-\frac{\left(X_q - X'_q\right)\left(X'_q - X''_q\right)}{\left(X'_q - X_{ls}\right)^2} - \frac{\left(X_q - X'_q\right)\left(X''_q - X_{ls}\right)^2}{X''_q\left(X'_q - X_{ls}\right)^2} \tag{A.56}$$

$$K_8 = -\frac{\left(X_q - X'_q\right)\left(X'_q - X''_q\right)X_{ls}}{X''_q\left(X'_q - X_{ls}\right)^2} \tag{A.57}$$

$$K_9 = \frac{\left(X_q - X'_q\right)\left(X''_q - X_{ls}\right)}{X''_q\left(X'_q - X_{ls}\right)} \tag{A.58}$$

$$K_{10} = -\frac{X_{ls}}{X''_q} \tag{A.59}$$

$$K_{11} = -\frac{X'_q}{X''_q} \tag{A.60}$$

$$K_{12} = -\frac{X'_q - X_{ls}}{X''_q}. \tag{A.61}$$

On the other hand, the effect of unbalance between the electromagnetic torque and the mechanical torque of the synchronous machine is obtained by applying the fundamental Newton's law [Sauer and Pai, 1998], [Van Cutsem and Vournas, 1998]:

$$\frac{2H}{\omega_0}\ddot{\delta} = T_m - T_e \tag{A.62}$$

where H is the moment of inertia and the electromechanical and mechanical torque are T_e and T_m, respectively, which in per unit on the machine base T_e is equal to the active power P_g generated while T_m is equal to the turbine mechanical power P_m. δ is the rotor angular position (in radians) with respect to the synchronous rotating reference given by [Kundur, 1994]:

$$\delta = \omega t - \omega_0 t + \delta_{initial}. \tag{A.63}$$

Using (A.63), the second-order differential equation (A.62) (known as the swing equation) can be decomposed into two first-order differential equations:

$$\frac{d\delta}{dt} = \omega - \omega_0 \tag{A.64}$$

$$\frac{d\omega}{dt} = \frac{\omega_0}{2H}\left(P_m - P_g - D\left(\omega - \omega_0\right)\right) \tag{A.65}$$

where D is the damping constant in (s/rad).

The active and reactive power generated by the synchronous machine can be obtained as follows. The complex power (in per unit) produced is given by

$$S_g = P_g + jQ_g = \mathbf{V}\mathbf{I}^* \tag{A.66}$$

where $\mathbf{V} = \left(V_d + jV_q\right)e^{j\left(\delta-\frac{\pi}{2}\right)}$ and $\mathbf{I} = \left(I_d + jI_q\right)e^{j\left(\delta-\frac{\pi}{2}\right)}$. Thus, using the definitions of ***V*** and ***I*** yields

$$P_g = I_d V_d + I_q V_q \tag{A.67}$$

$$Q_g = I_d V_q - I_q V_d\,. \tag{A.68}$$

Substituting (A.43)-(A.45) into (A.67)-(A.68) the active and reactive powers are expressed only in terms of meaningful variables:

$$\begin{aligned} P_g = {} & K_{13}E'_d V\cos\left(\delta-\theta\right) + K_{14}\psi_{2q}V\cos\left(\delta-\theta\right) + K_{15}E'_q V\sin\left(\delta-\theta\right) \\ & + K_{16}\psi_{1d}V\sin\left(\delta-\theta\right) + K_{17}V^2\sin\left(2\left(\delta-\theta\right)\right) \end{aligned} \tag{A.69}$$

$$\begin{aligned} Q_g = {} & -K_{13}E'_d V\sin\left(\delta-\theta\right) - K_{14}\psi_{2q}V\sin\left(\delta-\theta\right) + K_{15}E'_q V\cos\left(\delta-\theta\right) \\ & + K_{16}\psi_{1d}V\cos\left(\delta-\theta\right) - V^2\left(K_{18}\cos\left(\delta-\theta\right)^2 + K_{19}\sin\left(\delta-\theta\right)^2\right) \end{aligned} \tag{A.70}$$

where

$$K_{13} = -\frac{\left(X''_q - X_{ls}\right)}{X''_q\left(X'_q - X_{ls}\right)} \tag{A.71}$$

$$K_{14} = \frac{\left(X'_q - X''_q\right)}{X''_q\left(X'_q - X_{ls}\right)} \tag{A.72}$$

$$K_{15} = \frac{\left(X'_d - X_{ls}\right)}{X''_d\left(X'_d - X_{ls}\right)} \tag{A.73}$$

$$K_{16} = \frac{\left(X'_d - X''_d\right)}{X''_d\left(X'_d - X_{ls}\right)} \tag{A.74}$$

$$K_{17} = -\frac{\left(X''_q - X''_d\right)}{2X''_q X''_d} \tag{A.75}$$

$$K_{18} = -\frac{1}{X_d''} \tag{A.76}$$

$$K_{19} = -\frac{1}{X_q''}. \tag{A.77}$$

Thus, the generator model of order VI is given by six differential equations (A.46)-(A.49), (A.64)-(A.65) and two algebraic equations (A.69)-(A.70).

Finally, some generators can be equipped with an OvereXcitation Limiter and it necessary to compute the field current. Therefore, substituting (A.37), (A.44) and (A.45) into (4.36) yields

$$I_{fd} = -K_1 E_q' - K_2 \psi_{1d} - K_3 V \cos\left(\delta - \theta\right). \tag{A.78}$$

A.2 Generator model of order IV

A reduced-order synchronous machine model can be obtained (from the generator model of order IV) if the damper windings are neglected since the subtransient open-circuit time constants T_{qo}'', T_{do}'' are sufficiently small. Thus, the rotor circuit for this model is composed of the field winding and one amortisseur winding (denoted by *1q*) [Sauer and Pai, 1998]. Therefore, the generator of order IV is represented by the following voltage equations:

$$V_d = -R_a I_d - \frac{\omega}{\omega_0}\psi_q + \frac{1}{\omega_0}\frac{d\psi_d}{dt} \tag{A.79}$$

$$V_q = -R_a I_q + \frac{\omega}{\omega_0}\psi_d + \frac{1}{\omega_0}\frac{d\psi_q}{dt} \tag{A.80}$$

$$V_{fd} = R_{fd} I_{fd} + \frac{1}{\omega_0}\frac{d\psi_{fd}}{dt} \tag{A.81}$$

$$0 = R_{1q} I_{1q} + \frac{1}{\omega_0}\frac{d\psi_{1q}}{dt} \tag{A.82}$$

with the flux linkages per second as

$$\psi_d = -X_d I_d + X_{md} I_{fd} \tag{A.83}$$

$$\psi_q = -X_q I_q + X_{mq} I_{1q} \tag{A.84}$$

$$\psi_{fd} = -X_{md} I_d + X_{fd} I_{fd} \tag{A.85}$$

$$\psi_{1q} = -X_{mq} I_q + X_{1q1q} I_{1q}\,. \tag{A.86}$$

Hence, the synchronous machine model of order IV can expressed only in terms of meaningful variables following the same procedure as Section A.1 and under the same assumption:

$$T'_{do} \frac{dE'_q}{dt} = K_1 E'_q + K_3 V \cos(\delta - \theta) + E_{fd} \tag{A.87}$$

$$T'_{qo} \frac{dE'_d}{dt} = K_3 E'_d + K_4 V \sin(\delta - \theta) \tag{A.88}$$

$$\frac{d\delta}{dt} = \omega - \omega_0 \tag{A.89}$$

$$\frac{d\omega}{dt} = \frac{\omega_0}{2H}\left(P_m - P_g - D(\omega - \omega_0)\right) \tag{A.90}$$

$$\begin{aligned} P_g = {} & K_5 E'_d V \cos(\delta - \theta) + K_6 E'_q V \sin(\delta - \theta) \\ & + K_7 V^2 \sin\left(2(\delta - \theta)\right) \end{aligned} \tag{A.91}$$

$$\begin{aligned} Q_g = {} & -K_5 E'_d V \sin(\delta - \theta) + K_6 E'_q V \cos(\delta - \theta) \\ & - V^2 \left(-K_6 \cos(\delta - \theta)^2 + K_5 \sin(\delta - \theta)^2\right) \end{aligned} \tag{A.92}$$

where

$$K_1 = -\frac{X_d}{X'_d} \tag{A.93}$$

$$K_2 = -1 + \frac{X_d}{X'_d} \tag{A.94}$$

$$K_3 = -\frac{X_q}{X'_q} \tag{A.95}$$

$$K_4 = -1 + \frac{X_q}{X'_q} \tag{A.96}$$

$$K_5 = -\frac{1}{X'_q} \tag{A.97}$$

$$K_6 = \frac{1}{X'_d} \tag{A.98}$$

$$K_7 = \frac{X'_d - X'_q}{2X'_d X'_q}, \tag{A.99}$$

and the field current is expressed as

$$I_{fd} = -K_1 E'_q - K_2 V \cos\left(\delta - \theta\right). \tag{A.100}$$

The synchronous machine model of order IV is often referred to as a two-axis model [Sauer and Pai, 1998].

Appendix B

Power system stabilizer model

B.1 Transformation of the power system stabilizer

The functional block diagram of the Power System Stabilizer (PSS) system is shown in Figure B.1 [Kundur, 1994].

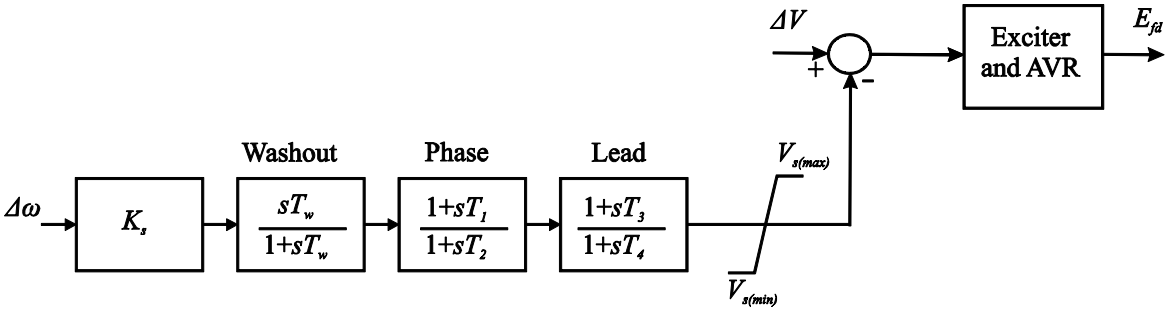

Figure B.1: Power system stabilizer.

The PSS system consists of three blocks: a phase compensation block (phase and lead), a signal washout block and a gain block. Each block is represented by a transference function that involves two differential equations. However, the integration method used in the present work cannot solve this type of transference function. Therefore, the PSS model must be expressed by only one ODE, which can be obtained by dividing each transference function as follows:

$$\frac{sTw}{1+sTw} = 1 - \frac{1}{1+sTw} \tag{B.1}$$

$$\frac{1+sT_1}{1+sT_2} = \frac{T_1}{T_2} - \frac{\left(1-\frac{T_1}{T_2}\right)}{1+sT_2} \tag{B.2}$$

$$\frac{1+sT_3}{1+sT_4} = \frac{T_3}{T_4} - \frac{\left(1-\frac{T_3}{T_4}\right)}{1+sT_4}. \tag{B.3}$$

Using (B.1), (B.2) and (B.3) the functional block diagram of the PSS system can be represented as shown in Figure B.2.

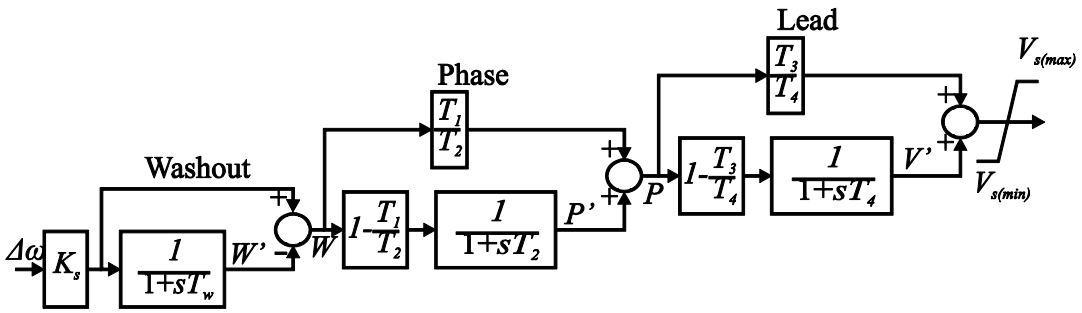

Figure B.2: Block diagram of the PSS.

By following the block diagram from Figure B.2, the model of the PSS can be expressed in terms of ODEs:

$$T_w \frac{dW'}{dt} = K_S \Delta\omega - W' \tag{B.4}$$

$$T_2 \frac{dP'}{dt} = c_1 \left(K_S \Delta\omega - W' \right) - P' \tag{B.5}$$

$$T_4 \frac{dV'}{dt} = c_2 \left(K_S \Delta\omega - W' \right) - c_3 P' - V' \tag{B.6}$$

with the compensation V_s of the PSS system given by

$$V_s = c_4\left(K_s\Delta\omega - W'\right) + c_5 P' + V' \tag{B.7}$$

where W', P' and V' are the new state variables associated with the washout block, phase and lead, respectively. Finally, the constants c_i are given by

$$c_1 = 1 - \frac{T_1}{T_2} \tag{B.8}$$

$$c_2 = 1 - \frac{T_3}{T_4} \tag{B.9}$$

$$c_3 = \frac{T_1}{T_2} - \frac{T_1 T_3}{T_2 T_4} \tag{B.10}$$

$$c_4 = \frac{T_1 T_3}{T_2 T_4} \tag{B.11}$$

$$c_5 = \frac{T_3}{T_4}. \tag{B.12}$$

Appendix C

Induction machine model

C.1 Induction motor model of order III

The induction motor model used in this work is derived with the same procedure described for the synchronous machine. Figure B.1 shows the winding arrangement for a 2-pole, 3-phase (v_a, v_b, v_c), symmetrical induction machine. The stator and rotor windings are sinusoidally distributed winding, displaced 120°, respectively. This representation can be employed for both the squirrel-cage rotor and the wound rotor.

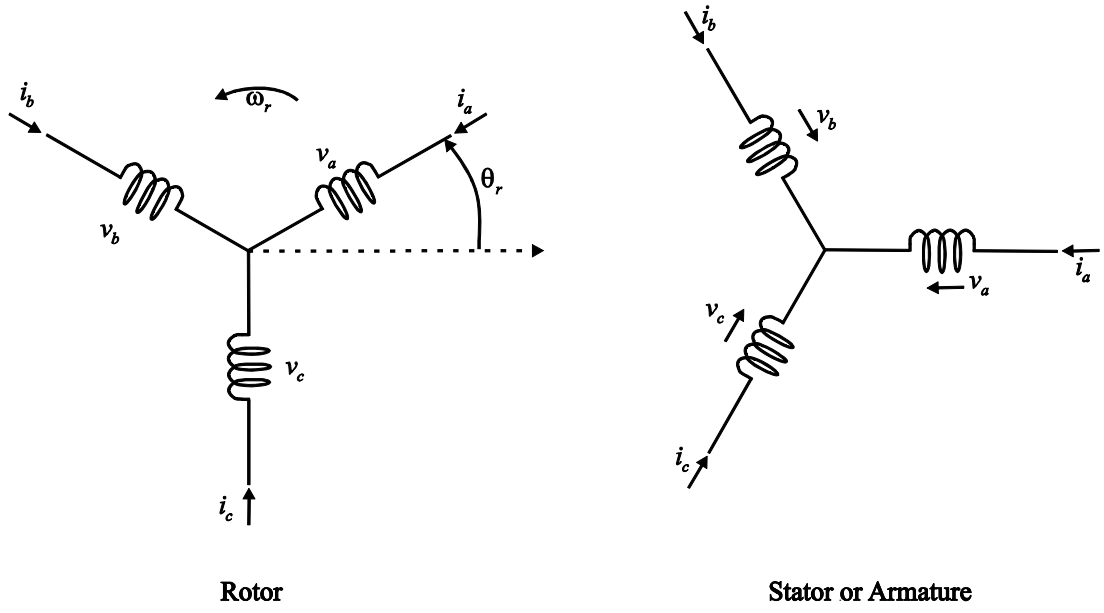

Figure C.1: Schematic diagram of the induction machine.

The stator and rotor equations expressed in terms of the *dq0* frame reference are obtained by applying Kirchhoff's, Faraday's fundamental laws and the Park transformation [Krause et al., 2002], [Kundur, 1994]:

$$V_{ds} = R_s I_{ds} - \frac{\omega_e}{\omega_0}\psi_{qs} + \frac{1}{\omega_0}\frac{d\psi_{ds}}{dt} \tag{C.1}$$

$$V_{qs} = R_s I_{qs} + \frac{\omega_e}{\omega_0}\psi_{ds} + \frac{1}{\omega_0}\frac{d\psi_{qs}}{dt} \tag{C.2}$$

$$V_{dr} = R_r I_{dr} - (1-\omega_r)\psi_{qr} + \frac{1}{\omega_0}\frac{d}{dt}\psi_{dr} \tag{C.3}$$

$$V_{qr} = R_r I_{qr} + (1-\omega_r)\psi_{dr} + \frac{1}{\omega_0}\frac{d\psi_{qr}}{dt} \tag{C.4}$$

with the flux-current relations [Lesieutre et al., 1995]

$$\psi_{ds} = X_{ss} I_{ds} + X_m I_{dr} \tag{C.5}$$

$$\psi_{qs} = X_{ss} I_{qs} + X_m I_{qr} \tag{C.6}$$

$$\psi_{dr} = X_m I_{ds} + X_{rr} I_{dr} \tag{C.7}$$

$$\psi_{qr} = X_m I_{qs} + X_{rr} I_{qr} \tag{C.8}$$

$$X_{ss} = X_s + X_m \tag{C.9}$$

$$X_{rr} = X_r + X_m \tag{C.10}$$

where ω_r is the actual rotor speed, and ω_e represents the speed of a rotating reference frame. X_s and X_r are the stator and rotor leakage reactances, whereas X_m is the magnetizing reactance. R_s is the stator resistance, V_{ds} and V_{qs} are the *d* and *q* stator voltages, I_{ds} and I_{qs} are the *d* and *q* stator currents ψ_{ds} and ψ_{qs} are the *d* and *q* stator flux linkages, and similarly for the rotor circuit.

Based on the dynamics of interest in the present work, the induction motor model can be rely on the following assumptions:

- The transformer voltages are neglected $(\dot{\psi}_{ds} = \dot{\psi}_{qs} = 0)$.
- The reference frame is rotating at synchronous speed, $(\omega_e = \omega_0)$.

- The rotor is assumed to be a squirrel-cage, $(V_{dr} = V_{qr} = 0)$.
- Magnetic saturation is neglected.

Based on the assumptions the motor equations (C.1)-(C.4) are expressed as

$$V_{ds} = R_s I_{ds} - \psi_{qs} \tag{C.11}$$

$$V_{qs} = R_s I_{qs} + \psi_{ds} \tag{C.12}$$

$$\frac{1}{\omega_0}\frac{d\psi_{dr}}{dt} = -R_{dr} I_{dr} + \psi_{qr} - \omega_r \psi_{qr} \tag{C.13}$$

$$\frac{1}{\omega_0}\frac{d\psi_{dr}}{dt} = -R_{qr} I_{qr} - \psi_{dr} + \omega_r \psi_{dr}\,. \tag{C.14}$$

The induction motor model can be obtained using the following definition [Lesieutre et al., 1995], [Kundur, 1994]:

$$X_s' = \frac{X_{ss} X_{rr} - X_m^2}{X_{rr}} \tag{C.15}$$

$$e_q' = \frac{X_m}{X_{rr}} \psi_{dr} \tag{C.16}$$

$$e_d' = -\frac{X_m}{X_{rr}} \psi_{qr} \tag{C.17}$$

$$T_o' = \frac{X_{rr}}{\omega_0 R_r} \tag{C.18}$$

$$s = 1 - \omega_r \tag{C.19}$$

where e_q' and e_d' are the voltage magnitudes behind transient impedances. T_o' is the transient open-circuit time constant, and s is the slip speed in p.u.

Hence, the rotor currents are obtained by substituting (C.15)-(C.17) into (C.7)-(C.8)

$$I_{dr} = \frac{e_q' + (X_s' - X_{ss}) I_{ds}}{X_m} \tag{C.20}$$

$$I_{qr} = -\frac{e'_d + (X'_s - X_{ss})I_{qs}}{X_m}. \tag{C.21}$$

The stator currents are determined from (C.11)-(C.12) using the rotor currents equations and stator flow linkages (C.5)-(C.6):

$$I_{ds} = \frac{R_s\left(V_{ds} - e'_d\right)}{R_s^2 + X_s'^2} + \frac{X'_s\left(V_{qs} - e'_q\right)}{R_s^2 + X_s'^2} \tag{C.22}$$

$$I_{qs} = \frac{R_s\left(V_{qs} - e'_q\right)}{R_s^2 + X_s'^2} - \frac{X'_s\left(V_{ds} - e'_d\right)}{R_s^2 + X_s'^2}. \tag{C.23}$$

On the other hand, the stator voltages can be represented in a complex form [Lesieutre et al., 1995], [Kundur, 1994]

$$Ve^{j\theta} = \left(V_{ds} + jV_{qs}\right) = V\cos\theta + jV\sin\theta \tag{C.24}$$

where V and θ are the magnitude and phase angle of the voltage measured at the load bus terminal.

Using (C.24), the stator currents can be represented in terms of terminal voltage as

$$I_{ds} = \frac{-R_s e'_d - X'_s e'_q + R_s V\cos\theta + X'_s V\sin\theta}{R_s^2 + X_s'^2} \tag{C.25}$$

$$I_{qs} = \frac{X'_s e'_d - R_s e'_q + R_s V\sin\theta - X'_s V\cos\theta}{R_s^2 + X_s'^2}. \tag{C.26}$$

Substituting the stator and rotor currents equations into (C.13)-(C.14), the induction motor model is expressed as

$$T'_o\frac{de'_q}{dt} = M_3 e'_q + \left[M_2 + M_1\left(1-\omega_r\right)\right]e'_d - M_2 V\cos\theta + M_4 V\sin\theta \tag{C.27}$$

$$T_o' \frac{de_d'}{dt} = \left[-M_2 + M_1 \left(1 - \omega_r\right) \right] e_q' + M_3 e_d' + M_4 V \cos\theta + M_2 V \sin\theta \tag{C.28}$$

where

$$M_1 = \frac{X_{rr}}{R_r} \tag{C.29}$$

$$M_2 = \frac{R_s \left(X_{ss} - X_s' \right)}{R_s^2 + X'^2_s} \tag{C.30}$$

$$M_3 = -\frac{R_s^2 + X_{ss} X_s'}{R_s^2 + X_s'^2} \tag{C.31}$$

$$M_4 = \frac{X_s' \left(X_{ss} - X_s' \right)}{R_s^2 + X_s'^2} \tag{C.32}$$

$$M_5 = -\frac{R_s}{R_s^2 + X_s'^2} \tag{C.33}$$

$$M_6 = \frac{X_s'}{R_s^2 + X_s'^2} . \tag{C.34}$$

The rotor motion can be represented by the differential equation in terms of the rotor angular speed, ω_r, in p.u.

$$\frac{d\omega_r}{dt} = \frac{1}{2H_m} \left(T_e - T_m \right) \tag{C.35}$$

where H_m is the moment of inertia, and T_e is the electromagnetic generated torque, which is given by [Krause et al., 2002]

$$T_e = \psi_{qr} I_{dr} - \psi_{dr} I_{qr} . \tag{C.36}$$

Introducing (C.7)-(C.8) and the rotor and stator currents in (C.36) yields

$$T_e = -M_5 e'_d V\cos\theta + M_6 e'_d V\sin\theta - M_6 e'_q V\cos(\theta) - M_5 e'_q V\sin\theta + M_5\left[\left(e'_d\right)^2 + \left(e'_q\right)^2\right] \quad . \tag{C.37}$$

Similarly, T_m is the mechanical load torque, and its model is composed of both the constant and the quadratic torque models. Thus, the composite mechanical load torque takes the following general form [Van Cutsem and Vournas, 1998], [Kundur, 1994]:

$$T_m = T_0 + T_1\omega_r + T_2\omega_r^2 \tag{C.38}$$

where T_0, T_1 and T_2 are constants whose values are calculated with the initial condition as discussed in Section 2.6.4.1.

The active and reactive power absorbed by the induction motor can be expressed only in terms of meaningful bus variables:

$$P_{Lm} = M_5 e'_d V\cos\theta + M_6 e'_d V\sin\theta - M_6 e'_q V\cos\theta + M_5 e'_q V\sin\theta - M_5 V^2 \tag{C.39}$$

$$Q_{Lm} = -M_6 e'_d V\cos\theta + M_6 e'_d V\sin\theta - M_5 e'_q V\cos\theta - M_6 e'_q V\sin\theta + M_6 V^2 \quad . \tag{C.40}$$

Therefore, the induction motor model of order III is composed of three differential equations (C.27), (C.28), (C.35) and four algebraic equations (C.37)-(C.40).

Appendix D

Electric power system data

D.1 One-machine infinite-bus system data

Table D.1: Transmission line parameters

Buses		R(p.u.)	X(p.u.)	B(p.u.)
1	2	0	0.055	0
1	2	0	0.055	0

Table D.2: Synchronous machine parameters

Bus	S_{nom} (MVA)	P_{nom} (MW)	X_{ls} (p.u.)	X_d (p.u.)	X'_d (p.u.)	X''_d (p.u.)	T'_{qo} (s)	T''_{qo} (s)	X_q (p.u.)	X'_q (p.u.)	X''_q (p.u.)	T'_{do} (s)	T''_{do} (s)	H (s)	D (s/rad)
1	1100	935	0.125	1	0.31	0.256	10.2	0.0245	0.69	0.356	0.08	0.6	0.054	4.2	5

D.2 2-machine, 4-bus system data

Table D.3: Transmission line parameters

Buses		R(p.u.)	X(p.u.)	B(p.u.)
1	4	0	0.055	0
1	4	0	0.055	0

Table D.4: Transformer parameters

Buses		R_s(p.u.)	X_s(p.u.)	Tap: T_v	Tap: U_v
2	4	0	0.016	1.04	1.0
3	4	0	0.004	1.0	1.0

Table D.5: LTC parameters

Buses		V_{con}(p.u.)	r_{max}(p.u.)	r^{min}(p.u.)	Δr(p.u.)	db(p.u.)	$T_{d0}+T_m$(s)	$T_{d1}+T_m$(s)
3	4	1.0	1.1	0.8	0.01	0.01	20	10

Table D.6: Static load parameters

Bus	P_L(MW)	Q_L(MVR's)
3	600	150

Table D.7: Load restoration parameters

Bus	T_P(s)	T_Q(s)	α_t	β_t
3	20	20	0.2	0.2

Table D.8: Induction motor parameters

Bus	S_{nom} (MVA)	fP_L	fQ_L	R_s (p.u.)	X_s (p.u.)	X_m (p.u.)	R_r (p.u.)	X_r (p.u.)	H (s)	T_1/T_0	T_2/T_0
3	800	0.4	0.4	0.0	0.1	3.2	0.018	0.18	0.5	0	0

Table D.9: Synchronous machine parameters

Bus	S_{nom} (MVA)	P_{nom} (MW)	X_{ls} (p.u.)	X_d (p.u.)	X'_d (p.u.)	X''_d (p.u.)	T'_{qo} (s)	T''_{qo} (s)	X_q (p.u.)	X'_q (p.u.)	X''_q (p.u.)	T'_{do} (s)	T''_{do} (s)	H (s)	D (s/rad)
1	100000	100000	0.2	2.1	0.414	0.25	6.682	0.052	2.1	0.813	0.25	4.52	0.221	3.5	0
2	500	450	0.2	2.1	0.414	0.25	6.682	0.052	2.1	0.813	0.25	4.52	0.221	3.5	0

Table D.10: Exciter parameters

Bus	T_E(s)	G_E	$E_{fd(max)}$(p.u.)	$E_{fd(min)}$ (p.u.)
1	0.1	50	5	0
2	0.1	50	5	0

Table D.11: OXL parameters

Bus	$I_{fd}^{\lim}$ (p.u.)	S_1	S_2	B_1	B_2	B_3	B_r	c_i
2	2.825	1	2	20	0.1	1	1	0.1

Table D.12: Governor and turbine parameters

Bus	R (p.u.)	T_{GV} (s)	$\frac{dP_{GV}}{dt}^{\max}$ (p.u.)	$\frac{dP_{GV}}{dt}^{\min}$ (p.u.)	T_{CH} (s)	F_{HP}	T_{RH} (s)	F_{IP}	T_{CO} (s)
1	0.4	0.1	0.1	-0.1	0.2	0.4	4	0.3	0.3
2	0.4	0.1	0.1	-0.1	0.2	0.4	4	0.3	0.3

D.3 3-machine, 9-bus WSCC system data

Table D.13: Transmission line parameters

Buses		R(p.u.)	X(p.u.)	B(p.u.)
4	5	0.0100	0.0850	0.176
5	7	0.0320	0.1610	0.306
7	8	0.0085	0.0720	0.149

Buses		R(p.u.)	X(p.u.)	B(p.u.)
8	9	0.0119	0.1008	0.209
9	6	0.039	0.1700	0.358
6	4	0.0170	0.9200	0.158

Table D.14: Transformer parameters

Buses		R_s(p.u.)	X_s(p.u.)	Tap: T_v	Tap: U_v
1	4	0	0.0625	1.0	1.0
2	7	0	0.0576	1.0	1.0
3	9	0	0.0586	1.0	1.0

Table D.15: Static load parameters

Bus	P_L(MW)	Q_L(MVR's)
5	125	50
6	90	30
8	100	35

Table D.16: Synchronous machine parameters

Bus	S_{nom} (MVA)	X_{ls} (p.u.)	X_d (p.u.)	X'_d (p.u.)	T'_{qo} (s)	X_q (p.u.)	X'_q (p.u.)	T'_{do} (s)	H (s)	D (s/rad)
1	100	0.0	0.146	0.0608	8.96	0.0969	0.0969	0.31	23.64	0.01254
2	100	0.0	0.8958	0.1198	6.0	0.8645	0.1969	0.535	6.4	0.0068
3	100	0.0	1.3125	0.1813	5.89	1.2578	0.25	0.6	3.01	0.0048

Table D.17: Exciter parameters

Bus	T_E(s)	G_E	$E_{fd(max)}$(p.u.)	$E_{fd(min)}$ (p.u.)
1	0.2	20	5	-5
2	0.2	20	5	-5
3	0.2	20	5	-5

D.4 10-machine, 39-bus New England system data

Table D.18: Transmission line parameters

Buses		R(p.u.)	X(p.u.)	B(p.u.)
1	2	0.00350	0.04110	0.69870
1	39	0.00100	0.02500	0.75000
2	3	0.00130	0.01510	0.25720
2	25	0.00700	0.00860	0.14600
3	4	0.00130	0.02130	0.22140
3	18	0.00110	0.01330	0.21380
4	5	0.00080	0.01280	0.13420
4	14	0.00080	0.01290	0.13820
5	6	0.00020	0.00260	0.04340
5	8	0.00080	0.01120	0.14760
6	7	0.00060	0.00920	0.11300
6	11	0.00070	0.00820	0.13895
7	8	0.00040	0.00460	0.07800
9	8	0.00230	0.03630	0.38040
9	39	0.00100	0.02500	1.20000
10	11	0.00040	0.00430	0.07290
10	13	0.00040	0.00430	0.07290

Buses		R(p.u.)	X(p.u.)	B(p.u.)
13	14	0.00090	0.01010	0.17250
14	15	0.00180	0.02170	0.36600
15	16	0.00090	0.00940	0.17100
16	17	0.00070	0.00890	0.13420
16	19	0.00160	0.01950	0.30400
16	21	0.00080	0.01350	0.25480
16	24	0.00030	0.00590	0.06800
17	18	0.00070	0.00820	0.13190
17	27	0.00130	0.01730	0.32160
21	22	0.00080	0.01400	0.25650
22	23	0.00060	0.00960	0.18450
23	24	0.00220	0.03500	0.36100
25	26	0.00320	0.03230	0.51300
26	27	0.00140	0.01470	0.23960
26	28	0.00430	0.04740	0.78020
26	29	0.00570	0.06250	1.02900
28	29	0.00140	0.01510	0.24900

Table D.19: Transformer parameters

Buses		R_s(p.u.)	X_s(p.u.)	Tap: T_v	Tap: U_v
2	30	0.0	0.01810	1.02500	1.0
6	31	0.0	0.02500	1.07000	1.0
10	32	0.0	0.02000	1.07000	1.0
12	13	0.00160	0.04350	1.00600	1.0
19	33	0.00070	0.01420	1.07000	1.0
20	34	0.00090	0.01800	1.00900	1.0

Buses		R_s(p.u.)	X_s(p.u.)	Tap: T_v	Tap: U_v
22	35	0.0	0.01430	1.02500	1.0
23	36	0.00050	0.02720	1.0	1.0
25	37	0.00060	0.02320	1.02500	1.0
29	38	0.00080	0.01560	1.02500	1.0
12	11	0.00160	0.04350	1.00600	1.0
19	20	0.00070	0.01380	1.06000	1.0

Table D.20: LTC parameters

Buses		V_{con}(p.u.)	r_{max}(p.u.)	r^{min}(p.u.)	Δr(p.u.)	db(p.u.)	T_{d0}+T_m(s)	T_{d1}+T_m(s)
12	13	1.0	1.1	0.8	0.01	0.01	20	10
12	11	1.0	1.1	0.8	0.01	0.01	20	10
20	19	1.0	1.1	0.8	0.01	0.01	20	10

Table D.21: Static load parameters

Bus	P_L(MW)	Q_L(MVR's)
3	322	2.4
4	500	184
7	233	84
8	522	176
12	7.5	88
15	320	153
16	329	32.3
18	158	30
20	628	103
21	274	115

Bus	P_L(MW)	Q_L(MVR's)
23	247.5	84.6
24	308.6	-92.2
25	224	47.2
26	139	17
27	281	75.5
28	206	27.6
29	283.5	26.9
39	1104	250
31	9.2	4.6

Table D.22: Synchronous machine parameters

Bus	S_{nom} (MVA)	P_{nom} (MW)	X_{ls} (p.u.)	X_d (p.u.)	X'_d (p.u.)	X''_d (p.u.)	T'_{qo} (s)	T''_{qo} (s)	X_q (p.u.)	X'_q (p.u.)	X''_q (p.u.)	T'_{do} (s)	T''_{do} (s)	H (s)	D (s/rad)
30	1100	935	0.125	1.0	0.31	0.256	10.2	0.0245	0.69	0.356	0.08	0.6	0.054	4.2	0
31	750	675	0.262	2.212	0.523	0.327	6.56	0.034	2.115	1.275	0.327	1.5	0.038	4.04	0
32	1000	850	0.304	2.495	0.531	0.424	5.7	0.039	2.37	0.876	0.424	1.5	0.053	3.58	0
33	1000	850	0.295	2.63	0.436	0.348	5.69	0.040	2.58	1.66	0.348	1.5	0.051	2.86	0
34	800	680	0.432	5.36	1.056	0.285	5.4	0.0345	4.96	1.328	0.285	0.44	0.023	3.25	0
35	1000	850	0.224	2.54	0.5	0.31	7.3	0.0379	2.41	0.814	0.31	0.4	0.023	3.48	0
36	800	680	0.257	2.36	0.392	0.314	5.66	0.04	2.336	1.488	0.314	1.5	0.038	3.3	0
37	800	680	0.224	2.32	0.456	0.285	6.7	0.0345	2.24	0.729	0.285	0.41	0.023	3.04	0
38	1000	850	0.298	2.106	0.57	0.356	4.79	0.0245	2.05	0.587	0.356	1.96	0.054	3.45	0
39	10000	8500	0.3	2	0.6	0.375	7	0.0356	1.9	0.8	0.375	0.7	0.021	5	0

Table D.23: Exciter and derivative feedback parameters

Bus	T_E(s)	G_E	$E_{fd(max)}$(p.u.)	$E_{fd(min)}$ (p.u.)	K_F	$T_{F)}$(p.u.)
30	0.1	5.0	5.0	-5.0	0.1	4
31	0.95	6.2	5.0	-5.0	0.114	3
32	0.1	5.0	5.0	-5.0	0.12	4
33	0.1	5.0	5.0	-5.0	0.12	4
34	0.07	40	5.0	-5.0	0.07	3
35	0.07	5.0	5.0	-5.0	0.115	4
36	0.07	40	5.0	-5.0	0.07	3
37	0.07	5.0	5.0	-5.0	0.15	4
38	0.07	40	5.0	-5.0	0.08	3
39	0.08	6.2	5.0	-5.0	0.12	6

Table D.24: Governor and turbine parameters

Bus	R (p.u.)	T_{GV} (s)	$\frac{dP_{GV}}{dt}^{\max}$ (p.u.)	$\frac{dP_{GV}}{dt}^{\min}$ (p.u.)	T_{CH} (s)	F_{HP}	T_{RH} (s)	F_{IP}	T_{CO} (s)
30	0.4	0.1	0.1	-0.1	0.2	0.4	4	0.3	0.3
31	0.4	0.1	0.1	-0.1	0.2	0.4	4	0.3	0.3
32	0.4	0.1	0.1	-0.1	0.2	0.4	4	0.3	0.3
33	0.4	0.1	0.1	-0.1	0.2	0.4	4	0.3	0.3
34	0.4	0.1	0.1	-0.1	0.2	0.4	4	0.3	0.3
35	0.4	0.1	0.1	-0.1	0.2	0.4	4	0.3	0.3
36	0.4	0.1	0.1	-0.1	0.2	0.4	4	0.3	0.3
37	0.4	0.1	0.1	-0.1	0.2	0.4	4	0.3	0.3
38	0.4	0.1	0.1	-0.1	0.2	0.4	4	0.3	0.3
39	0.4	0.1	0.1	-0.1	0.2	0.4	4	0.3	0.3

D.5 46-machine, 190-bus Mexican power system data

The system data are taken from [Messina and Vittal, 2005]. However, for this work all generators are equipped with a steam turbine. Furthermore, the parameter for all speed governors and steam turbine are equal and given in Table D.25.

Table D.25: Governor and turbine parameters

R (p.u.)	T_{GV} (s)	$\frac{dP_{GV}}{dt}^{\max}$ (p.u.)	$\frac{dP_{GV}}{dt}^{\min}$ (p.u.)	T_{CH} (s)	F_{HP}	T_{RH} (s)	F_{IP}	T_{CO} (s)
0.4	0.1	0.1	-0.1	0.2	0.4	4	0.3	0.3

Table D.26: LTC parameters

Buses		R_s (p.u.)	X_s (p.u.)	Tap: T_v	Tap: U_v	V_{con} (p.u.)	r_{max} (p.u.)	$r^{\min}$ (p.u.)	Δr (p.u.)	db (p.u.)	$T_{d0}+T_m$ (s)	$T_{d1}+T_m$ (s)
182	182fa	0.0007	0.0138	1.0	1.0	1.0	1.1	0.8	0.01	0.01	20	10
183	183fa	0.0007	0.0138	1.0	1.0	1.0	1.1	0.8	0.01	0.01	20	10
184	184fa	0.0007	0.0138	1.0	1.0	1.0	1.1	0.8	0.01	0.01	20	10